

THE DEVELOPMENT OF NOVEL NUCLEAR MAGNETIC
RESONANCE TECHNIQUES FOR THE STUDY OF
SOLIDS, THIN FILMS AND SURFACES WITH
PARTICULAR APPLICATION TO AMORPHOUS
SEMICONDUCTING SILICON-HYDROGEN FILMS

Thesis by

Jeffrey Allen Reimer

In Partial Fulfillment of the Requirements
for the Degree of
Doctor of Philosophy

California Institute of Technology
Pasadena, California

1981

(Submitted October 28, 1980)

This thesis is dedicated to the late Professor Robert W. Vaughan...

*"There is an appointed time for everything. And
there is a time for every event under heaven —*

*A time to give birth, and a time to die;
A time to plant, and a time to uproot
what was planted.*

*A time to kill, and a time to heal;
A time to tear down, and a time to
build up.*

*A time to weep, and a time to laugh;
A time to mourn, and a time to dance.
A time to throw stones, and a time to
gather stones;*

*A time to embrace, and a time to shun
embracing.*

*A time to search, and a time to give
up as lost;*

A time to keep, and a time to throw away.

*A time to tear apart, and a time to
sew together;*

A time to be silent, and a time to speak.

A time to love, and a time to hate;

A time for war, and a time for peace...

*I know that every thing God does will remain forever;
there is nothing to add to it and nothing to take from it,
for God has so worked that men should fear Him."*

from Ecclesiastes, Chapter 3

ACKNOWLEDGMENTS

I am very grateful to a number of people who have supported, trained, and disciplined me during my four years of graduate study. It is very difficult to mention only a few of their names....

Shortly after Professor Vaughan was killed, I became acquainted with Dr. John C. Knights at the Xerox Palo Alto Research Center. John has provided enthusiasm, motivation, and direction for my final seventeen months of graduate study. I respect him a great deal, and perhaps can thank him best by pursuing scientific problems with the same ingenuity and lack of compromise that I found in his approach to research. I would also like to thank Professor Sunney I. Chan for his guidance during this same period. His advice has always been sound and he has devoted many selfless hours toward helping me finish this thesis and secure postgraduate employment. Professor Bernard C. Gerstein has also been very helpful, especially by allowing me to utilize his one-of-a-kind experimental set-ups.

I have learned a great deal while working with several former students and postdocs. Mike Stoll and Lex Vega have taught me most everything I know about solid state magnetic resonance. I shared an office with Mike Duncan for over three years, and while Mike and I are in some ways opposites, Bob Vaughan recognized this as a potential for both of us and made sure we were put together. I hope Mike learned a few things from me because I certainly learned many things from him. Indeed, the whole Vaughan research group was important in my graduate training; notably Doug Carson, Mike Duncan, Jim Gleeson, Albert Highe,

Micha Polak, John Schlup, Mike Stoll and Lex Vega. Also several of the scientists at Xerox P.A.R.C. have been very helpful. They include Dave Biegelsen, Jim Boyce, Bob Nemanich, Bob Street, Nobel Johnson, and Rene Lujan.

Life here at Caltech has been enriched by several close friends. Russ Bone and I shared lots of ups and downs while sharing an apartment, and of course the same for Mike Duncan and I while sharing an office. I was on a marvelous softball team for three summers with great athletes such as Bill Olbricht, Gary Whatley, Doug Carson, John Schlup, Samir Barudi, to name just a few. These guys are all good friends along with Pat Thiel and Barry Bentley. My off-campus life has been blessed by four very special people: Gordon, Darlene, Michelle and Sherri Reisig. None of them has ever ceased loving and supporting me through the best and worst of times.

I have grown greatly through excellent Bible teaching and Christian fellowship in two churches: Lake Avenue Congregational and Calvary Baptist Church. I am especially grateful to Pastors Tom, Bob and John for ministry opportunities, prayer support, and advice during the past two years. Also, two fellow scientists and Christians, John Schlup and Gerry Garwood, have been very diligent in prayer support over the years of my graduate training.

The people who have really made this thesis possible are my parents. They have been supportive, loving, interested, and self-sacrificing throughout my entire college education. I have learned much by watching their successes (and, yes, failures too) over the years; they have never

once denied me the opportunity to learn, stumble and re-learn again. And to this day they, along with my brother and sister, continue to teach me important lessons on life and parenthood.

Late in 1973 I met a new next-door neighbor: a blonde-haired, blue-eyed girl from San Clemente. At that time I had no idea that in September of 1978 she would become my wife ... and now I have no idea how to thank her enough. She has helped me learn to enjoy what I have now without sacrificing goals for tomorrow. And while she has a Masters degree, she has little scientific training and yet manages to put up with the three weekly and two monthly journals delivered to our home, as well as numerous papers, books, phone calls, nights in the lab, trips to who-knows-where, group meetings, seminars ... and now so busy, loving and caring for our daughter, Jennifer. Thank you Nona. I hope this thesis has taught me as much about being a better husband as it has you about being a better wife.

I would like to thank the National Science Foundation for my financial support during my years as a graduate student. NSF has paid my stipend through the Energy Traineeship program as well as fund the laboratory and research expenses accrued during my stay at Caltech.

Finally, I would like to thank Kathy Lewis for typing most of my thesis and Sharon Vigario for typing several of my manuscripts. Both of these ladies are a pleasure to work with and are experts at their craft.

ABSTRACT

Part 1

Proton magnetic resonance data are presented for twenty different plasma-deposited amorphous silicon-hydrogen films. The two phase compositional inhomogeneity observed in these films is found to be independent of film thickness down to less than 1μ . Models for various structural configurations show that these films contain heavily monohydride clustered regions such as divacancies and voids, as well as $(\text{SiH}_2)_n$ and SiH_3 local bonding configurations. The presence of the divacancies in films showing predominantly monohydride vibrational modes provides some insight into the controversy over the assignment of the 2090 cm^{-1} vibrational mode. The films also contain regions in which monohydride groups are distributed at random. Based on changes in a film whose proton NMR lineshapes are metastable as deposited, a model based on strain relief is proposed for film development which explains the ubiquitous presence of the two phase inhomogeneity. Examination of the changes in proton NMR data as a function of deposition conditions furnishes new insight on the role SiH_2 and SiH_x^+ groups have in models for the gas phase reactions involved in the developing films. Finally, p- or n-type doping is found to increase the the hydrogen content of the films, and, under heavy p-type doping with diborane, boron clustering may occur within the films. Proton NMR lineshapes are also presented as a function of annealing temperature up to 650°C . The data indicate that hydrogen diffuses internally before major

evolution occurs, that transfer of hydrogen occurs from a heavily clustered phase to a dilute phase coincident with evolution and that evolution occurs initially from the heavily clustered phase. Internal hydrogen diffusion is found to be concomitant with the reduction in paramagnetic center density.

Silicon-29 and hydrogen magic angle sample spinning experiments on amorphous silicon-hydrogen films (involving cross-polarization and homonuclear multiple pulse techniques respectively) fail to yield quantitative determinations of local silicon-hydrogen bonding environments. However, the ^{29}Si data are qualitatively consistent with infra-red assignments of $(\text{SiH}_2)_n$ groups. Furthermore, the lack of significant line narrowing for the ^{29}Si spectra upon magic angle sample spinning shows that there are large chemical shift dispersions, indicative of the disorder in the amorphous lattice.

Proton spin-lattice relaxation data are presented for several plasma deposited amorphous silicon-hydrogen films when (i), homonuclear dipolar interactions are suppressed, (ii), deuterium is isotopically substituted for hydrogen, and (iii), films are annealed. These data are consistent with a model in which proton nuclei are relaxed by hydrogen-containing disorder modes. Analysis of these data shows that the density of disorder modes is $\sim 30\%$ higher in the low hydrogen density domain and that more than one hydrogen nucleus is associated with each disorder mode. The behavior of T_1 upon annealing indicates that a small fraction of unpaired spins or "dangling bonds" may be associated with the disorder modes. These results suggest that the role of hydrogen in amorphous silicon is more

complex than passivation of "dangling bond" intrinsic defects.

Finally, proton magnetic resonance data are presented for the hydrogen alloys of plasma-deposited amorphous boron, carbon, silicon carbide and silicon nitride. Linewidth and lineshape analysis leads to the conclusion that hydrogen nuclei are clustered in a-Si/C:H, a-C:H, and a-Si/N:H. Both a-Si/C:H and a-C:H data show hydrogen exists in two phases. Modeling of linewidths in a-Si/C:H indicates that the two phases are heavily hydrogenated carbon clusters imbedded in a weakly hydrogenated a-Si lattice. In addition, evidence is presented for the presence of motionally narrowed hydrogen spectra in a-Si/N:H, a-B:H, and a-C:H. It is suggested that the hydrogen nuclei giving rise to these spectra are associated with disorder modes.

Part 2

The production of heteronuclear dipolar modulated chemical shift spectra of specific protons within polycrystalline solids is described by consideration of explicit double resonance pulse schemes which remove both heteronuclear and homonuclear dipolar interactions. These spectra furnish an accurate method of determining bond distances in local environments of complicated chemical systems. When used in conjunction with selectively observed chemical shift spectra, these schemes present a means for characterization of both geometrical and electronic properties in the solid state. To demonstrate the utility of these experiments, selective proton observed NMR results are presented for the carbonyl protons of

adsorbed formic acid on ammonium-Y zeolite and the hydrogen bonded proton in polycrystalline acetanilide. Chemical shift information for the adsorbed formic acid shows a chemisorbed species consistent with formate ions. The data for the amide bond in polycrystalline acetanilide show a hydrogen bond with a chemical shift anisotropy of 17.7 ppm and a N-H distance of $1.05 \pm 0.01 \text{ \AA}$.

Table of Contents

	<u>Page</u>
Dedication	<i>ii</i>
Acknowledgments.	<i>iii</i>
Abstract	<i>vi</i>
Part 1: Magnetic Resonance Studies of Plasma-Deposited Inorganic Films	1
Chapter 1: Introduction.	1
Chapter 2: Film Microstructure as Determined by Proton Magnetic Resonance Lineshapes	15
A. Amorphous Silicon	15
B. Annealed Amorphous Silicon.	52
C. Amorphous Boron, Carbon, Silicon Nitride and Silicon Carbide	66
Chapter 3: Local Bonding Environments in Amorphous Silicon via Magic Angle Sample Spinning NMR	84
Chapter 4: Disorder Modes in Amorphous Silicon as Determined by Proton Spin Lattice Relaxation.	99
Part 2: Selective Proton Observed NMR in Solids	123
Chapter 5: Introduction: Selective Proton Observed NMR.	124
Chapter 6: Selective Proton Observed Heteronuclear Dipolar Modulated Chemical Shift Spectra in Solids.	130
Chapter 7: The Application of Selective Proton NMR to the Study of Surface Adsorbed Formic Acid and Polycrystalline Acetanilide	145
Propositions	159

PART 1: MAGNETIC RESONANCE STUDIES OF
PLASMA-DEPOSITED INORGANIC FILMS

Chapter 1
INTRODUCTION

One of the fundamental pursuits of chemistry is an understanding of the way in which structure affects reactivity. The structure of a molecule is reflective of its quantum mechanical wavefunctions and energy eigenvalues, which in turn may be used to understand bond-making and bond-breaking processes. In semiconductor physics, the same relationship between structure and energy eigenvalues exists; however, the goal of understanding this relationship is not the design of molecular reactions, rather, it is the design of semiconductor devices, the heart of the booming electronics industry.

The lack of understanding of the relationship between structure and the density of electronic energy eigenvalues is particularly acute in the field of amorphous semiconductors. In these materials, the absence of long-range order precludes the use of theories (1) intended to study crystalline systems. A brief examination of a recent model of the electronic states of amorphous semiconductors (2,3) (due to Mott, Davis, Cohen, Fritzsche and Ovshinsky) is useful in determining some of the important structural questions in amorphous semiconductors. Figure 1 (from Reference 2) shows that a single energy band within the solid may

SCHEMATIC DIAGRAM OF THE DENSITY OF STATES OF AN ISOLATED ENERGY BAND WITHIN A DISORDERED SOLID. THE SHADED REGIONS CORRESPOND TO LOCALIZED STATES.

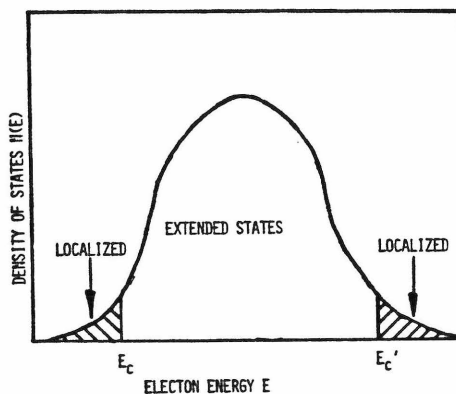
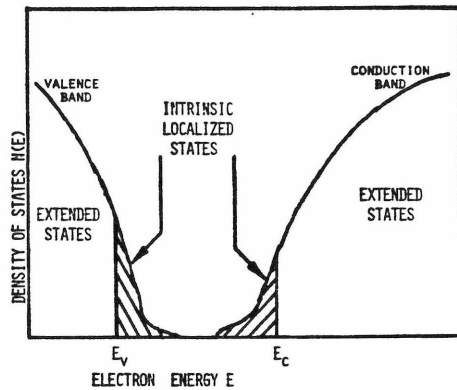


Figure 1

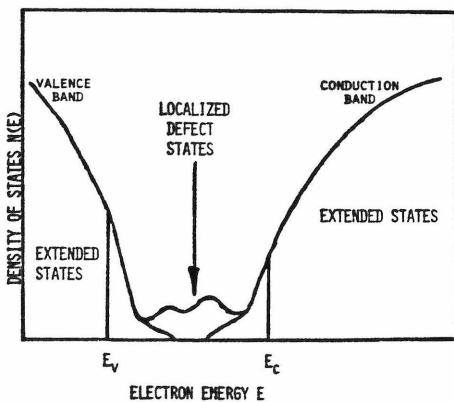
be composed of states which are localized in space and those which are not (extended). Figure 2 shows a band model of an ideal amorphous semi-



BAND MODEL DIAGRAM OF AN IDEAL AMORPHOUS SEMICONDUCTOR. NOTE THE NARROW ENERGY RANGES FOR THE INTRINSIC LOCALIZED STATES. THE VALENCE BAND STATES ARE LOCALIZED AT ENERGIES GREATER THAN E_v ; THE CONDUCTION BAND STATES ARE LOCALIZED AT ENERGIES LESS THAN E_c .

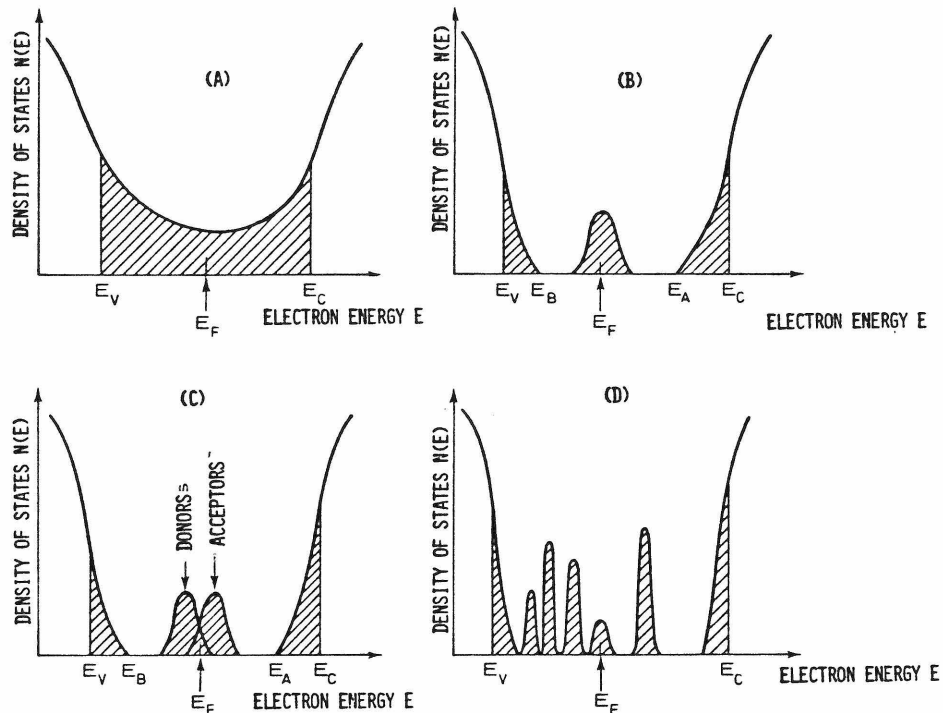
Figure 2

conductor with the localized states near the valence and conduction band edges, while the extended states are within the valence and conduction bands. Since amorphous semiconductors may be doped p- or n-type, there exists an analogy between defects and impurities in crystalline semiconductors (which result in discrete states in the energy gap) and amorphous semiconductors. This analogy is described in Figures 3 and 4 (from References 2 and 3, respectively). It is thus seen that localized



BAND MODEL DIAGRAM OF A REAL AMORPHOUS SEMICONDUCTOR WITH IMPURITIES AND DEFECTS GIVING RISE TO STATES WITHIN THE GAP.

Figure 3

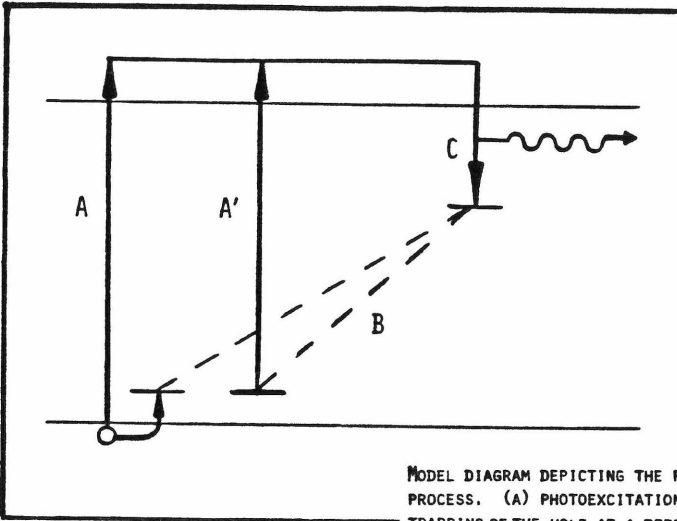


SCHEMATIC DIAGRAM SHOWING THE DEVELOPMENT OF BAND MODELS FOR THE DESCRIPTION OF AMORPHOUS SEMICONDUCTORS. (A) THE COHEN-FRITZSCHE-OVSHINSKY MODEL, (B) THE DAVIS-MOTT MODEL (WITH A BAND OF COMPENSATED LEVELS AT THE MIDDLE OF THE BAND GAP), (C) MODIFIED MOTT-DAVIS MODEL, AND (D), A MORE REALISTIC MODEL OF A REAL GLASS WITH DEFECT STATES.

Figure 4

states may exist in the band gap by design (i.e. doping) or as a result of defects. Since states in the band gap affect electronic and/or optical properties significantly, some important questions are: what are the structural features of the defects giving rise to states within the gap? What is the role of the short-range order in determining the shape of the intrinsic localized states?

The role defects play in optimizing the optical or electric properties of amorphous semiconductors is perhaps best visualized by considering luminescence experiments (3). Figure 5 (from Reference 3) shows a



MODEL DIAGRAM DEPICTING THE PHOTOGENERATION AND LUMINESCENCE PROCESS. (A) PHOTOEXCITATION ACROSS THE GAP FOLLOWED BY RAPID TRAPPING OF THE HOLE AT A DEFECT CENTER, (A') CORRESPONDS TO DIRECT EXCITATION OF THE DEFECT CENTER. (B) SHOWS THE RELAXATION OF THE DEFECT LEVEL TO A POINT HIGHER IN THE GAP. THE ELECTRON AND HOLE THEN RECOMBINE RADIATIVELY PRODUCING A LUMINESCENCE SPECTRUM AT ENERGIES LESS THAN THE ABSORPTION ENERGIES. THE SHIFT OF ENERGY BETWEEN ABSORBANCE AND LUMINESCENCE IS RELATED TO THE DISTORTION ENERGY OF THE DEFECT CENTER.

Figure 5

model (due to Street) for luminescence processes in amorphous semiconductors. Photoexcitation from the valence band or from a defect center produces an electron-hole pair, each of which is rapidly trapped at defect centers near the conduction or valence band edges, respectively. The defect center then distorts and moves its energy level to a new position (higher) in the gap. The electron and hole then recombine radiatively. The difference in energy between the absorption and luminescence energies is then related to the distortion energy of the defect site. Of course, not all defect sites are the same and there are some defects which allow for rapid nonradiative recombination of the electron and hole. The luminescence efficiency is then a measure of radiative versus nonradiative electron-hole recombination processes. It is worth noting that, in general, the longer the electron and hole

remain separated, the better the semiconductor is for device applications (2). This means, for instance, that higher luminescence efficiencies results in materials with excellent photoconductivities and photoreceptor properties. As a result, there is an important structural question relating to luminescence efficiency in amorphous semiconductors: what is the structure of defect sites responsible for nonradiative recombination of electron-hole pairs?

Since amorphous semiconductors are by definition highly disordered, the usual structural tools for studying crystalline materials fall short of describing structure in amorphous materials. The structural tools employed to date for the study of amorphous semiconductors are (i) X-ray, electron or neutral diffraction data, (ii) vibrational spectroscopy, (iii) EXAFS, and (iv) electron (scanning or transmission) microscopy. X-ray, electron or neutron diffraction data are most often employed and result in radial distribution functions (RDF) describing local coordination (4,5) of atoms. Extended X-ray absorption fine structure (EXAFS) has also been shown (3) to yield local coordination numbers for impurity atoms in amorphous semiconductors. Raman and infrared vibrational spectroscopy have been used extensively to study vibrational modes in amorphous materials (3,6). From a structural point of view, vibrational modes due to bond bending or bond stretching are most important as they also yield information on local bonding configurations. Electron microscopy is useful in determining microstructural features such as voids, columns, cracks, etc. to a resolution of tens of angstroms (7). All of these methods have been applied to the study of amorphous

semiconductors. The purpose of Part I of this thesis is to use nuclear magnetic resonance techniques to probe structural features of one amorphous semiconductor in particular: plasma-deposited silicon-hydrogen films. The structural information obtained is unique vis-à-vis other structural tools and provides information on both microstructure and defects responsible for nonradiative electron-hole recombination.

Amorphous silicon-hydrogen films were first investigated by Chittick *et al.* in 1969 (8). These films were produced by glow discharge decomposition of silane and were shown to be good photoconductors and receptive to both p- and n-type doping. A more definitive study by Spear and LeComber (9) in 1975 showed that p,n junctions could easily be synthesized. In 1976, Carlson and Wronski at RCA Laboratories synthesized the first a-Si:H solar cells (10). Since fabrication of a-Si:H cells is very inexpensive (a few dollars per square foot), there has been considerable motivation to study a-Si:H films and design deposition conditions to optimize optical and electronic properties.

The production of inorganic thin films by glow discharge has been described in the literature in a number of reviews (11-13). The apparatus used in these studies is shown in Figure 6. The walls of the chamber are stainless steel held at ground potential while rF is applied to one of the two electrodes. Because of the difference in mobilities of the ions and the electrons in the discharge, the rF applied electrode becomes cathodic with a large negative D.C. bias. Table I describes the range of deposition parameters used in production of many of the films reported herein.

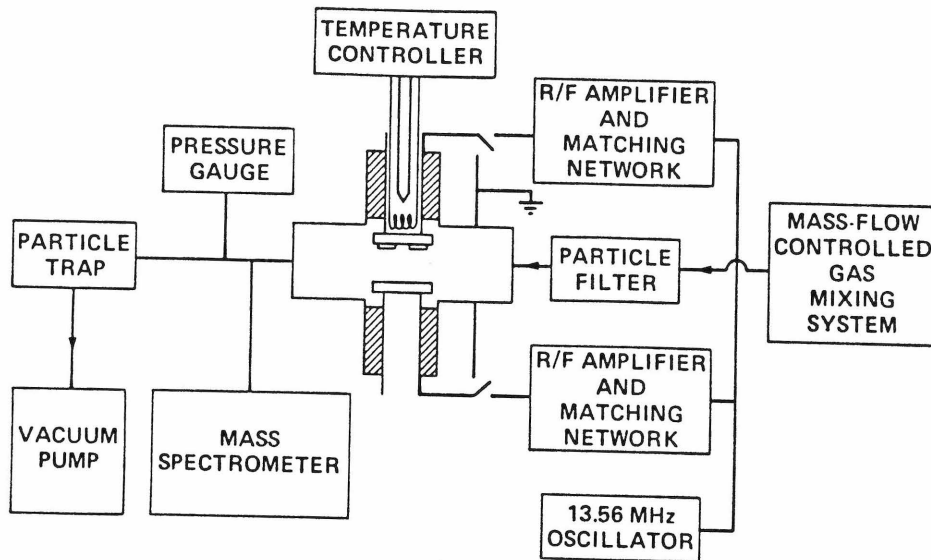


Fig. 1. Schematic of plasma-deposition system.

Figure 6

Table I. Deposition parameters.

Parameter	Range
Pressure	0.05–1.0 Torr
Flow (total)	50–200 sccm
Concentration (silane in argon)	0.1–100%
RF power	0.5–40 watts
Bias(-ve)	0–40 volts
Substrate temperature	–125–450°C

The range given here is that typically used during experiments at this laboratory with a particular system.

Table I

The remarkable electronic properties of hydrogenated amorphous silicon (a-Si:H) are apparently related to the presence of hydrogen within the films. In 1978, Pankove (14,15) showed that luminescence

efficiency decreased when hydrogen was removed by annealing. Furthermore, upon rehydrogenation by exposure to atomic hydrogen, the films recovered their original luminescence characteristics. Soon afterward, electron spin resonance studies (16 - 18) showed that the number of unpaired electron spins associated with broken Si-Si bonds (so-called dangling bonds) was decreased by several orders of magnitude upon hydrogenation. The ostensible role of hydrogen is then "passivation" of the dangling bond intrinsic defects. One then associates the dangling bonds with nonradiative recombination centers and the role of hydrogen in the electronic properties of a-Si:H is thus understood.

During 1978-80, the research group at Xerox (mainly Knights, Street, Biegelsen, Lucovsky and Nemanich) reported some pioneering studies (19 - 22) on correlations between electron spin resonance, luminescence efficiency, and vibrational spectroscopy measurements. Since the vibrational spectroscopy measurements detail the local bonding configurations of hydrogen on silicon [e.g. SiH, SiH₂, (SiH₂)_n], by correlating ESR/luminescence data with specific vibrational modes they discovered that *defect sites responsible for nonradiative recombination in a-Si:H are related to the way hydrogen is incorporated into the samples*. However, the details of the defect structure remain uncertain. The book is by no means closed on the role hydrogen plays in determining the electronic properties of a-Si:H.

The role hydrogen plays in crystalline devices is apparently no less important (29 - 34). Although details of device manufacturing are usually proprietary, it has become clear (29 - 32) that high temperature treatment of devices with hydrogen is necessary for them to work.

Hydrogen, in the form of SiOH and SiH groups, appears to be responsible for a large decrease in the number of surface charge states at Si/SiO₂ interfaces (29 - 32). Most recently, it has been shown (34) that diffusion of hydrogen into the Si/SiO₂ interface decreases the ambient electron spin resonance signal. It appears then that a study of the role hydrogen plays in a-Si:H defect structures may have important consequences for the design and manufacture of MOS devices.

The fact that deposition parameters can be adjusted to optimize the electronic properties of a-Si:H (3) implies that there is yet another frontier in the study of these films: how does the chemistry of the glow discharge affect the properties of the resultant film? How do films grow on substrates and does film growth affect the electronic properties as well? There have been several studies in the recent literature (35 - 41) on effects of gas phase chemistry on models for film growth yet none of these works is definitive. These works have been prompted by the desire to understand how defect structures responsible for electron-hole nonradiative recombination are formed, and hence, how they may be minimized.

Part I of this thesis may be divided into three sections. Chapter 2 discusses the structural consequences of the proton NMR lineshapes in a-Si:H (and to a lesser extent, a-C:H, a-Si/C:H, a-Si/N:H, and a-B:H). It is shown that these data reveal useful and unique structural information which, when taken as a function of deposition conditions, furnish insight into models for chemical reactions in the glow discharge as well as for film growth. In addition, studies on annealed a-Si:H films show how structure and hydrogen content changes with concomitant changes in

electron spin resonance and luminescence efficiency data. Chapter 3 details the efforts to determine quantitatively the different types of local bonding configurations via ^{29}Si and ^1H magic-angle sample spinning experiments. These experiments reveal information about the disorder in the amorphous silicon lattice. Finally, Chapter 4 reports the results of proton spin-lattice relaxation experiments in a-Si:H films and yields new evidence for the structure of the defect sites responsible for non-radiative recombination.

Each of the chapters that follow has been published or is currently being submitted for publication. Hence, the figures, references, experimental methods, introductions, and conclusions are local to each chapter.

References

1. C. Kittel, Introduction to Solid State Physics, (John Wiley and Sons, New York, 1971).
2. R. Dalven, Introduction to Applied Solid State Physics, (Plenum Press, New York, 1980).
3. M. Brodsky, Ed., Amorphous Semiconductors, (Plenum Press, New York, 1980).
4. A. C. Wright: in Advances in Structure Research by Diffraction Methods, Vol. 5, W. Hoppe, R. Mason, eds. (Pergamon Press, Oxford, 1974).
5. A. C. Wright, A. J. Leadbetter, Phys. Chem. Glasses 17, 122 (1976).
6. M. H. Brodsky, M. Cardona, J. Non-Crys. Solids 31, 81 (1978).
7. J. C. Knights, R. A. Lujan, Appl. Phys. Lett. 35, 244 (1978).
8. R. C. Chittick, J. H. Alexander, H. F. Sterling, J. Elec. Soc. Solid State 116, 77 (1969).
9. W. E. Spear, P. G. LeComber, Solid State Commun. 17, 1193 (1975).
10. D. E. Carlson, C. R. Wronski, Appl. Phys. Lett. 11, 671 (1976).
11. A. R. Reinberg, Ann. Rev. Mater. Sci. 9, 341 (1979).
12. M. H. Brodsky, Thin Solid Films 50, 57 (1978).
13. J. C. Knights, Jap. J. Appl. Phys. 18, 101 (1979).
14. J. I. Pankove, M. A. Lampert, M. L. Tarng, Appl. Phys. Lett. 32, 439 (1978).
15. J. I. Pankove, Appl. Phys. Lett. 32, 812 (1978).
16. R. S. Title, M. H. Brodsky, J. J. Cuomo, in Proceedings of the Seventh International Conferences on Amorphous and Liquid

- Semiconductors, ed. W. E. Spear (University of Edinburgh, Edinburgh, 1977), p. 424.
17. P. A. Thomas, M. H. Brodsky, D. Kaplan, D. Lepine, Phys. Rev. B 18, 3059 (1978).
 18. D. K. Biegelsen, R. A. Street, C. C. Tsai, J. C. Knights, Phys. Rev. B 20, 4839 (1979).
 19. R. A. Street, J. C. Knights, D. K. Biegelsen, Phys. Rev. B 18, 1880 (1978).
 20. C. Tsang, R. A. Street, Phys. Rev. B 19, 3027 (1980).
 21. J. C. Knights, G. Lucovsky, R. J. Nemanich, J. Non-Crys. Solids 32, 393 (1979).
 22. R. Street, D. Biegelsen, J. Stuke, Phil. Mag. B 40, 451 (1979).
 23. M. H. Brodsky, M. Cardona, J. J. Cuomo, Phys. Rev. B 16, 3556 (1977).
 24. J. C. Knights, G. Lucovsky, R. J. Nemanich, Phil. Mag. B 37, 467 (1978).
 25. M. H. Brodsky, M. Cardona, J. Non-Crys. Solids 31, 81 (1978).
 26. G. Lucovsky, R. J. Nemanich, J. C. Knights, Phys. Rev. B 19, 2064 (1979).
 27. H. Shanks, C. J. Fang, L. Ley, M. Cardona, F. J. Demand, S. Kalbitzer, Phys. Stat. Sol. B 100, 43 (1980).
 28. W. Paul, Solid State Commun. 34, 283 (1980).
 29. E. Kooi, Philips Res. Rep. 21, 477 (1966).
 30. K. H. Beckman, N. J. Harrick, J. Electrochem. Soc. Solid State Science 118, 614 (1971).
 31. B. E. Deal, J. Electrochem. Soc. Reviews and News 121, 198C (1974).

32. A. G. Revez, J. Electrochem. Soc. Solid State Science 124, 1811 (1977).
33. W. R. Knolle, H. R. Maxwell, Jr., R. E. Benerson, J. Appl. Phys. 51, 4385 (1980).
34. D. Biegelsen, N. Johnson, Moier in Physics of MOS Insulators, (Pergamon Press, New York, 1980, in press).
35. J. C. Knights. J. Non-Crys. Solids 35/36, 159 (1980).
36. P. Kocian, *ibid.*, 35/36, 195 (1980).
37. A. Matsuda, K. Nakagawa, K. Tanaka, M. Matsumura, S. Yamasaki, H. Okushi, S. Iizima, *ibid*, 35/36, 183 (1980).
38. G. Turban, Y. Catherine, B. Grolleau, Thin Solid Films, 67, 309 (1980).
39. B. A. Scott, M. H. Brodsky, D. C. Green, P. B. Kirby, R. M. Plecenik, E. E. Simonyi, Appl. Phys. Lett. 37, 725 (1980).
40. J. C. Knights, R. A. Lujan, M. P. Rosenblum, R. A. Street, D. K. Biegelsen, J. A. Reimber, Appl. Phys. Lett. (submitted).
41. G. Turban, Y. Catherine, B. Grolleau, Thin Solid Films (submitted).

Chapter 2

FILM MICROSTRUCTURE AS DETERMINED BY
PROTON MAGNETIC RESONANCE LINESHAPES

A: Amorphous Silicon

(This section is essentially two articles by J. A. Reimer, R. W. Vaughan and J. C. Knights. They are: (i) "Proton Magnetic Resonance Spectra of Plasma-Deposited Amorphous Si:H Films", Physical Review Letters 44, 193 (1980); and (ii) "Proton Nuclear Magnetic Resonance Studies of Microstructure in Plasma-Deposited Amorphous Silicon-Hydrogen Films", which has been submitted to Physical Review B.)

Abstract

Proton magnetic resonance data are presented for twenty different plasma-deposited amorphous silicon-hydrogen films. The two phase compositional inhomogeneity observed in these films is found to be independent of film thickness down to less than 1μ . Models for various structural configurations show that these films contain heavily monohydride clustered regions such as divacancies and voids, as well as $(\text{SiH}_2)_n$ and SiH_3 local bonding configurations. The presence of the divacancies in films showing predominantly monohydride vibrational modes provides some insight into the controversy over the assignment of the 2090 cm^{-1} vibrational mode. The films also contain regions in which monohydride groups are distributed at random. Based on changes in a film whose proton NMR lineshapes are metastable as deposited, a model based on strain relief is proposed for film development which explains the ubiquitous presence of the two phase inhomogeneity. Examination of the changes in proton NMR data as a function of deposition conditions furnishes new insight on the role SiH_2 and SiH_x^+ groups have in models for the gas phase reactions involved in the developing films. Finally, p- or n-type doping is found to increase the hydrogen content of the films, and, under heavy p-type doping with diborane, boron clustering may occur within the films.

1. INTRODUCTION

Considerable attention has been focused recently on hydrogenated amorphous silicon (a-Si:H) films (1a) because of their electronic properties (16) and application to p,n and Schottky barrier junctions (2-4), photovoltaic energy conversion devices (5), and xerographic photoreceptors (13,14). There have been several studies on the role film microstructure plays in determining the electronic properties of the films. In particular, scanning and transmission electron microscopy (6) has shown a strong correlation between columnar morphology and the presence of nonradiative recombination centers which limit luminescence efficiency. Small angle X-ray and neutron scattering results have shown (7,8) that strong isotropic low angle scattering exists in samples that show no microstructure via TEM or SEM. Vibrational spectroscopy measurements (15,16) have led to the conclusion (16) that growth of columnar microstructure is paralleled by an increase in $(\text{SiH}_2)_n$ "poly-silane" oscillator strengths.

More recently, proton nuclear magnetic resonance (NMR) data have posed some new questions on the role of hydrogen in structural properties of a-Si:H films. Linewidth and lineshape data have shown (10) direct evidence for two-phase compositional inhomogeneity. The two domains differ in the density of hydrogen, however, in both domains the hydrogen nuclei are clustered. Modeling of proton distributions led to the conclusion that the high hydrogen density domain could be due to

local clustering on silicon atoms [e.g. $(\text{SiH}_2)_n$ "polysilane" regions] or monohydride clustering on internal surfaces. Monohydride clustering was confirmed by further proton NMR studies (11) of annealed a-Si:H films. In those studies we showed that upon annealing hydrogen in the less clustered domain (predominantly monohydride) diffuses internally (prior to evolution) concomitant with the reduction in paramagnetic center density (12). Further combined NMR and infrared studies on the effects of inert gas dilution on film formation and growth (17) have shown that high deposition rates achieved with He and Ne diluent gases are associated with high levels of hydrogen incorporation in the form of heavily clustered monohydride configurations. Thus, inhomogeneous microstructure occurs not only when $(\text{SiH}_2)_n$ is present but when clustered SiH are present as well.

The purpose of this work is to propose structural models for the proton NMR lineshapes and examine the microstructural implications of changing deposition parameters. Specifically, we wish to show: (i) saturation experiments which confirm that the two proton dipolar reservoirs are indeed isolated; (ii) that the two component behavior is independent of film thickness (down to 1 μ); (iii) that the two components may be modeled by local bonding configurations and a random distribution of protons; (iv) that divacancies are a common microstructural feature (which may be responsible, in part, for the 2090 cm^{-1} vibrational mode); (v) that the spatial isolation of the two proton domain may be understood in terms of strain in the film during deposition; (vi) that gas phase chemistry in the discharge influences the microstructural properties of the films; and finally (vii) that p- or

n-type doping increases the hydrogen content of the films and heavy p-type doping with diborane may lead to boron-clustering within the films.

2. EXPERIMENTAL

Proton magnetic resonance data were taken with an NMR spectrometer described previously (18). The spectra were obtained by Fourier transformation of the free induction decay (FID) of the magnetization following a preparatory pulse. This usually is a simple 90° pulse, although in the saturation experiments a weak "tickling" field was applied prior to the 90° pulse. The 90° pulse lengths were always less than 2 μ seconds. In all experiments, the FID's were signal averaged prior to Fourier transformation with 500 acquisitions typically accumulated. Full spin-lattice relaxation was allowed between acquisitions in order to obtain accurate counts of proton spins. The hydrogen content of the films was determined from proton spin counts and sample weight. Spin-lattice relaxation times were measured by the inversion-recovery method (19). All spectra were least-squares fitted to the sum of a Gaussian component (broad line) and a Lorentzian component (narrow line). The resulting fits were excellent and, based on values of χ^2 resulting from a variety of initial starting parameters, the errors are ± 1 kHz in the FWHM (full width at half maximum) of the broad component (± 0.3 kHz narrow component) and ± 0.3 atom percent in the distribution between broad and narrow components.

The samples were prepared in an rF-diode deposition described elsewhere (20). The samples were deposited onto ~ 2 -inch diameter

aluminum foil substrates in thicknesses of ~ 0.1 to 100μ resulting in sample masses in the range $\sim 0.5 - 100$ mg after removal of the substrates with a dilute hydrochloric acid etch. Tables 1, 2 and 3 detail (i) the deposition conditions for a variety of samples, (ii) the hydrogen content, distribution and linewidths from the FID spectra, and (iii) the spin-lattice relaxation times.

3. RESULTS

A. Saturation Experiments

Figure 1 details the "hole-burning" experiment designed to test the hypothesis that the broad and narrow components of the observed FID spectra are due to spatially-isolated dipolar reservoirs. A weak pulse of magnitude $\omega_1^{\text{sat}} \sim 1$ kHz is applied to the sample at frequency ω_{sat} such that $\omega_{\text{sat}} - \omega_0 \gg \text{FWHM}_{\text{narrow}}$ where ω_0 is the center of the narrow component lineshape and $\text{FWHM}_{\text{narrow}}$ is the full width at half-maximum of the narrow component. The effect of this pulse is to saturate those components of the lineshape that are in rapid spin-spin communication with those components at ω_{sat} . This saturation pulse is then followed by a short, intense 90° pulse which places the remaining thermally induced magnetization into the x,y plane to be detected by the spectrometer. This is shown schematically in part (A) of Figure 1. If one compares this experiment to a standard 90° pulse/FID measurement [part (B) of Figure 1] by taking the difference between the standard experiment and the hole-burning experiment, one obtains only the lineshape that was saturated by the hole-burning process. The bottom of Figure 1

shows the results of this experiment for two a-Si:H samples. The figure shows both the FID spectra and the results of the difference experiment. The difference spectra are superimposed on a Gaussian line whose width is given by a best fit to the broad component of the FID spectra. These results show clearly that the broad component of the FID spectra has little spin-spin communication with the narrow component.

B. Effects of Film Thickness

A series of samples was prepared by the conditions of sample L (Table 1), but the total deposition time, hence film thickness, was allowed to vary. The proton FID spectra were obtained for the range 0.1 μ to 10 μ in order to determine if proton NMR parameters varied with film thickness. Figure 2 shows the hydrogen content as a function of film thickness over this range as well as the content in the broad and narrow components over the range 1 - 10 μ . The 0.1 μ sample FID spectrum, while exhibiting two-component behavior, was not deconvolved because of poor signal-to-noise. Figure 2 shows the hydrogen content and distribution to be roughly constant over the 0.1 - 10 μ range of film thicknesses.

C. Effects of Various Deposition Parameters

Tables 1 and 2 show the proton NMR parameters for 15 samples which differ in their deposition parameters. While these data do not represent a systematic survey of the full range of parameters, several trends are worth noting.

- (i) In all samples, the hydrogen content in the narrow component is 2 - 5 atom% (mean, 3.5; standard deviation, 0.8) with linewidth of 1 - 5 kilohertz (mean, 3.2; standard deviation, 1.0).
- (ii) The effect of the diluent gas, notably argon vs. helium, may be realized by comparing samples F and DD and samples G and L. These data show the samples deposited in helium have an increased clustering in the narrow component and a higher total hydrogen content. Note in cathode samples the effects of Ar vs. He are negligible.
- (iii) The effect of rF power may be realized by comparing samples G and F, A and H, and I and C. For anode samples deposited at high temperatures, the effect of rF power appears to be negligible. For anode samples deposited at room temperature, decreasing rF power causes less clustering in the narrow component and a shorter T_1 . For cathode samples, decreasing rF power results in increased clustering of protons in the narrow component and longer T_1 's.
- (iv) The effects of a diluent gas (Ar or He) vis-à-vis deposition from pure silane may be realized by comparing samples AA, F and DD, and samples KK, G and L. The total hydrogen content appears to increase with addition of the diluent gas. In low rF power samples (AA, F and DD), the increase in hydrogen content is in the broad component.
- (v) The effect of substrate temperature on NMR parameters may be realized by comparing samples A and G, and samples N and

D. Increasing temperature results in a lower hydrogen content, predominantly reflected in the broad component.

D. Effect of Doping with P or B

Table 3 details the deposition conditions for several samples where dopant gases, diborane or phosphane, were introduced into the deposition system. The effects of doping on the proton NMR parameters may be summarized as follows:

- (i) In 100% SiH_4 anode samples deposited at 230°C (compare samples CC and BB from Table 3 with sample AA from Table 1), the hydrogen content increases when either PH_3 or B_2H_6 is introduced. The phosphorus-doped sample has a shorter T_1 than both the undoped and boron-doped sample.
- (ii) In 5% SiH_4 in helium samples (anode) deposited at 230°C (compare sample W from Table 3 with sample L from Table 1), introduction of diborane reduced the T_1 .

The proton FID spectrum of this doped sample (W) is complicated by an additional broad component (~ 50 kHz FWHM) and narrow component (800 hertz FWHM). The narrow component is temperature dependent (Figure 3) such that reducing the temperature broadens the narrow component to the point where it appears to lack any contribution to the observed spectrum. The total hydrogen content in the additional broad and narrow component, however, is less than ~ 2 atom%.

E. Effects of Time on a High Defect Density Sample

A high defect density sample ($>10^{19}$ spins/cm³) was prepared by depositing from 5% SiH₄/Ar at 25°C with an rF power of 18 watts. Figure 4 compares the proton FID spectra of the sample freshly deposited (A) with the same sample allowed to stand in dry air for approximately six months. As deposited, the NMR spectra yields the hydrogen content to be 23.8% with 18.1% broad (25.8 khz FWHM), 5.0% narrow (1.65 khz FWHM), and ~1.5% very narrow (~1 khz FWHM). The proton spectrum of the "aged" sample yields 29.5 atom% H with 20.9% broad (26.8 hkHz FWHM) and 3.7% narrow (2.8 khz FWHM).

4. DISCUSSION

A. Structural Models for a-Si:H

Having established that the proton NMR lineshapes are dipolar-broadened (10), and that the two components are indeed spatially isolated (Figure 1), we may consider specific structural features which may give rise to these observed lineshapes. It is well known that the second moment (M_2) of a dipolar-broadened spectrum in an amorphous material is given by (21)

$$M_2 = \frac{3}{5} \gamma^4 n^2 I(I+1) \sum_{j,k} \frac{1}{r_{kj}^6} \quad (1)$$

where γ is the proton gyromagnetic ratio, I the value of the nuclear spin ($\frac{1}{2}$ for protons), and $\sum_k \frac{1}{r_{jk}^6}$ represents a lattice sum of distances

to other proton nuclei. Following our earlier work (10), we shall apply

Equation (1) to two types of models. The first, using Equation (1) directly, models local bonding configurations of hydrogen on silicon. The second model is a calculation of the second moment of a known number of spins dispersed on a simple cubic lattice.

Table 4 shows the results of applying Equation (1) to various local bonding configurations. Given the sensitivity of the calculations to slight changes in interatomic distances, we make only general comments. The hydrogenated monovacancy yields a linewidth much larger than those observed, hence we conclude that there few, if any, of these defects present. This is consistent with the knowledge that monovacancies in crystalline silicon are not stable (22). All of the other configurations may give rise to the broad component and their presence would be given by the deposition conditions. Of particular interest is the persistence of the broad component in samples which show no microstructure by small angle X-ray and neutron scattering experiments (7) (note samples D, AA, DD, CC, BB and ZZ in Tables 1 and 3). In addition, these samples show predominantly monohydride signatures in their vibrational spectra. Table 4 shows that the hydrogenated divacancy may yield the broad component and would probably be too small to be detected as a void by the scattering experiments [although small isotropic scattering persists in many samples (25)]. The assignment of the broad component in the NMR spectrum to these divacancies scattered throughout the film may yield a natural explanation to the current controversy over the assignment of the 2090 cm^{-1} vibrational mode (23,24). This mode has been assigned previously (15,16) to $-\text{SiH}_2$ groups though two recent studies (23,24) of

sputtered films give strong evidence for an as yet unidentified species (although a hydrogenated void has been postulated). We suggest that indeed the hydrogenated divacancy may be responsible for this 2090 cm^{-1} mode, and that it is contributing to the broad component in the observed NMR spectra. In samples such as AA (Table 1), where only monohydride vibrational spectra are observed, the 4.2 atom% hydrogen in the broad component would correspond to a "divacancy density" of approximately $3 \times 10^{20}/\text{cc}$, or an average separation between divacancies of about 15 \AA (assuming the density of a-Si:H is 2 grams/cc). Note that once the deposition conditions are changed so that SiH_x ($x > 1$) vibrational species are observed and/or larger scale microstructure appears, a variety of configurations may give rise to the broad component.

To model the protons in the narrow component, we consider the modification of Equation (1) to the configuration of a simple cubic lattice (21):

$$M_2 = 5.1 \gamma^4 \hbar^2 I(I + 1) \frac{1}{d^6} , \quad (2)$$

where d is the lattice constant (and nearest neighbor distance). We then take the known hydrogen content in the narrow component and disperse it homogeneously throughout the fraction of the film not occupied by the broad component (plus some buffer region to assure spatial isolation of the two dipolar reservoirs). The inverse cube root of the resulting spin density yields a value for d which, when inserted into Equation (2), yields a value for M_2 which may be compared with experiment. Figure 5 shows the experimentally observed narrow component linewidth (mean and standard deviation of the samples shown in Tables

1 - 3) and the predicted linewidth for a homogeneous distribution of the known hydrogen content in the narrow component (mean and standard deviation in Tables 1 - 3), assuming 25% of the a-Si lattice is excluded due to the broad component protons and buffer region. The discrepancy between the model linewidths and the observed linewidths shown in Figure 5 has led previously (10) to the conclusion that the narrow component is predominantly clustered monohydride.

Since this narrow component has nearly the same hydrogen content ($3.5 \pm 0.8\%$) and linewidth (3.2 ± 1 kHz) in all films, including those which show only monohydride vibrational spectra, we concur that the narrow component is due only to monohydride species. However, the observed broadening may be explained by considering a *random* distribution of proton spins rather than a *homogeneous* (cubic lattice) distribution. We modify the lattice sum in Equation (1) with a probability distribution $P(r)$

$$M_2 = A \int_{r_i}^{r_f} \frac{1}{r^6} P(r) dr \quad (3)$$

where A is the usual collection of fundamental constants, and r_i and r_f minimum and maximum distances considered. We assume a Gaussian distribution,

$$P(r) = e^{-\frac{(r - r_0)^2}{2\Delta^2}} \quad (4)$$

of distances about the r_0 determined from the inverse cube root of the spin density. Inspection of Figure (5) and numerical solution of Equation (3) shows that when $r_0 = 7.7 \text{ \AA}$ and $\Delta = 1.7 \text{ \AA}$, we get an

excellent match of the observed linewidth with the random distribution model. Therefore, we conclude that the narrow component is due to monohydride groups distributed at random in the a-Si lattice.

An important structural question is the dimensions of the buffer region between the high and low hydrogen density domains (broad and narrow linewidths, respectively). A minimum distance would be given by the average separation between protons in the narrow component since the broad component protons have a T_2 roughly eight times shorter than the narrow component protons. This places minimum of 5 - 6 Å on the dimensions of the buffer zone between the high density hydrogen region and low density region. In the sample AA (Table 1), we estimated previously a divacancy density of $3 \times 10^{20}/\text{cc}$, and assuming a 5 - 6 Å buffer region, we calculate that 5 - 30% of the a-Si lattice is taken up by high hydrogen density and buffer zone regions, in reasonable agreement with the modeling shown in Figure 5.

The identification of the broad component with structural inhomogeneities (voids, divacancies, $(\text{SiH}_2)_n$ regions, etc.) and the narrow component with interstitial monohydride groups provides a natural explanation as to why the disorder mode density, responsible for proton spin-lattice relaxation (26a), is higher for the narrow component protons than the broad component protons (26b). The narrow component protons "feel" the fluctuating fields due to a three-dimensional distribution of disorder modes whereas protons situated on a void see a lower dimensionality distribution of disorder modes. Hence, the narrow component protons would be expected to relax faster [under conditions of homonuclear dipolar interaction suppression (26b)] than the broad component

protons.

The observation of this two-phase compositional homogeneity presents another interesting question: Is the structure of these films determined by surface/bulk processes during deposition or by gas phase reactions. We shall argue that, in fact, both factors influence film microstructure. However, the persistence of the two-phase structure as seen by NMR, regardless of the deposition conditions, would imply a bulk or surface rearrangement of the film during growth. To test this hypothesis, we prepared a high unpaired spin density ($>10^{19} \text{ cm}^{-3}$), high hydrogen content a-Si:H sample and recorded the NMR spectrum just after deposition and then recorded the spectrum six months later. As Figure 4 illustrates, the hydrogen content and distribution appears to undergo rearrangement. It has been shown previously (26b) by NMR relaxation data that the hydrogen content of this sample, as determined by NMR lineshapes, is artificially low ($\sim 8 \text{ atom\%}$) because of large dipolar broadening of the hydrogen spins by the abundant electron spins. Nonetheless, we propose that the "stabilization" process shown in Figure 3 may serve as a model for what may happen during film growth, namely, hydrogenation of dangling and strained bond interfaces by diffusion of hydrogen from other regions in the lattice. We then picture areas of high strain during film growth as "sweeping" the hydrogen out of the immediately surrounding lattice and forming a hydrogenated void, thereby stabilizing the lattice and spatially isolating the hydrogen in the void from that in the bulk. It is worth noting that during growth of films in which there are $(\text{SiH}_2)_n$ polymer phases, the same process may occur with the polymer phase playing

the same role as the hydrogenated void: a mechanism by which the strain in the continuous random network is relieved. Finally, we should comment on the role oxygen may play in the stabilization process shown in Figure 4. Studies on sputtered a-Si:H films have shown that oxygenated films have remarkably different photoconductivity, photoluminescence, and optical absorption properties (27). However, a recent study (28) of plasma-deposited films has shown that changes in optical absorption and luminescence data occur monotonically with addition of oxygen. Furthermore, in samples in which there was up to 0.1% oxygen in the silane during deposition, there was observed to be no change in ESR data. Hence, we conclude that some oxygen may have been incorporated in the film shown in Figure 3 over time, but is not responsible for the observed changes in hydrogen distribution.

B. Effects of Film Thickness

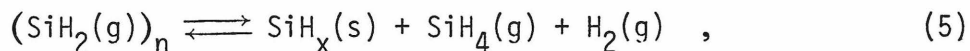
Figure 2 shows that the microstructure and hydrogen content of a-Si:H films are roughly constant at least to the 1 μ level. There have been several recent studies (29 - 33) on the effects of film thickness on optical properties (31 - 33) and hydrogen content (29,30). Nuclear reaction techniques (29) have shown that the hydrogen content decreases within 0.1 μ of an interface for some samples (30), and increases for others (29). Unfortunately, the data reported herein have insufficient signal-to-noise ratios to study this phenomenon. However, the use of superconducting solenoids and/or lower temperatures would allow proton NMR studies of samples with $\sim 1 \times 10^{17}$ proton spins, or about 100 - 1000 \AA

films prepared with our deposition apparatus.

C. The Influence of Deposition Conditions on NMR Parameters

While all the samples reported herein have two-component proton NMR spectra, there are considerable variations between the samples as to the atom% hydrogen, particularly the atom% hydrogen contained within the broad component. We wish to point out the trends in these proton data (vide supra) may be understood in terms of some gas phase reactions and models for film growth.

There have been several papers published recently which propose models for film growth and gas phase chemistry (34 - 40). These papers include structural studies of the films (34), films prepared from higher silanes (38), mass spectroscopy of the glow discharge (37,40), optical absorption studies of the glow discharge (35,36), and effects of inert gas dilution of the silane (39). The consensus of these works concludes that film growth may be written as



where the role of ionic species is somewhat clouded. A recent model (39), used to explain the differences between films deposited in Ar or Kr versus He or Ne, proposed that ions "scour" the surface of the growing film and thus remove segments of $(\text{SiH}_2)_n$ chains formed on the surface. We wish to propose that Equation (5) and the "scouring theory" are sufficient to explain the trends (ii) - (v) discussed in the Results section.

Consider the data for films AA, F and DD (Table 1) which compare the effects of deposition from pure silane, 5% silane in Ar, and 5% silane in He. The deposition rates for these films are in the order $100\% \text{SiH}_4 < 5\% \text{SiH}_4/\text{Ar} < 5\% \text{SiH}_4/\text{He}$. Inspection of Equation (5) shows that more $\text{SiH}_2(\text{g})$ or less $\text{H}_2(\text{g})$ will provide for faster growth of the film. Mass spectroscopic studies (37,40) have shown the concentration of $\text{H}_2(\text{g})$ to be higher in the pure SiH_4 deposition than deposition from Ar, consistent with Equation (5) and the deposition rates. The observed increase in hydrogen content in the films over this same trend may be the result of trapping of hydrogen in the growing film, i.e. faster film growth implies more H is trapped in the growing film. This faster growth implies a more strained a-Si lattice which in turn is relaxed by the formation of divacancies or other microstructural features. Accordingly, faster deposition rates would imply an increase in the broad component in the NMR spectra, consistent with the observed data. Whether or not the broad component corresponds to divacancies or to $(\text{SiH}_2)_n$ regions, voids, cracks, etc., depends on the availability of ions (SiH_x^\oplus) to "scour" the surface. As discussed previously (39), deposition in He or pure SiH_4 results in higher ion densities (more scouring) than deposition in Ar because Ar has a metastable energy less than the ionization potentials of SiH_x , ($x = 1,3$) and thus absorbs most of the plasma electron energy. Hence, films deposited in He and pure SiH_4 have only monohydride signature in their vibrational spectra and finer scale inhomogeneities as seen by electron microscopy (broad component = divacancies).

The dependence of the films deposited from 100% SiH₄, 5% SiH₄/Ar, 5% SiH₄/He on rF power is worth considering in light of these models for film growth. Samples KK, G and L represent the same deposition conditions as AA, F and DD except the rF power has been increased from 1 watt to 18 watts. The samples deposited from 5% SiH₄ in He or Ar show little changes in their NMR spectra yet the sample deposited from pure SiH₄ shows an increase in the broad component, the deposition rate and structural morphology (34). We propose that the availability of (SiH₂)_(g) is increased with increasing rF power in pure SiH₄ deposition whereas this effect is mediated in the inert gas mixtures as the metastables of the inert gas atoms are responsible for absorption of most of the plasma energy.

The scouring of the developing film surface by ions should be affected by magnetic or electric fields and temperature. An increase in substrate temperature would presumably result in increased mobility of (SiH₂)_n groups on the surface and hence allow for more effective scouring. Furthermore, increasing the substrate temperature would shift Equation (5) to the left, slowing film growth. Hence, we expect higher substrate temperatures to decrease the total hydrogen content and minimize large scale microstructure and (SiH₂)_n formation. This is consistent with these proton NMR data as well as microstructural studies (7, 8, 34) [compare samples N with D, as well as A with G (Table 1)]. Samples deposited on cathode substrates have a large negative D.C. bias which would prevent scouring of the developing film surface with ions. These NMR data are consistent with this concept as the effects of Ar vs. He diluent gas on NMR parameters is negligible on cathode substrates

(samples B and S in Table 2). In the recent literature there have also been reports on the effects of electric and magnetic fields on a-Si:H deposition (41 - 43).

D. The Effects of Doping on the Observed NMR Parameters

A recent study (32) of the hydrogen content of phosphorus (n-type) and boron (p-type) doped a-Si:H films via nuclear reaction techniques has shown that the hydrogen content varies linearly with the Fermi level position. Their reported values of the hydrogen content range from ~ 4 atom% for highly n-type films to ~ 10 atom% for highly p-type materials (intrinsic values of ~ 7.5 atom%). Inspection of our data for samples CC, BB (Table 3), and AA (Table 1) may be compared to this study since the deposition conditions are roughly comparable. Our data show both the n-type and p-type material to increase in hydrogen content relative to the intrinsic material with the largest increase observed for phosphorus (n-type) doping. The reason for the discrepancy between our data and the Dundee group nuclear reaction results is unclear, perhaps being due to differences in the deposition apparatuses. It is worth noting, however, that both B_2H_6 and PH_3 are expected to absorb electron energies less than 11 eV (44) from the plasma and may influence the ion concentrations, deposition rates, and hydrogen content in a similar fashion as Ar and Kr diluent gases. The data from Table 3 are consistent with the Ar diluent gas effects.

Figure 3 shows that when deposited in helium, high p-type doping results in a motionally narrowed component in the proton NMR spectrum.

An analysis of the FID prior to Fourier transformation shows a small broad component (~ 50 kHz) in the spectra as well. We attribute these proton spectra to protons experiencing an amorphous-boron type environment. Previous proton NMR studies (45) have shown that a-BiH films deposited from B_2H_6 in helium yield two-component spectra where one component is motionally narrowed and the broad component is further broadened beyond that expected from H-H dipolar interactions by heteronuclear ($^{10}B/^{11}B$) dipolar interactions. We conclude that some boron clustering is present under 5% $SiH_4/1\%$ B_2H_6/He deposition conditions. This implies that boron preferentially bonds to other boron neighbors during film growth at high boron doping levels.

5. SUMMARY AND CONCLUSIONS

In summary, we have presented proton NMR spectra for a-Si:H films under a variety of deposition conditions. The two-component lineshapes observed in all spectra are modeled in terms of local bonding configurations, and both homogeneous and random distributions of protons. The heavily clustered phase (broad component) corresponds to those protons associated with microstructure such as voids, hydrogenated surfaces and polysilane regions. In films which show predominantly monohydride vibrational spectra, divacancies may give rise to the broad component with a minimal number of monovacancies. The protons in the divacancies may be responsible for at least part of the 2090 cm^{-1} vibrational modes observed in the literature. The lightly clustered phase (narrow component) is predominantly composed of monohydride groups that are distributed randomly

throughout the film. The spatial separation of the broad and narrow component protons may arise from regions of high strain during film growth "sweeping" hydrogen nuclei out of the neighboring a-Si lattice and forming hydrogenated voids which in turn relieve local strain. We have shown that this is the case in at least one sample which, as deposited, was "metastable" and microstructural changes, via the NMR lineshapes, were found to occur with time. The two domain proton inhomogeneity was found to be independent of film thickness down to 1 μ . Furthermore, changes in the details of the NMR lineshapes as a function of deposition conditions have been described in terms of film formation from SiH_2 gas phase species and film scouring due to the presence of SiH_x^\oplus ions. Finally, we have shown that doping of the films, either p-type or n-type, results in an increase in the total hydrogen content of the films, and when high boron levels are present in the gas phase, boron clustering occurs within the films.

We conclude that proton NMR lineshapes are useful probes of the hydrogen distribution in a-Si:H films. More experiments are required to better understand the relationship between gas phase chemistry and film properties as well as the relationship between NMR parameters and optical properties. Such understandings may lead to the design of cheap, efficient photovoltaic and xerographic devices.

6. ACKNOWLEDGMENTS

The authors wish to thank R. A. Lujan for his expert assistance with sample preparations, and Drs. S. I. Chan and T. M. Duncan for their help

in preparing this manuscript. Also, we thank James Gleeson, Dave Biegelsen, Jim Boyce and Bob Nemanich for helpful discussions. This work was supported by the National Science Foundation under Grant # DMR-77-21394.

References

1. (a) M. H. Brodsky, Ed., Topics in Applied Physics 36 (Springer-Verlag, Berlin, 1979).
(b) D. E. Carlson, C. R. Wronski, J. I. Pankove, P. J. Zanzucchi and D. L. Staebler, RCA Rev. 38, 211 (1977).
2. W. Paul, A. J. Lewis, G. A. N. Connell, T. D. Moustakas, Solid State Comm. 20, 969 (1976); G. A. N. Connell and J. R. Pawlik, Phys. Rev. B 13, 787 (1976).
3. W. F. Spear, P. G. LeComber, S. Kinmond, M. H. Brodsky, Appl. Phys. Lett. 28, 105 (1976).
4. D. E. Carlson and C. R. Wronski, Appl. Phys. Lett. 28, 671 (1976).
5. D. E. Carlson, EIII Trans. on Electron Dev. ED-24, 449 (1977).
6. P. D'Antonio and J. H. Konnert, Phys. Rev. Lett. 43, 1161 (1979).
7. A. J. Leadbetter, A. A. M. Rashid, R. M. Richardson, A. F. Wright and J. C. Knights, Solid State Comm. 33, 973 (1980).
8. J. C. Knights and R. A. Lujan, Appl. Phys. Lett. 35, 244 (1979).
9. R. A. Street, J. C. Knights and D. K. Biegelsen, Phys. Rev. B 18, 1880 (1978).
10. J. A. Reimer, R. W. Vaughan, J. C. Knights, Phys. Rev. Lett. 44, 193 (1980).
11. J. A. Reimer, R. W. Vaughan and J. C. Knights, Solid State Comm., submitted.
12. D. K. Biegelsen, R. A. Street, C. C. Tsai and J. C. Knights, Phys. Rev. B 20, 4839 (1979).
13. I. Shimizu, T. Komatsu, K. Saito and E. Inoue, J. Non-Crys. Solids 35, 773 (1980).

14. J. Mort, S. Grammatica, J. Knights and R. Lyan, Solar Cell Materials, in press.
15. M. H. Brodsky, M. Cardona, J. J. Cuomo, Phys. Rev. B 16, 3556 (1977).
16. G. Lucovsky, R. J. Nemanich and J. C. Knights, Phys. Rev. B 19, 2064 (1979).
17. J. C. Knights, R. A. Lujan, M. P. Rosenblum, R. A. Street, D. K. Biegelsen and J. A. Reimer, Appl. Phys. Lett., submitted.
18. R. W. Vaughan, D. D. Elleman, L. M. Stacey, W.-K. Rhim and J. W. Lee, Rev. Sci. Instrum. 43, 1356 (1972).
19. T. C. Farrar and E. D. Becker, Pulse and Fourier Transform NMR (Academic Press, New York, 1971).
20. R. A. Street, J. C. Knights and D. K. Biegelsen, Phys. Rev. B 18, 1880 (1978).
21. A. Abragam, The Principles of Nuclear Magnetism (Clarendon, Oxford, England, 1961).
22. W. E. Spear, P. G. LeComber, Phil. Mag. 33, 935 (1976).
23. W. Paul, Solid State Commun. 34, 283 (1980).
24. H. Shanks, C. J. Fang, L. Ley, M. Cardona, F. J. Demond and S. Kalbitzer, Phys. Stat. Sol. (b) 100, 43 (1980).
25. J. C. Knights, J. Non-Cryst. Solids 35/36, 159 (1980).
26. (a) W. E. Carlos, P. C. Taylor, Phys. Rev. Lett. 45, 358 (1980).
(b) J. A. Reimer, R. W. Vaughan and J. C. Knights, Phys. Rev. B, submitted.
27. M. A. Paesler, D. A. Anderson, E. C. Freeman, G. Moddel and W. Paul, Phys. Rev. Lett. 41, 1492 (1978).
28. J. C. Knights, R. A. Street, G. Lucovsky, J. Non-Cryst. Solids 35/36, 279 (1980).

29. M. H. Borsky, M. A. Frisch, J. F. Ziegler, W. A. Lanford, Appl. Phys. Lett. 30, 561 (1977).
30. D. G. Ast, M. H. Brodsky, Phil. Mag. B 41, 273 (1980).
31. D. G. Ast, M. H. Brodsky, J. Non-Crys. Solids 35/36, 611 (1980).
32. G. Müller, F. Demond, S. Kalbitzer, H. Damjantchitsch, W. E. Spear, P. G. LeComber, R. A. Gibson, Phil. Mag. B 41, 571 (1980).
33. I. Solomon, M. H. Brodsky, J. Appl. Phys. 51, 4548 (1980).
34. J. C. Knights, J. Non-Crys. Solids 35/36, 159 (1980).
35. P. Kocian, *ibid.*, 35/36, 195 (1980).
36. A. Matsuda, K. Nakagawa, K. Tanaka, M. Matsumura, S. Yamasaki, H. Okushi, S. Iizima, *ibid.*, 35/36, 183 (1980).
37. G. Turban, Y. Catherine, B. Golleau, Thin Solid Films 67, 309 (1980).
38. B. A. Scott, M. H. Brodsky, D. C. Green, P. B. Kirby, R. M. Plecenik, E. E. Simonyi, Appl. Phys. Lett. 37, 725 (1980).
39. J. C. Knights, R. A. Lujan, M. P. Rosenblum, R. A. Street, D. K. Biegelsen, J. A. Reimer, Appl. Phys. Lett.
40. G. Turban, Y. Catherine, B. Grolleau, Thin Solid Films, submitted.
41. M. Taniguchi, M. Hirose, Y. Osaka, J. Non-Crys. Solids 35/36, 189 (1980).
42. H. Okamoto, T. Yamaguchi, Y. Nitta, Y. Hamakawa, *ibid.*, 35/36, 201 (1980).
43. L. J. Dimmey, P. L. Jones, F. H. Locks, Thin Solid Films 67, L13 (1980).
44. G. Herzberg, Molecular Spectra and Molecular Structure III (Van Nostrand Reinhold, New York, 1966) shows that both ionization

potentials and B-H (or P-H) bond dissociation energies are less than 11 eV.

45. J. A. Reimer, R. W. Vaughan, J. C. Knights, R. A. Lujan, Appl. Phys. Lett., submitted.

TABLE 1: ANODE FILMS

SAMPLE	RF ⁽¹⁾ POWER (WATTS)	SUBSTRATE TEMP.	GAS ⁽²⁾ COMP.	ATOM % HYDROGEN: ⁽³⁾			LINEWIDTH (KWHM,kHz)		T ₁ (SECONDS)
				TOTAL	NARROW	BROAD	NARROW	BROAD	
A	18	RT	5%/Ar	32.3	2.6	29.7	4.7	25.4	2.47
D	2	230° C	100%	7.8	3.4	4.4	3.8	26.3	2.98
F	1	230° C	5%/Ar	11.6	3.8	7.8	2.0	26.2	2.01
G	18	230° C	5%/Ar	12.9	4.5	8.4	1.0	22.4	2.68
H	11	RT	5%/Ar	30.1	2.4	27.7	1.3	26.3	1.80
L	18	230° C	5%/He	15.8	4.1	11.7	3.0	24.2	3.60
N	2	RT	100%	29.0	3.6	25.4	3.6	27.7	--
AA	1	230° C	100%	7.8	3.6	4.2	3.1	31.5	2.48
DD	1	230° C	5%/He	15.1	4.7	10.4	3.5	23.4	--
KK	18	230° C	100%	12.6	2.8	9.8	2.8	26.5	--

(1) Net into matching network.

(2) Percentage silane in diluent gas.

(3) Determined from integrated spin density and sample weight.

TABLE 2: CATHODE FILMS

SAMPLE	RF ⁽¹⁾ POWER (WATTS)	SUBSTRATE TEMP.	GAS ⁽²⁾ COMP.	ATOM % HYDROGEN:			LINEWIDTH (KWHM, kHz)		T ₁ (SECONDS)
				TOTAL ⁽³⁾	NARROW	BROAD	NARROW	BROAD	
B	18	RT	5%/Ar	16.3	2.2	14.1	3.9	22.1	6.02
C	1	RT	5%/Ar	12.6	3.5	9.1	4.7	29.5	7.09
I	18	RT	5%/Ar	15.4	2.0	13.4	2.9	22.2	6.02
M	2	RT	100%	23.1	4.6	18.5	5.4	24.0	--
S	18	RT	5%/He	16.5	4.0	12.5	2.3	19.4	4.50

(1) Net in matching network.

(2) Percentage silane in diluent gas.

(3) Determined from integrated proton spin density and sample weight.

TABLE 3: DOPED FILMS

SAMPLE	RF ⁽¹⁾ POWER (WATTS)	SUBSTRATE TEMP.	GAS ⁽²⁾ COMP.	ATOM % HYDROGEN:			LINEWIDTH (KWHM, khz)		T ₁ (SECONDS)
				TOTAL ⁽³⁾	NARROW	BROAD	NARROW	BROAD	
V	18,C	RT	5%/He 1% B ₂ H ₆	14.8	3.1	11.7	2.5	19.2	2.4
W ⁽⁴⁾	18,A	230 ^o C	5%/He 1% B ₂ H ₆	14.2	3.3	10.1	4.5	24.2	2.2
CC	1,A	230 ^o C	100% 1% PH ₃	11.5	4.1	7.4	3.5	31.7	1.4
BB	1,A	230 ^o C	100% 1% B ₂ H ₆	8.5	3.1	5.4	2.9	28.3	2.6
ZZ	2,A	230 ^o C	100% 0.1% B ₂ H ₆ 0.1% PH ₃	9.5	4.0	5.5	3.7	28.1	2.3

(1) Net into matching network. A or C refers to anode or cathode substrates.

(2) Percentage silane in diluent gas followed by percentage dopant gas.

(3) Determined from integrated proton spin density and sample weight.

(4) A third line is observed in this sample; 0.8 atom % and FWHM 0.79 khz.

Table 4

<u>Configuration</u>	<u>Full Width at Half Maximum^(a) (khz)</u>
SiH ₂ ^(b)	13.6
(SiH ₂) _n	17.1
SiH ₃	19.2
cSi[111] (hydrogenated)	23.5
cSi monovacancy (hydrogenated)	36.8
cSi divacancy (hydrogenated)	24.8
observed ^(c)	25.4 ± 3.4

^(a) Calculated using equation (1).

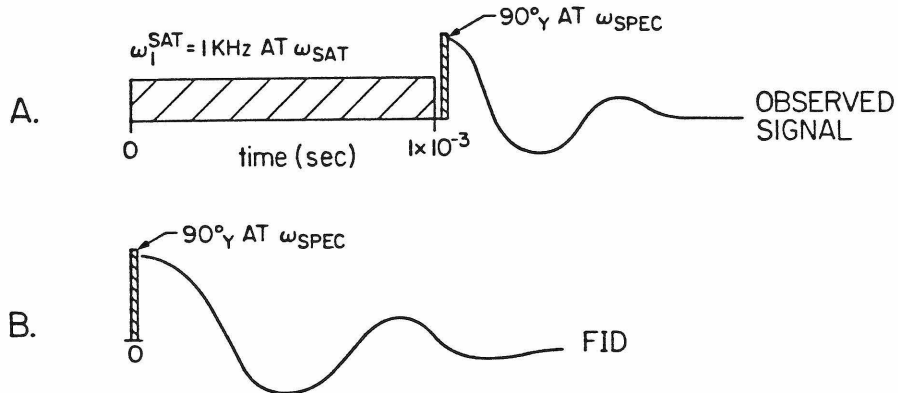
^(b) SiH₂ will give rise to a Pake doublet, however, in the amorphous matrix the doublet components will be expected to broaden to the point where no structure will be observed in the spectrum.

^(c) Mean and standard deviation of the values in Tables 1, 2 and 3.

Figure Captions

- Figure 1: Schematic diagram (*top*) of the pulse sequences used in the "hole-burning" experiments. Below, the results for two samples. The dark line in the difference spectra (A-B) are Gaussians best fit to the broad component of the FID spectra.
- Figure 2: Changes in the total hydrogen content and the hydrogen content in the broad and narrow components of the proton NMR spectra for films of varying thickness.
- Figure 3: Room temperature and low temperature proton NMR spectra for a heavily doped p-type a-Si:H film. At the bottom is the difference (room temperature - 100 K) of the two spectra, which clearly show the motionally narrowed component in the room temperature spectra.
- Figure 4: Proton NMR spectra for (A), a freshly deposited a-Si:H sample (RT, 18 watts, 5% SiH₄/Ar, anode), and (B) for the same sample after exposure to dry air for ~ six months.
- Figure 5: Schematic diagram, from Equation (2) in the text, showing that a homogeneous distribution of protons in the narrow component of the proton NMR spectrum will not give rise to the observed linewidths. The points and error bars are the mean and standard deviation of the linewidths and hydrogen content of the narrow components of 15 different a-Si:H samples.

SATURATION EXPERIMENTS



A-B YIELDS LINESHAPE THAT
 WAS SATURATED

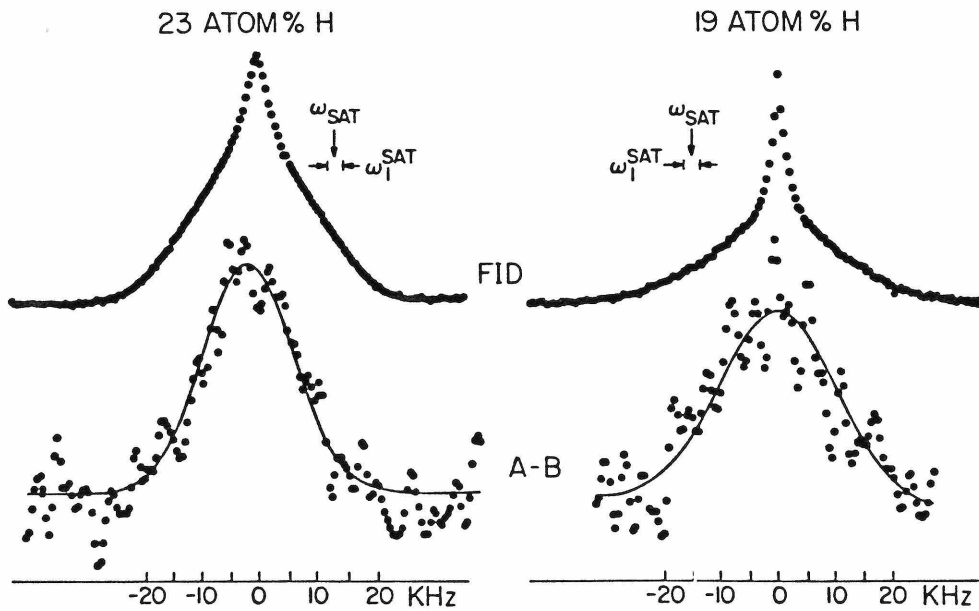


Figure 1

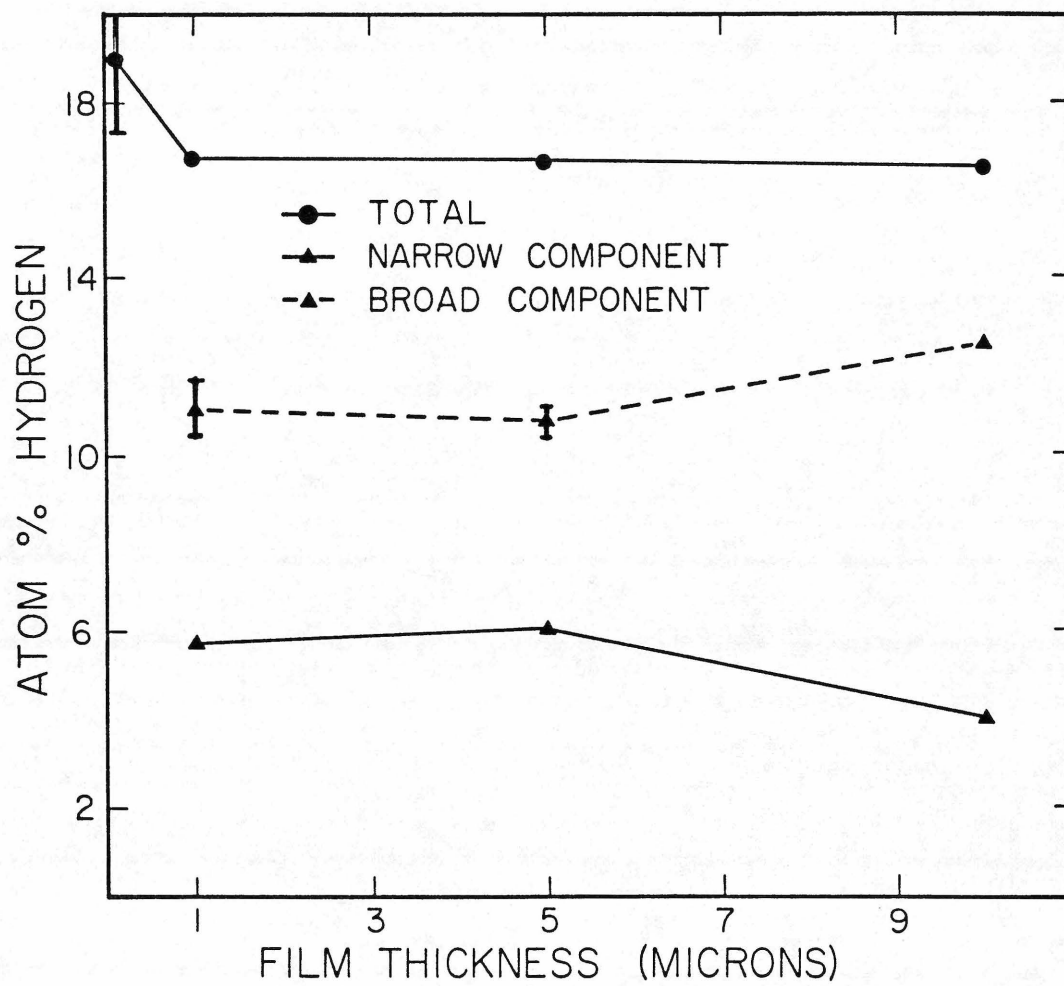


Figure 2

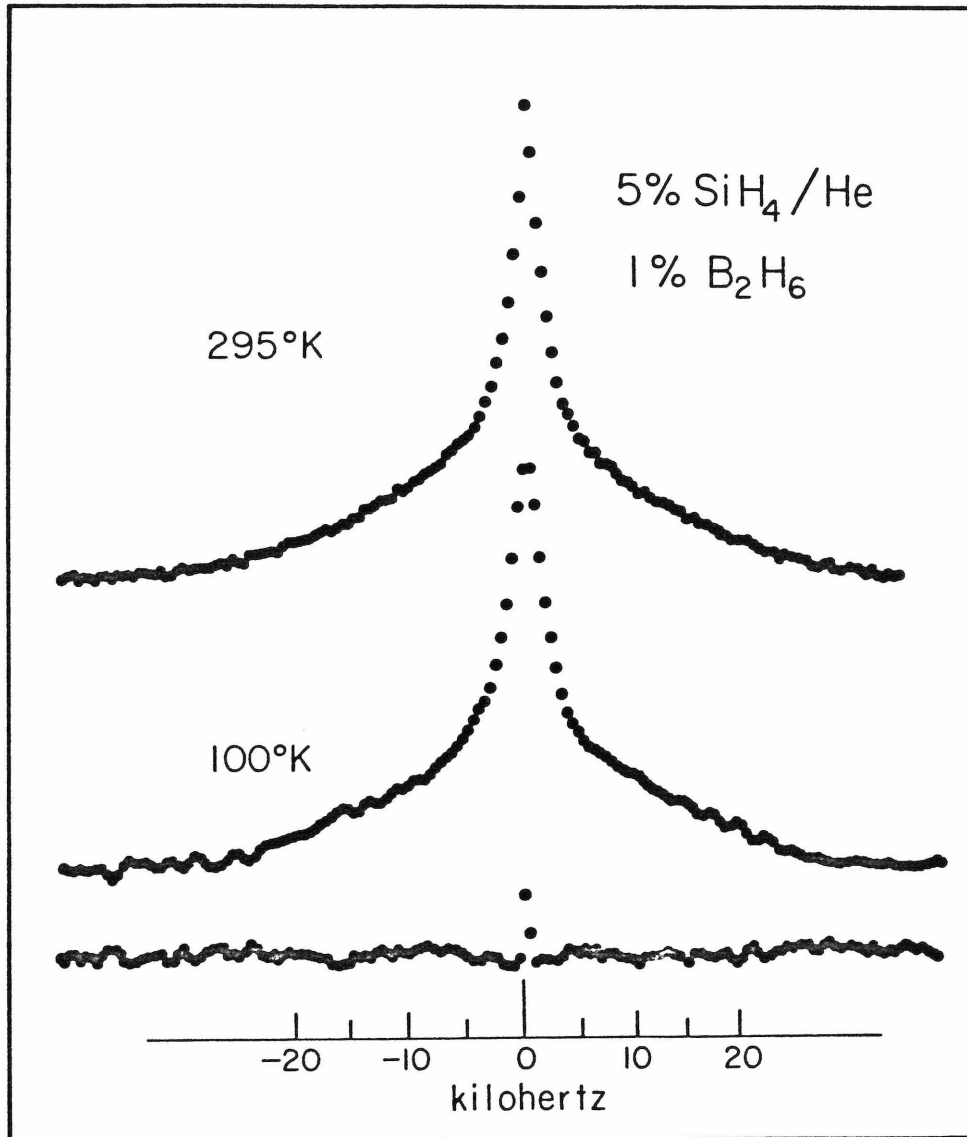


Figure 3

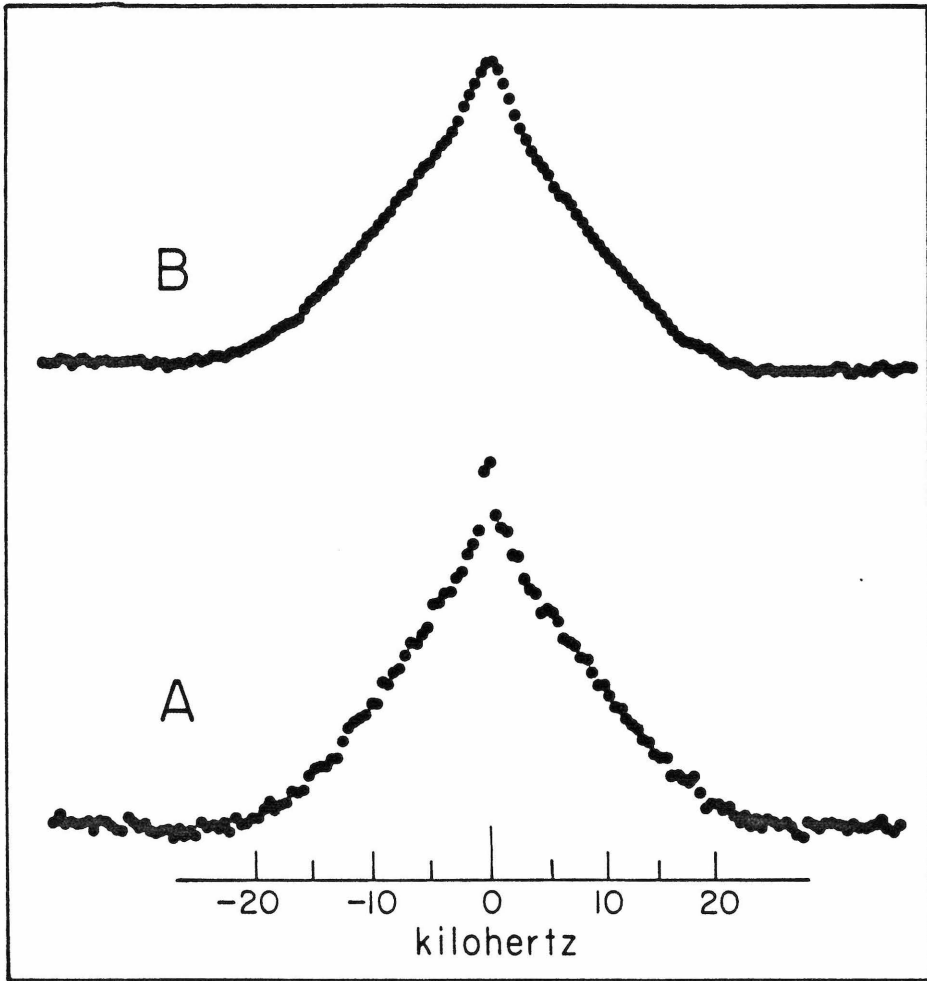


Figure 4

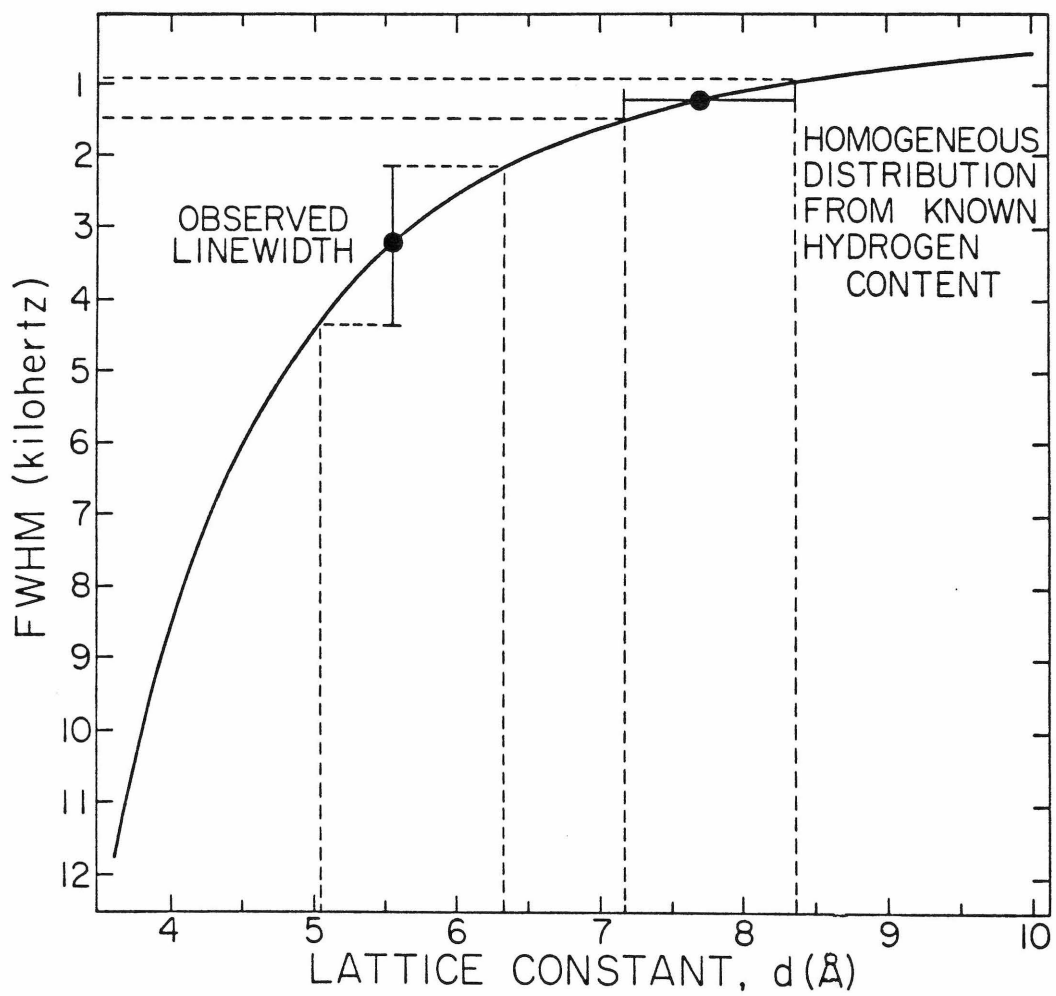


Figure 5

B: Annealed Amorphous Silicon Films

(This section is essentially an article by J. A. Reimer, R. W. Vaughan and J. C. Knights entitled "Proton NMR Studies of Annealed Plasma-Deposited Amorphous Silicon-Hydrogen Films", which has been scheduled for the December 1980 issue of Solid State Communications.)

Abstract

Proton magnetic resonance data are presented for plasma-deposited amorphous Si:H as a function of annealing temperature up to 650⁰C. The data indicate that hydrogen diffuses internally before major evolution occurs, that transfer of hydrogen occurs from a heavily clustered phase to a dilute phase coincident with evolution and that evolution occurs initially from the heavily clustered phase. Comparison with infrared data indicates that the heavily clustered phase can be either SiH_x (x = 2,3) or SiH.

It has been recently established (1) that proton magnetic resonance data reveal unique information on the degree of clustering or intermingling of local hydrogen environments in amorphous silicon-hydrogen films. Specifically, there is two-phase compositional behavior of the hydrogen with the two phases differing in their local density of hydrogen, the more dilute containing hydrogen only in monohydride SiH configurations. It has also been shown that annealing of a-Si:H films in the temperature range 100⁰C - 650⁰C results in changes in paramagnetic defect densities and evolution of hydrogen accompanied by changes in the Si-H vibrational spectra (2,3). It is the purpose of this letter to report proton magnetic resonance data from similarly annealed samples that indicate: (1) that hydrogen diffusion occurs in the dilute phase coincident with the paramagnetic center density reduction, (2) that hydrogen transfer from the heavily clustered to the dilute phase occurs at the onset of evolution, and (3) that evolution at low (<400⁰C) temperatures occurs exclusively from the heavily clustered phase independent of the species identified from vibrational spectroscopy as being reduced in density by annealing.

The samples were prepared in an rf-diode deposition system (4) and the proton NMR data taken with a solid state pulse Fourier transform spectrometer operating at 56.4 MHz (1.3 Tesla) (5). The NMR spectra were obtained by Fourier transformation of the free induction decay following a 90⁰ pulse. Signal averaging was required in all samples with the number of acquisitions varying from 128 to 1024 averages depending on the hydrogen content of the sample. Care was taken to allow

full spin-lattice relaxation between acquisitions so that accurate spin counts could be obtained.

We have studied proton resonance in annealed samples deposited under a wide range of conditions. Since we find that the behavior is qualitatively similar in all samples studied, we describe here data from one sample that best illustrates all the features observed. This sample was deposited under the following conditions: 5% silane in argon, 18 watts net rf power into matching network, $\sim 25^{\circ}\text{C}$ substrate temperature and a negative DC self-bias of ~ 220 volts. The sample was deposited into ~ 2 -inch diameter aluminum foil with a thickness of $\sim 50\ \mu$ which resulted in ~ 0.1 g of material after removal of the substrate with a dilute acid etch. The sample was then placed in a quartz NMR tube and isochronally annealed at various temperatures under flowing nitrogen for 20 minutes. The NMR data were taken after allowing the sample to cool to room temperature subsequent to each 50°C increase in annealing temperature. All spectra were found to be temperature independent down to 80 K as well as field independent. The two-component NMR spectra were least squares fitted assuming the broad component to be Gaussian and the narrow component Lorentzian (6). The resulting excellent fits, as exemplified in Fig. 1, gave values for the linewidths and relative areas of the two components. The errors are estimated from the reproducibility of the fits resulting from different starting parameters. Figure 2 shows the atom % hydrogen in the film as a function of annealing temperature and Fig. 3 shows how the full width at half-maximum (FWHM) changes for two components. Note that up to 600°C anneal the two-phase compositional behavior is still observable.

It is useful to consider the data in Figs. 2 and 3 in order of increasing annealing temperature. The first apparent change in these data appears at 150°C when there is a slight loss of hydrogen from the highly clustered (broad component) phase. Infrared and hydrogen evolution data have shown (3) that in this temperature region samples deposited at room temperature with SiH₃ sites evolve hydrogen. The NMR result is consistent with this explanation although the hydrogen loss is too small to be detected with IR in this particular sample. The second change is in the linewidth of the narrow component. While the hydrogen content associated with this line is roughly constant or even increasing up to 400°C, Fig. 3 shows a large reduction in the FWHM of the narrow component between 200°C and 400°C. The dipolar contribution (1) to the FWHM is given by

$$\text{FWHM} = 2.36\sqrt{M_2} = 2.36 \left(\frac{3}{5} \gamma^4 \hbar^2 I(I+1) \sum_{i,j} r_{ij}^{-6} \right)^{\frac{1}{2}}, \quad (1)$$

where I is the nuclear spin, $\frac{1}{2}$ for protons, γ is the nuclear gyromagnetic ratio, and $\sum r_{ij}^{-6}$ is the lattice sum of internuclear distances. It is thus seen that the FWHM is proportional to the density of protons. The dipolar contribution to the FWHM of the narrow component is readily obtained from the observed FWHM since the only other contribution to the FWHM is from the proton chemical shift which is known from previous multiple pulse studies (1). Figure 4 shows that the density change given by the dipolar contribution to the FWHM for the narrow component is an activated process with an activation energy of 0.31 eV. This density change is not due to hydrogen evolution since the atom % hydrogen

does not decrease in this temperature range. We conclude then that the 0.31 eV activation energy corresponds to hydrogen diffusion to a less clustered state, which, from Eq. (1), is found to correspond to a homogeneous dilute distribution of monohydride species. It is interesting to note that this diffusion coincides with the reduction of the electron spin density (3), suggesting that hydrogen diffusion to defects is indeed the mechanism by which the spin density is reduced.

Above 300°C inspection of Figs. 2 and 3 show continuous hydrogen evolution from the highly clustered environment. From 300°C to 400°C, the loss of hydrogen from this environment results both in evolution from the film and an increase in the total amount of hydrogen in the dilute environment. This increase could occur either by an increase in the volume occupied by this phase due to spatially inhomogeneous evolution from the highly-clustered environment or by diffusion of protons between the two environments. Although there is insufficient evidence to distinguish between these alternatives at present, the former would require not only a reduction in proton concentration but also the creation of a barrier or barriers to spin communication with the remaining highly-clustered protons and the opening of pathways for spin diffusion to the dilute phase. We therefore suggest that straightforward proton transfer is a more likely mechanism, particularly since diffusion is already occurring within the dilute phase. Inspection of Fig. 3 shows the effect of the hydrogen evolution on the FWHM of the broad component: above 400°C the loss of hydrogen causes the dipolar linewidth to reduce drastically. The corresponding changes after annealing in the SiH

vibrational spectra for a similar sample indicate that the evolution below 400°C occurs exclusively from the environment which has a Si-H stretch frequency of 2000 cm^{-1} . This frequency is universally associated with SiH monohydride groups (7,8). In other samples, we observe that this same temperature regime corresponds to evolution from environments with SiH mode frequencies of 2100, 890 and 845, a combination associated with $(\text{SiH}_2)_n$ groups (8). These results confirm the earlier indication (1) that the heavily clustered environment identified by NMR can arise from clustering of monohydride groups as well as dihydride, trihydride, etc. Finally, above 450°C , hydrogen evolves from both environments until, at temperatures greater than 650°C , the two-phase behavior disappears and ~ 1 atom % of hydrogen remains in a dilute homogeneous phase.

In conclusion, we have shown the annealing behavior of the two phases of hydrogen in plasma-deposited amorphous Si:H to be different. The low hydrogen-density phase disperses to a homogeneous dilute bath of protons at annealing temperatures up to 400°C with an activation energy of 0.31 eV. After a slight loss due to evolution from $-\text{SiH}_3$ sites, the highly clustered phase evolves hydrogen above annealing temperatures of 300°C . Above 450°C both phases evolve hydrogen, until 650°C , clustered phase can no longer be identified and a single dilute phase containing ~ 1 atom % hydrogen is left. Of particular significance, is the fact that the dispersion of hydrogen to a homogeneous dilute bath coincides with the paramagnetic center reduction observed previously (3) and that monohydride clustering, presumably on internal surfaces, is clearly

present in some films.

The authors wish to acknowledge the expert assistance of R. A. Lujan in sample preparation, and helpful discussions with S. I. Chan. This work was supported by the National Science Foundation under Grant No. DMR-77-21394, and by the Solar Energy Research Institute under Contract No. XJ-0-9079-1.

References

1. J. A. Reimer, R. W. Vaughan and J. C. Knights, Phys. Rev. Lett. 44, 193 (1980).
2. C. C. Tsai and H. Fritzsche, Solar Energy Mat. 1, 29 (1979).
3. D. K. Biegelsen, R. A. Street, C. C. Tsai and J. C. Knights, Phys. Rev. B 20, 4939 (1979).
4. R. A. Street, J. C. Knights and D. K. Biegelsen, Phys. Rev. B 18, 1880 (1978).
5. R. W. Vaughan, D. D. Elleman, L. M. Stacey, W. K. Rhim and J. W. Lee, Rev. Sci. Instrum. 43, 1356 (1972).
6. We find that the narrow component, previously found in a limited set of samples to be Gaussian (1) can be either Lorentzian or Gaussian depending on the precise deposition conditions.
7. M. H. Brodsky, M. Cardona and J. J. Cuomo, Phys. Rev. B 16, 3550 (1977).
8. G. Lucovsky, R. J. Nemanich and J. C. Knights, Phys. Rev. B 19, 2064 (1979).

Figure Captions

- Figure 1: Experimental spectra with Gaussian and Lorentzian fits showing the quality of the fits. On the left is the spectrum of the sample as deposited; on the right is the spectrum of the same sample annealed to 400°C.
- Figure 2: Atom % hydrogen for high and low density hydrogen phases in a sample deposited at room temperature from 5% SiH₄/Ar onto a cathode substrate. T_{anneal} refers to the temperature the sample was annealed to.
- Figure 3: The full width at half maximum (FWHM) for both high and low density phases of hydrogen in the sample shown in Fig. 1. Note the two different scales for the two components.
- Figure 4: Activation process of the reduction in dipolar linewidth of the low density phase.

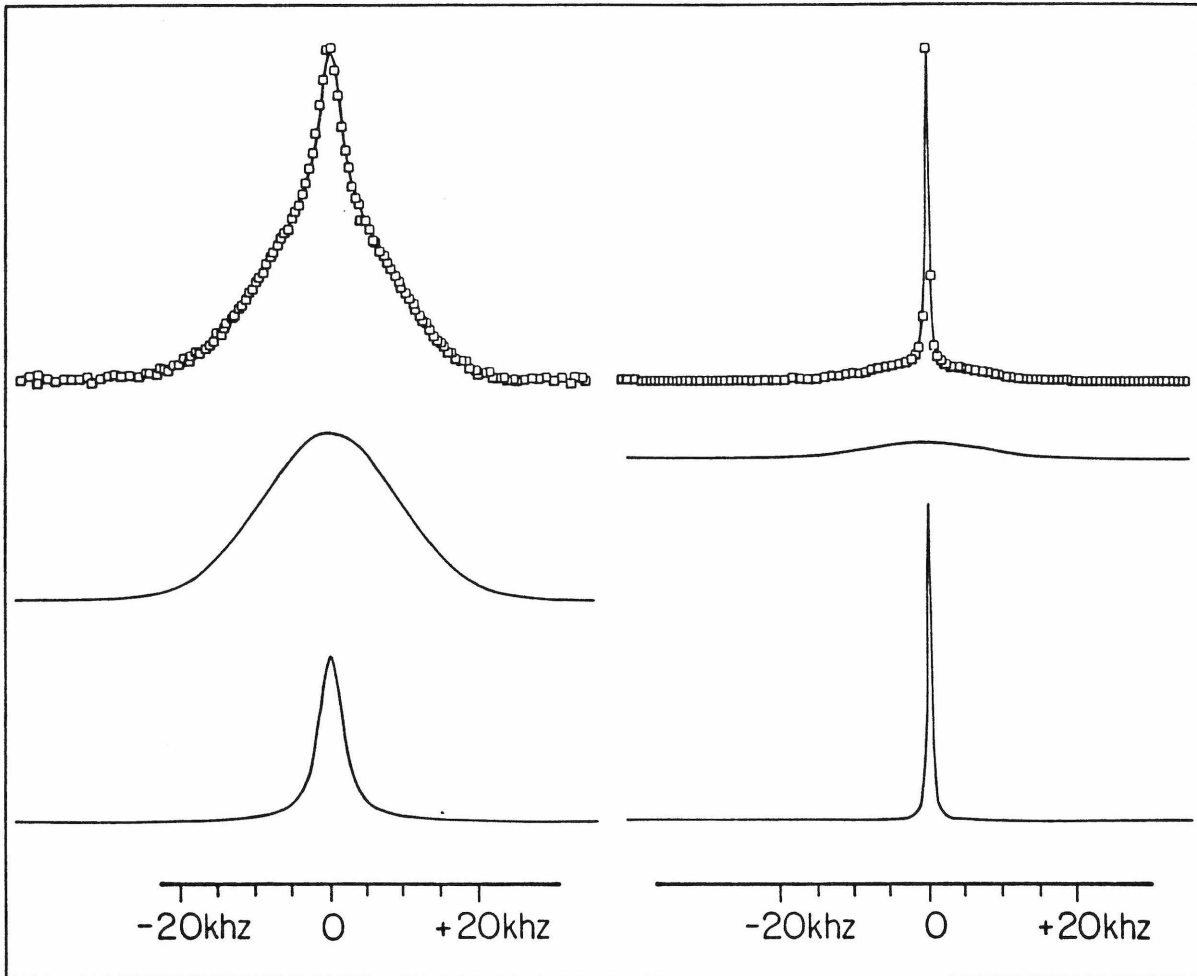


Figure 1

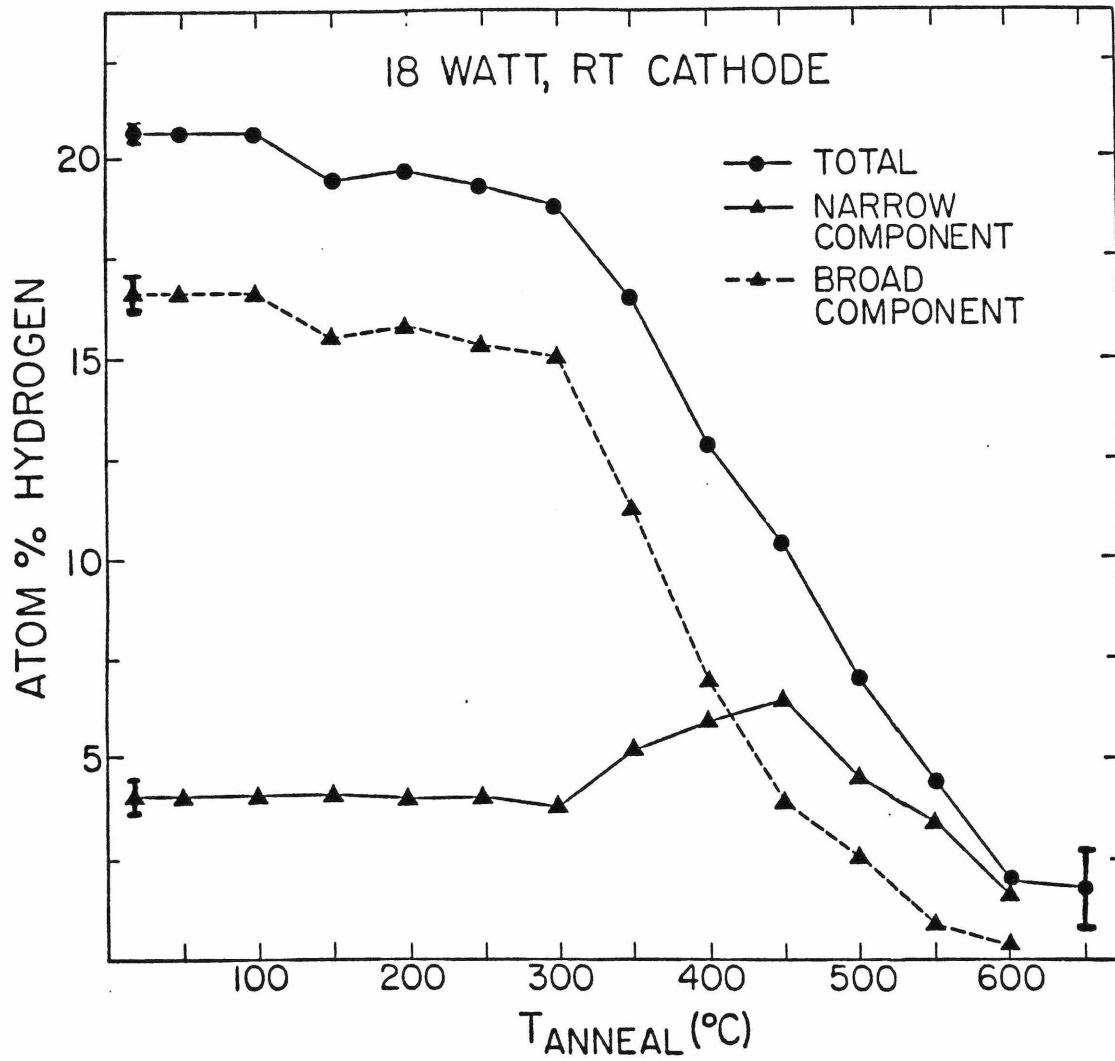


Figure 2

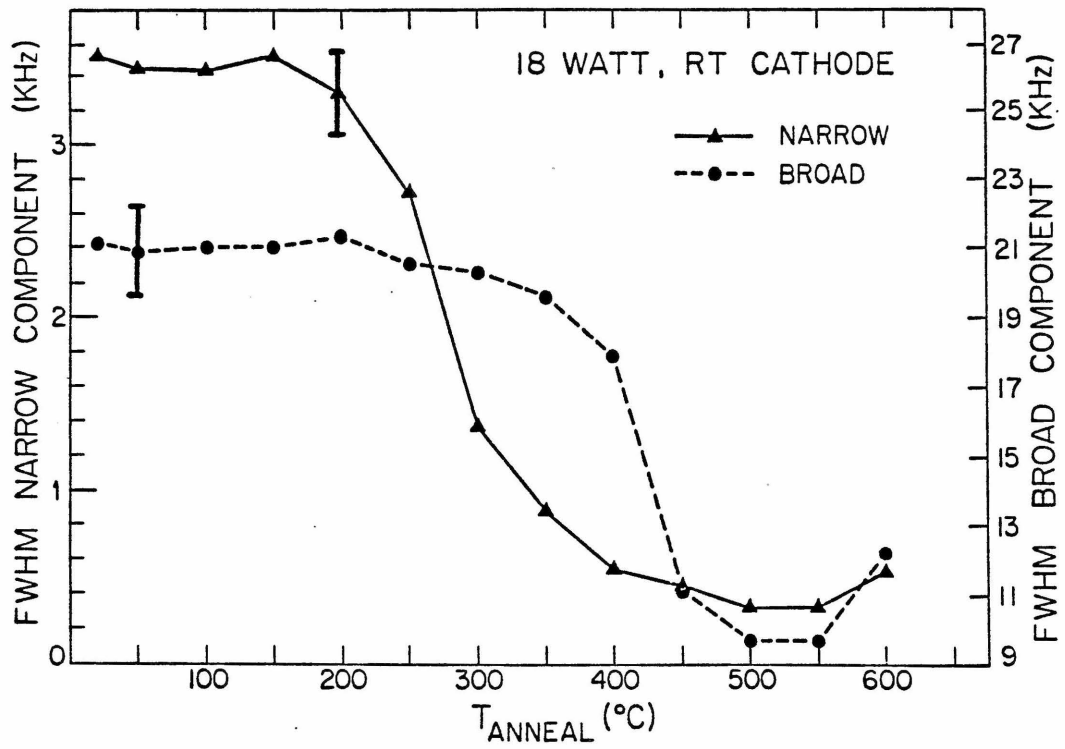


Figure 3

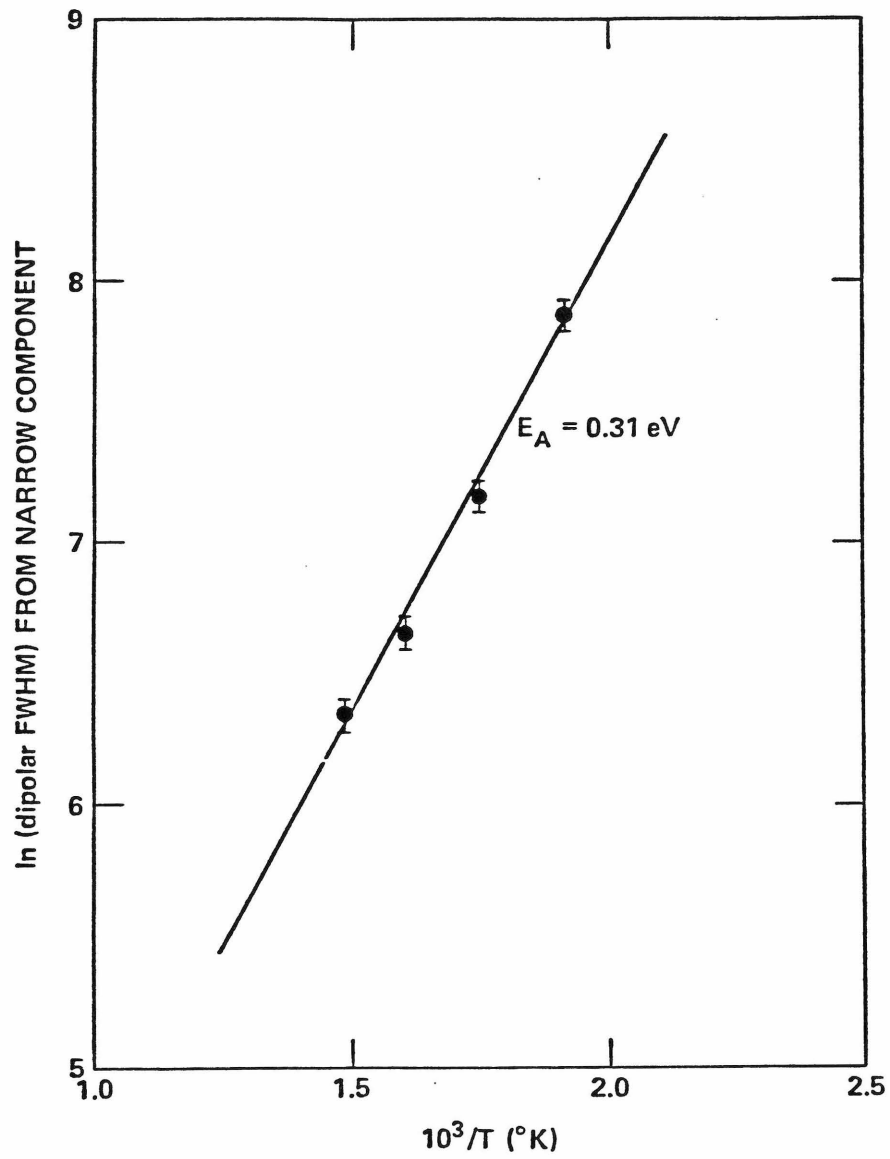


Figure 4

C. Amorphous Boron, Carbon,
Silicon Nitride and Silicon Carbide.

(This Section is essentially an article by J. A. Reimer, R. W. Vaughan, J. C. Knights and R. A. Lujan entitled "Proton Magnetic Resonance Spectra of Plasma-Deposited Inorganic Thin Films". This paper has been submitted for publication in Applied Physics Letters.)

Abstract

Proton magnetic resonance data are presented for the hydrogen alloys of plasma-deposited amorphous boron, carbon, silicon carbide and silicon nitride. Linewidth and lineshape analysis leads to the conclusion that hydrogen nuclei are clustered in a-Si/C:H, a-C:H, and a-Si/N:H. Both a-Si/C:H and a-C:H data show that the hydrogen exists in two phases. Modeling of linewidths in a-Si/C:H indicates that the two phases are heavily hydrogenated carbon clusters imbedded in a weakly hydrogenated a-Si lattice. Finally, evidence is presented for the presence of motionally narrowed hydrogen spectra in a-Si/N:H, a-B:H, and a-C:H. It is suggested that the hydrogen nuclei giving rise to these spectra are associated with disorder modes.

INTRODUCTION

Inorganic thin films prepared either by plasma-deposition or reactive sputtering techniques have attracted a great deal of attention recently (1) because of their technological importance. Plasma deposited silicon nitrides have proven attractive for use as passivation layers in high reliability silicon integrated circuits and amorphous silicon has been doped successfully to form p,n and Schottky barrier junctions, as well as solar cells (2). The role of hydrogen in these films is not well understood, although it is generally accepted that hydrogen passivates dangling bond intrinsic defects and thus decreases the density of states in the gap (2 - 4).

It has been recently shown (6) that proton magnetic resonance data reveal unique information on the degree of clustering and intermingling of local hydrogen bonding environments in amorphous plasma-deposited silicon-hydrogen films. Hydrogen also plays an important role in the properties of other films such as silicon nitride (3,7-10), silicon carbide (3,11,12), carbon (4,13-15) and boron. It is the purpose of this Letter to report two-component dipolar broadened proton magnetic resonance spectra of the hydrogen alloys of these plasma-deposited amorphous substances. It will be shown that data for a-C:H, a-Si/N:H, and a-Si/C:H lead to the conclusion that the hydrogen nuclei are clustered. In addition, the data for a-C:H and a-Si/C:H show direct evidence for two-phase compositional inhomogeneity, where modeling of local bonding environments in a-Si/C:H suggests that the two phases are due to heavily hydrogenated carbon clusters imbedded in a weakly hydrogenated a-Si

lattice. Furthermore, temperature dependent data for a-B:H, a-Si/N:H and a-C:H indicate that a small fraction of the protons in these films have spectra which are motionally narrowed. We associated them with disorder modes in the lattice.

Materials and Methods

The samples were prepared by deposition (16) under the conditions detailed in Table 1. All samples were deposited onto ~2 inch diameter aluminum foil substrates in thicknesses ranging from 1μ to 100μ resulting in sample masses in the range of 5 - 100 milligrams after removal of the substrates with dilute acid etch. Silicon/carbon and silicon/nitrogen ratios were determined using Rutherford backscattering. A pulse NMR spectrometer (17) was used at an operating frequency of 56.4 MHz (1.3 Tesla). The resonance techniques and the least-squares fitting of the observed lineshapes to the sum of a Gaussian (broad component) and a Lorentzian (narrow component) have been described previously (6). The ^1B spectrum was obtained on a standard pulse spectrometer operating at 86.7 Mhz (6.3 Tesla). Only the $\frac{1}{2} \rightarrow -\frac{1}{2}$ transition is shown.

Results and Discussion

Figure 1 shows a comparison of spectra at room temperature and 125 K for the samples described in Table 1. The observed linewidths reflect contributions from (i) homonuclear dipolar interactions, (ii) heteronuclear dipolar interactions (iii) chemical shift interactions. When multiple pulse cycles (18 - 20) were applied (which remove the homonuclear

dipolar broadening), the lines narrowed significantly. Thus, for a-C:H, a-Si/C:H, and a-Si/N:H, the homonuclear dipolar interaction is the dominant broadening mechanism in the proton spectra. In a-B:H, the heteronuclear dipolar interaction due to nearby ^{10}B and ^{11}B nuclei was estimated (5) and was found to be as large or larger than the homonuclear dipolar interaction.

The spectra for all the samples may be decomposed into at least two components. Multicomponent lineshapes in these films may arise from the following situations: (i) motion in a domain or at a defect site which decouples spin-spin communication (5) with the rest of the dipolar reservoir; (ii) the existence of spatially-isolated [$\geq 8\text{\AA}$ (21)] dipolar reservoirs with differing densities of spins such that there is no spin-spin communication between them; or (iii) both (i) and (ii). The first case has been observed in partially crystalline polyethylene (22) and case (ii) in amorphous silicon hydrogen films (1). Effects on the lineshapes due to motion may often be removed by reducing the temperature, hence, cases (i) and (ii) may be readily distinguished. Inspection of Figure 1 and Table 2 shows that at low temperature, where motional narrowing is not expected, both a-C:H and a-Si/C:H spectra still exhibit two-component behavior. In a-Si/N:H, a-B:H, and a-C:H, a small fraction of the protons have lineshapes that do appear to be motionally narrowed at room temperature. However, this fraction accounts for no more than 3% of the total proton spins. Hence, we conclude that a-Si/C:H is best described by case (ii), a-B:H and a-Si/N:H by case (i), and a-C:H by case (iii). The low temperature spectra for a-B:H and a-Si/N:H show no evidence for case (ii), however, we shall present evidence suggesting

that the hydrogen nuclei in a-Si/N:H are clustered. In a-B:H we estimate (5) the heteronuclear dipolar interaction to be 70 - 102 kHz, hence no structural information is expected from proton lineshapes.

Further insight on the distribution of hydrogen can be derived from analysis of the low temperature data shown in Figure 1 and Table 2 according to models for local proton configurations. The homonuclear and heteronuclear dipolar interactions in polycrystalline or amorphous solids give rise to Gaussian lineshapes whose second moments are given by, respectively (5),

$$M_2^{II} = 3/5 \gamma_I^4 \hbar^2 I(I+1) \sum_{i,j} 1/r_{ij}^6 \quad (1)$$

$$M_2^{IS} = 4/15 \gamma_I^2 \gamma_S^2 \hbar^2 S(S+1) \sum_{i,j} 1/r_{ij}^6 \quad (2)$$

where γ_I is the nuclear gyromagnetic ratio for a nucleus of spin I and r_{ij} is the internuclear distance between spins i and j . For a-C:H, a-Si/C:H and a-Si/N:H, two types of proton configurations to which Equation 1 simply applies have been considered. The first is one of local clustering into configuration such as CH_3 , $(\text{CH}_2)_n$, $(\text{SiH}_2\text{CH}_2)_n$, SiNH_2 , and a hydrogenated [111]c-carbon surface. The corresponding Si-H clustering has been previously calculated (6). The results of these calculations and an estimate (23) of the linewidth (FWHM) for isolated CH_2 are as follows: CH_2 , 33.1 kHz (SiH_2 , 13.5 kHz); CH_3 , 46.9 kHz (SiH_3 , 19.2 kHz); $(\text{CH}_2)_n$, 44.1 kHz ($(\text{SiH}_2)_n$, 17.1 kHz); $(\text{SiH}_2\text{CH}_2)_n$, 36.1 kHz; and C[111], 57.4 kHz (Si[111], 23.5 kHz) and SiNH_2 , 37.8 kHz. Given the sensitivity of the calculation to small changes in internuclear distances

and the errors involved in the fitting procedures, we conclude that any of the local configurations on carbon could give rise to the broad component in both a-C:H and a-Si/C:H spectra. Since the width of the broad component is >45 kHz in both of the a-Si/C:H samples and the broadest component expected for protons clustered on silicon is 23.5 kHz and on $(\text{SiH}_2\text{CH}_2)_n$ is 36.1 kHz, we conclude that for silicon carbide the broad line is due to predominantly "polyacetylene" type environments. This is especially true for the higher carbon content sample where the observed broad component linewidth is identical to that of amorphous carbon. This implies that the spatial inhomogeneity in the protons is reflective of carbon clusters which are heavily hydrogenated imbedded in a weakly hydrogenated amorphous silicon lattice.

The second situation to which Equation 1 may be simply applied is one where the spins are distributed uniformly on a cubic lattice whose spacing is equal to the inverse cube root of the spin density. The results of applying this model for Equation 1 to the narrow component of the a-Si/C:H and a-C:H lineshapes as well as the total lineshape in a-Si/N:H are shown in Table 3. These calculations show that the protons responsible for the narrow component of a-Si/C:H and a-C:H, as well as all the protons in a-Si/N:H, are clustered. Local clustering of hydrogen on nitrogen atoms is sufficient to explain the observed linewidth in a-Si/N:H. However, in a-Si/C:H and a-C:H, the clustering in the narrow component is not dominated by local multiply bonded species such as SiH_x or CH_x as those species yield much larger linewidths. We conclude that the narrow component is composed primarily of clustered monohydride species (CH or SiH).

There are several implications of these results from a-Si/C:H and a-C:H for models of microstructure and optimal properties. Microstructure in a-C:H films prepared from ethylene, acetylene and styrene (13 - 15) has been observed by SEM, TEM and low-angle X-ray scattering. In those studies, it was concluded that there are two phases, specifically, spheres imbedded in a polymer binder. It may be possible to identify the broad component in the FID spectra of a-C:H with those protons in the polymer binder and the narrow component with monohydride clustering on internal spheres. However, more detailed experiments are needed to confirm these suggestions.

The observation of carbon clusters in a-Si/C:H is consistent with recent photoluminescence results (11) on films prepared from $\text{SiH}_4/\text{C}_2\text{H}_4$ mixtures. In those data the visible photoluminescence consists of two bands which change in intensity with changing composition. The relatively low hydrogen content of the silicon-rich regions of these films (<1.5 atom %, from Table 2) represents a hydrogen content not accessible by plasma deposition of SiH_4 to form a-Si:H. Thus, the optical properties of plasma deposited a-Si/C:H may prove useful in the study of a-Si:H. Furthermore, the heavy hydrogen clustering for the carbon-rich regions may have implications in film growth and/or the chemistry of the plasma above the films.

The room temperature spectra of a-C:H, a-Si/N:H and a-B:H all show a small narrow component that increases in width as the temperature is decreased. Since these components do not decrease in intensity with extended evacuation of the samples, they are not due to adsorbed gases.

We conclude that they are motionally narrowed (18) spectra due to hydrogen nuclei which are indigenous to the films. Estimates of the dipolar broadening, including the effects of motion (18,24), in rotating local bonding configurations such as methyl groups yield values much larger than those observed. The central transition of the ^1B spectra for a-B:H shown in Figure 2 is a typical dipolar-broadened, second-order quadrupolar power pattern and shows no evidence for motionally narrowed ^1B nuclei. We suggest that these motionally narrowed proton lines correspond to hydrogen nuclei rapidly moving in a defect site or disorder mode. The existence of hydrogen-containing disorder modes has been proposed recently (25) in a-Si:H in order to explain the temperature and field dependence of proton spin-lattice relaxation (T_1), as well as other relaxation measurements (26). Their presence in a-C:H, a-Si/N:H, and a-B:H indicate that such modes may be ubiquitous to hydrogen containing amorphous materials. The relationship between these modes and defects affecting optical properties warrants further investigation.

Conclusion

In conclusion, we have shown that for a series of plasma-deposited inorganic thin films, hydrogen is spatially inhomogeneous on two levels. The first consists of hydrogen clustering which we have observed in a-C:H, a-Si/C:H and a-Si/N:H. The second, observed in a-C:H and a-Si/C:H, we conclude to be a two-phase compositional inhomogeneity. Furthermore, we have presented evidence that in a-Si/C:H, the inhomogeneity is due to heavily hydrogenated carbon clusters imbedded in a weakly hydrogenated

a-Si lattice. Finally, we have observed a small fraction of protons whose spectra are motionally narrowed. We attribute these protons to hydrogen-containing disorder modes within the lattices of a-B:H, a-C:H, and a-Si/N:H. These results imply that film microstructure, compositional inhomogeneity and rapidly moving hydrogen nuclei may be important in understanding both defect structures and optical properties in plasma-deposited inorganic thin films.

The authors thank S. I. Chan and T. M. Duncan for helpful comments on the manuscript and T. W. Sigmon for assistance with the Rutherford backscattering analysis. This work was supported by the National Science Foundation under Grant No. DMR 77-21394.

References

1. A. R. Reinberg, *Ann. Rev. Mat. Sci.* 9, 341 (1979).
2. H. Fritzsche, C. C. Tsai and P. Persans, *Solid State Tech.*, Jan., 55 (1978).
3. D. A. Anderson and W. E. Spear, *Phil. Mag.* 35, 1 (1977).
4. D. A. Anderson, *Phil. Mag.* 35, 17 (1977).
5. A. Abragam, *The Principles of Nuclear Magnetism*, (Oxford, London, 1961).
6. J. A. Reimer, R. W. Vaughan and J. C. Knights, *Phys. Rev. Lett.* 44, 193 (1980).
7. E. A. Taft, *J. Electrochem. Soc.: Solid State Science* 118, 1341 (1971).
8. H. R. Philipp, *ibid*, 120, 295 (1973).
9. P. S. Peercy, H. J. Stein, B. L. Doyle and S. T. Picraux, *J. Electronic Materials* 8, 11 (1979).
10. A. K. Sinha, *Solid State Tech.*, Apr., 133 (1980).
11. D. Engemann, R. Fischer and J. Knecht, *Appl. Phys. Lett.* 32, 567 (1978).
12. A. Guivarich, J. Richard, M. LeConteller, E. Ligeon and J. Fontenille, *J. Appl. Phys.* 51, 2167 (1980).
13. M. R. Havens, K. G. Mayhan and W. J. James, *J. Appl. Poly. Science* 22, 2793 (1975).
14. M. R. Havens, K. G. Mayhan and W. J. James, *ibid*, 22, 2799 (1978).
15. A. Moshonov and Y. Avny, *J. Appl. Poly. Science* 25, 771 (1980).
16. R. A. Street, J. C. Knights and D. K. Biegelsen, *Phys. Rev. B* 18, 1880 (1978).

17. R. W. Vaughan, D. D. Elleman, L. M. Stacey, W.-K. Rhim and J. W. Lee, *Rev. Sci. Instrum.* 43, 1356 (1972).
18. C. P. Slichter, Principles of Magnetic Resonance, (Springer-Verlag, Berlin, 1978).
19. M. Mehring in: NMR Basic Principles and Progress, eds. P. Diehl, E. Fluck and R. Kosfeld, (Springer-Verlag, Berlin, 1976).
20. U. Haeberlen in: Advances in Magnetic Resonance, Supplement 1, ed. J. S. Waugh, (Academic Press, New York, 1976).
21. Reference (5) shows the probability of mutual spin flips between neighbors to be $\sim \sqrt{M_2}/30$.
22. R. G. Pembleton, R. C. Wilson and B. C. Gerstein, *J. Chem. Phys.* 66, 5133 (1977).
23. Both CH_2 and SiH_2 give rise to Pake doublets. In an amorphous matrix, such doublets would be expected to broaden considerably and the values of 13.6 and 33.1 khz for SiH_2 and CH_2 , respectively, are an approximate measure of the linewidth.
24. H. S. Gutowsky and G. E. Pake, *J. Chem. Phys.* 18, 162 (1950).
25. W. E. Carlos and P. C. Taylor, *Phys. Rev. Lett.* 45, 358 (1980).
26. J. A. Reimer, R. W. Vaughan and J. C. Knights, submitted to *Phys. Rev. B*.

TABLE 1

SAMPLE CONDITIONS ^(a)	HYDROGEN CONTENT ^(b) (atom%)	MOLECULAR FORMULA
5% B ₂ H ₆ /He(C) 10 Watts, 25°C	25.1	a-B _{.75} H _{.25}
5% B ₂ H ₆ /He(A) 10 Watts, 230°C	20.6 ^(f)	a-B _{.79} H _{.21}
100% C ₂ H ₂ (A) 5 Watts, 230°C	35.2	a-C _{.65} H _{.35}
13% SiH ₄ /C ₂ H ₂ (A) 2 Watts, 230°C ^(e)	22.7	a-Si _{.20} C _{.57} H _{.23}
26% SiH ₄ /C ₂ H ₂ (A) 2 Watts, 230°C ^(d)	38.2 ^(f)	a-Si _{.26} C _{.36} H _{.38}
NH ₄ /N ₂ /SiH ₄ FLOW(A) Rates 100/50/6 SCCM 10 Watts, 300°C	23.0	a-Si _{.31} N _{.46} H _{.23} ^(c)

(a) The conditions refer to percentage gas in mixture, net RF power into matching network, substrate temperature, (A) refers to deposition on the grounded electrode (Anode) and (C) refers to the RF hot (Cathode) electrode.

(b) Determined from proton spin density, sample weight, and Si/C or Si/N ratios.

(c) Si/N ratio determined by Rutherford backscattering.

(d) Si/C ratio determined by Rutherford backscattering.

(e) Si/C ratio estimated from the Rutherford backscattering results for the 26% SiH₄/C₂H₂ sample and the ratio of silane percentages.

(f) Spectra not shown in Figure 1.

TABLE 2

SAMPLE		HYDROGEN DISTRIBUTION				T_1 (Seconds)	LINE WIDTH (FWHM, kHz)	
		%	Atom %	%	Atom %		Broad	Narrow
a-C _{.65} H _{.35}	293°K	93.5	32.7±.4	6.5	2.3±.3	0.4±.1	78.4±2.6	1.6±.7
	130°K	91.1	32.1±.4	8.9	3.1±.4		76.8±2.8	6.6±.2
a-B _{.75} H _{.25} (cathode)	293°K	98.9	24.8±.1	1.1	0.3±.1	4.6±.3	118±3	1.8±.1
	124°K	98.7	24.8±.1	1.3	0.3±.1		121±3	11.7±.6
a-B _{.79} H _{.21} ^(a) (anode)	293°K	98.5	20.7±.1	1.5	0.3±.1	5.1±.3	83.7±1.4	3.6±.7
a-Si _{.31} N _{.46} H _{.21}	293°K	97.0	22.3±.2	3.0	0.7±.2	4.6±.4	35.1±.3	2.2±.1
	124°K	97.8	22.5±.2	2.2	0.5±.2		55.6±.2	6.0±.2
a-Si _{.20} C _{.57} H _{.23} ^(b)	293°K	94.5	21.5±.3	5.5	1.2±.3	0.2±.05	69.0±.3	7.4±.3
	126°K	95.3	21.6±.3	4.7	1.1±.3		78.4±.4	7.0±.3
a-Si _{.26} C _{.36} H _{.38} ^(a)	293°K	98.1	37.5±.3	1.9	0.7±.3		45.6±.4	1.9±.2

(a) Spectra not shown in Figure 1.

(b) Estimated molecular formula (see Table 1).

TABLE 3

SAMPLE	ATOM % NARROW	FWHM NARROW (kHz)	HOMOGENEOUS ^(a) WIDTH (kHz)
a-C:H ^(b)	3.1	6.6	1.7
a-Si _{.26} C _{.36} H _{.38}	0.7	1.9	0.4
a-Si _{.20} C _{.57} H _{.23} ^(d)	1.2	7.0	0.6
a-Si _{.31} N _{.46} H _{.23}	23.0 ^(c)	55.6	12.9

(a) Calculated with use of Eq. (1).

(b) The low temperature values were chosen to eliminate motion effects.

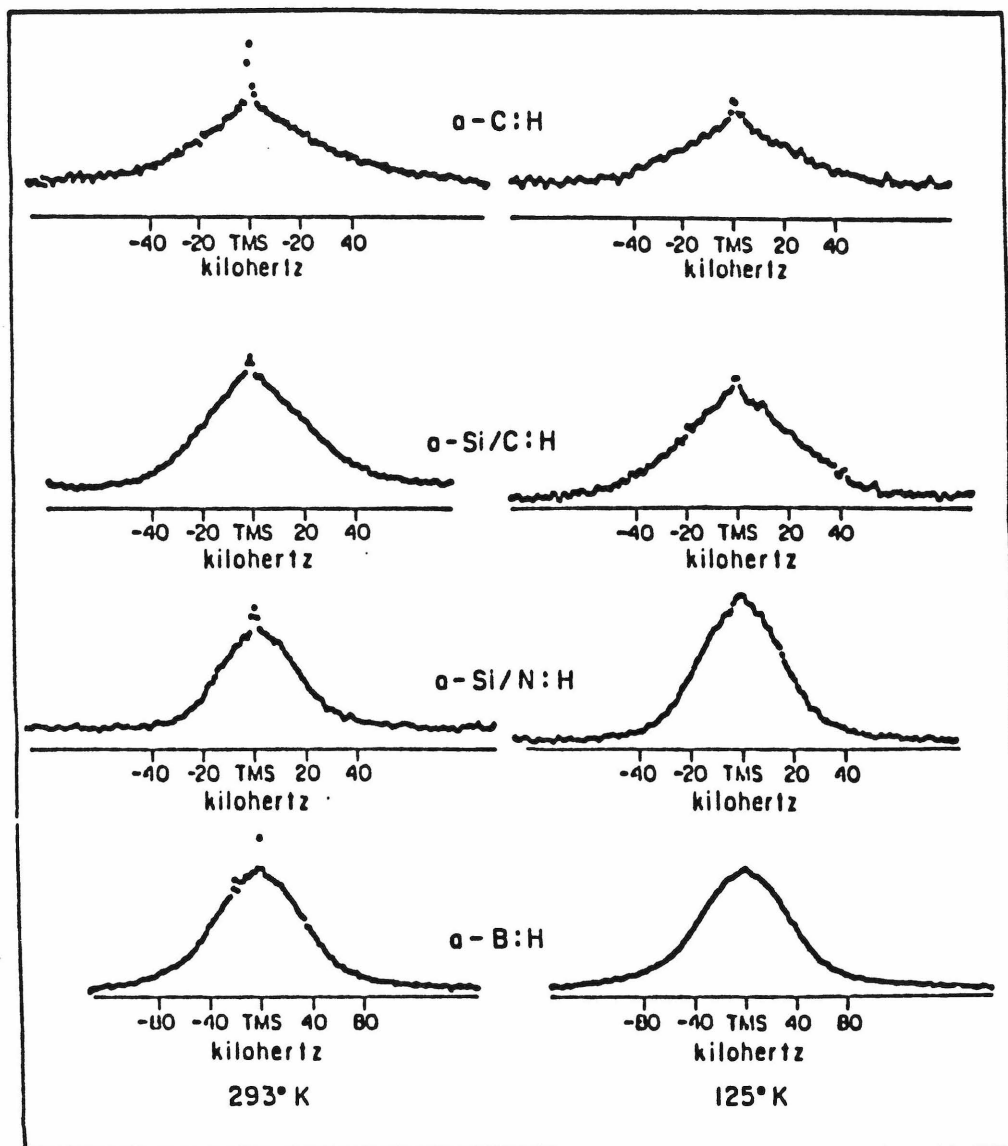
(c) Total hydrogen content.

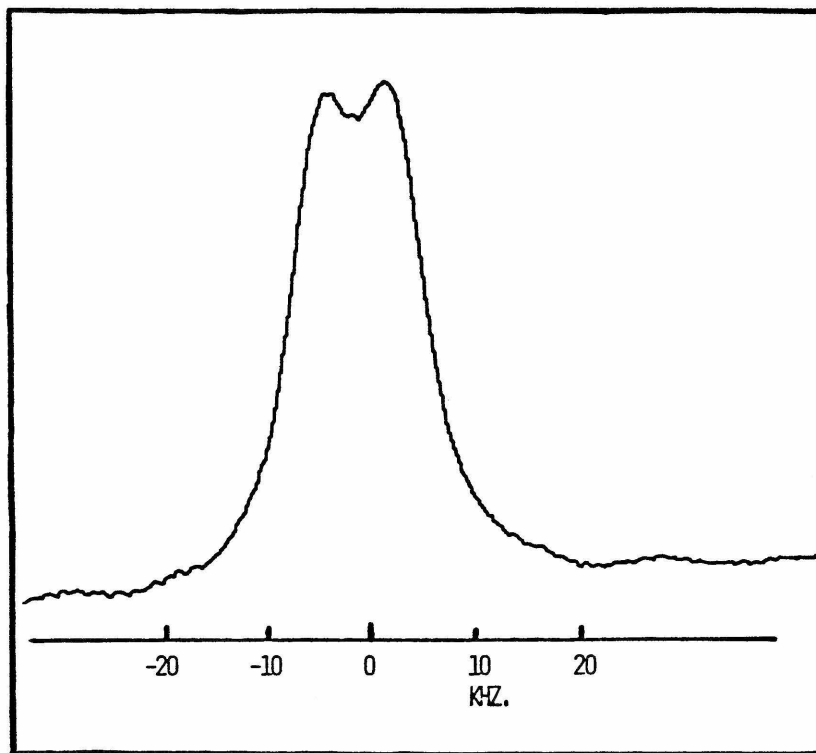
(d) Estimated molecular formula (see Table 1).

Figure Captions

Figure 1: Proton free-induction decay spectra for, from top to bottom, amorphous carbon, silicon carbide, silicon nitride and boron (cathode). Details of sample preparation conditions are shown in Table 1. At left are spectra at room temperature, at right, 125 K.

Figure 2: The $\frac{1}{2} \rightarrow \frac{1}{2}$ transition at room temperature of the "B spectra for a-B:H obtained at 86.8 Mhz. Note that there appear to be no motionally narrowed components.





Chapter 3

LOCAL BONDING ENVIRONMENTS IN AMORPHOUS SILICON
VIA MAGIC-ANGLE SAMPLE SPINNING NMR

(Much of Chapter 3 is from an article by J. A. Reimer, P. DuBois Murphy, B. C. Gerstein and J. C. Knights entitled "Silicon-29 Cross-Polarization Magic-Angle Sample Spinning Spectra in Amorphous Silicon-Hydrogen Films". This paper is scheduled for the January 1981 issue of the Journal of Chemical Physics.)

INTRODUCTION

The question of local hydrogen bonding environments in plasma-deposited amorphous silicon-hydrogen films has been addressed by vibrational spectroscopy in the recent literature (1-3). The interpretations of the various IR and Raman transitions, as shown in Table 1, are by no means well accepted, but nonetheless have been used to characterize films in attempts to model the structural origin of defects which act on non-radiative recombination centers and limit the luminescence efficiency in these films (4). Thus, it appears that quantitative characterization of local bonding environments in a-Si:H films may be important in terms of understanding both microstructure and defect chemistry.

Recent years have seen the development of NMR techniques (20) that allow near liquid spectra resolution for both dilute spins, such as ^{13}C or ^{29}Si , and protons in solids. In particular, magic-angle sample spinning (5,6), cross polarization and high power decoupling (7-10) between dilute spins and abundant protons, and proton multiple pulse dipolar narrowing (16-19) are techniques which have been developed for quantitative/qualitative NMR in solids. In the literature, there are several studies of disordered materials, such as polymers (6,11-13,19), where chemically distinct nuclei are resolved. We report here the first attempt to use both ^{29}Si and proton high resolution solid state NMR techniques to address the qualitative and quantitative question of local silicon-hydrogen bonding environments in plasma-deposited a-Si:H films.

Methods and Materials

The spectrometer used in these experiments has been described previously (23,24). Resonant frequencies for ^1H and ^{29}Si were 56.03 and 11.13 MHz, respectively. A single-coil doubly-tuned probe (24 - 26) was used. The Hartmann-Hahn condition (7) for cross-polarization was matched with rotating-frame fields: H_1 (proton) equal to 8 Gauss and H_1 (silicon-29) equal to 40 Gauss with the 8G proton irradiation also used for decoupling. For ^{29}Si experiments, varying the contact time for cross-polarization from 50 microseconds to 6 milliseconds only changed the observed signal-to-noise ratio; hence, only the data obtained at $T_{\text{CP}} = 6$ msec are shown here. Rotation rates for both ^{29}Si and ^1H data were typically 2.2 kilohertz. Accumulation of 5300 - 6500 acquisitions, with 15 - 20 seconds allowed between acquisitions to account for full proton spin-lattice relaxation, yielded the ^{29}Si spectra discussed herein. For ^1H spectra, between 350 and 1250 acquisitions were accumulated. The BR-24 pulse cycle (18) was utilized to remove homonuclear dipolar interactions while magic-angle spinning removed chemical shift anisotropies [CRAMPS, (19)]. The cycle time for the 24-pulse cycle was 36 μ seconds.

The samples were prepared in an rf-diode deposition system, details of which have been published elsewhere (27). Three samples were chosen that represent a proton content varying from 33 to 8 atom% produced by varying of the deposition parameters. Table 2 details the preparation conditions and the hydrogen content measured from the area of the proton to FID spectra. The samples were deposited on ~ 2 -inch diameter aluminum foil substrates in thicknesses from 20 to 110 μ resulting in sample

masses in the range $\sim 0.1 - 0.25$ grams after removal of the substrates with dilute acid etch.

Results

Figure 1 shows the **silicon-29** NMR spectrum of the room temperature anode sample obtained under conditions of cross-polarization by ^1H , and strong proton decoupling (top curve labeled X-POL), and with the addition of magic-angle sample spinning (X-POL, MASS). The full width at half maximum for the spectrum under MASS is 50.8 ppm, only 40% narrower than the 81.5 ppm spectrum obtained without spinning. Figure 2 compares the spectra of the RT anode and RT cathode samples under MASS. The center-of-mass of the RT anode and RT cathode spectra are 50.4 and 41.6 ppm upfield (shielded) with respect to TMS, respectively. The difference of the RT anode and RT cathode spectra is also shown in Figure 2; the RT anode spectrum clearly has components further upfield than the RT cathode spectrum.

The lack of narrowing of the cross-polarization spectra upon magic-angle spinning combined with lack of lineshape changes upon varying the contact time for cross-polarization (28) are indicative of large dispersions in the chemical shift of the silicon-29 nuclei. The contribution of bulk susceptibility to these magic-angle spectra may be estimated from combined multiple pulse/magic-angle sample spinning spectra (Figure 3) of the protons in these samples and is found to be less than 3 ppm. Thus the majority of the broadening in the magic-angle spectra must be due to variations in the local electronic environment of the silicon-29 nuclei.

The comparison of the RT anode and RT cathode spectra in Figure 2 is useful in light of an analogous comparison of their IR and Raman spectra. The RT anode film has IR and Raman bands attributed to polysilane $(\text{SiH}_2)_n$ bonding environments (3) which are lacking in the cathode film. These bonding environments are expected to yield silicon NMR resonances shifted to higher field — based upon analogies in liquid ^{29}Si chemical shifts (6,7). Figure 2 shows that the RT anode film does indeed have higher field components than the RT cathode film, consistent with the IR identification of polysilane-type local bonding.

Figure 3 and Table 3 show the ^1H proton CRAMPS data for films A and C. Again, local bonding environments are not discernible due to the 2 - 3 ppm susceptibility or dispersion effects. The ~ 2 ppm downfield shift of the protons in sample C is most likely due to susceptibility effects since sample A has ~ 200 ppm unpaired spins associated with dangling bonds while sample C has < 1 ppm of unpaired spins (1 - 3).

We conclude that these ^1H NMR spectra yield no information on the distribution of local bonding environments. However, as noted previously, the observed linewidths place an upper bound of ~ 3 ppm on the contributions of bulk susceptibility to the ^{29}Si chemical shifts.

Conclusions

In summary, we have presented both ^{29}Si and ^1H high resolution solid state NMR data in an effort to determine the local bonding environments of hydrogen on silicon in plasma deposited a-Si:H. These data show large chemical shift dispersions which we attribute to extensive

disorder in the silicon lattice. The ^{29}Si spectra yield qualitative agreement with the infrared assignment of $(\text{SiH}_2)_n$ species in room temperature anode films.

We gratefully acknowledge support from the National Science Foundation under Grant # DMR-77-21394.

Table 1

Structural Group	Bond Stretching	Bond Bending	Bond Rocking
SiH	2000	-	630
SiH ₂	2090	880	630
SiH ₃	2140	860 905	630
(SiH ₂) _n	(2090 - 2100)	845 890	630

Vibrational frequencies for H-containing units. The numbers in parentheses give the range of frequencies found in samples produced under different conditions. The mode at 845 cm⁻¹ for (SiH₂)_n is most probably a bond-wagging mode made active through anⁿintrachain coupling.

Table 2

Sample	Conditions ^(a)	Hydrogen ^(b) Content (at %)
A	5%; 18W; 25 C (A)	32.2
B	5%; 18W; 25 C (C)	16.3
C	100%; 2W; 230 C (A)	7.8

^aThe conditions refer to percentage silane in gas (diluent argon), rf power (net into matching network), and substrate temperature. (A) and (C) distinguish between deposition on grounded electrode (anode) or hot rF electrode (cathode).

^bDetermined from integrated proton spin density and sample weight.

Table III
Magic-Angle NMR Data

Sample	Nucleus	FWHM ^(A)	$\bar{\sigma}$ ^(A)
A	²⁹ Si	50.8	50.4
	¹ H	2.49	0.0 ^(B)
B	²⁹ Si	49.7	41.6
C	¹ H	2.98	-1.91

^AIn parts per million (ppm) where 1 ppm = 11.1 hertz for Si and 55.4 hertz for H.

^BArbitrary set to zero.

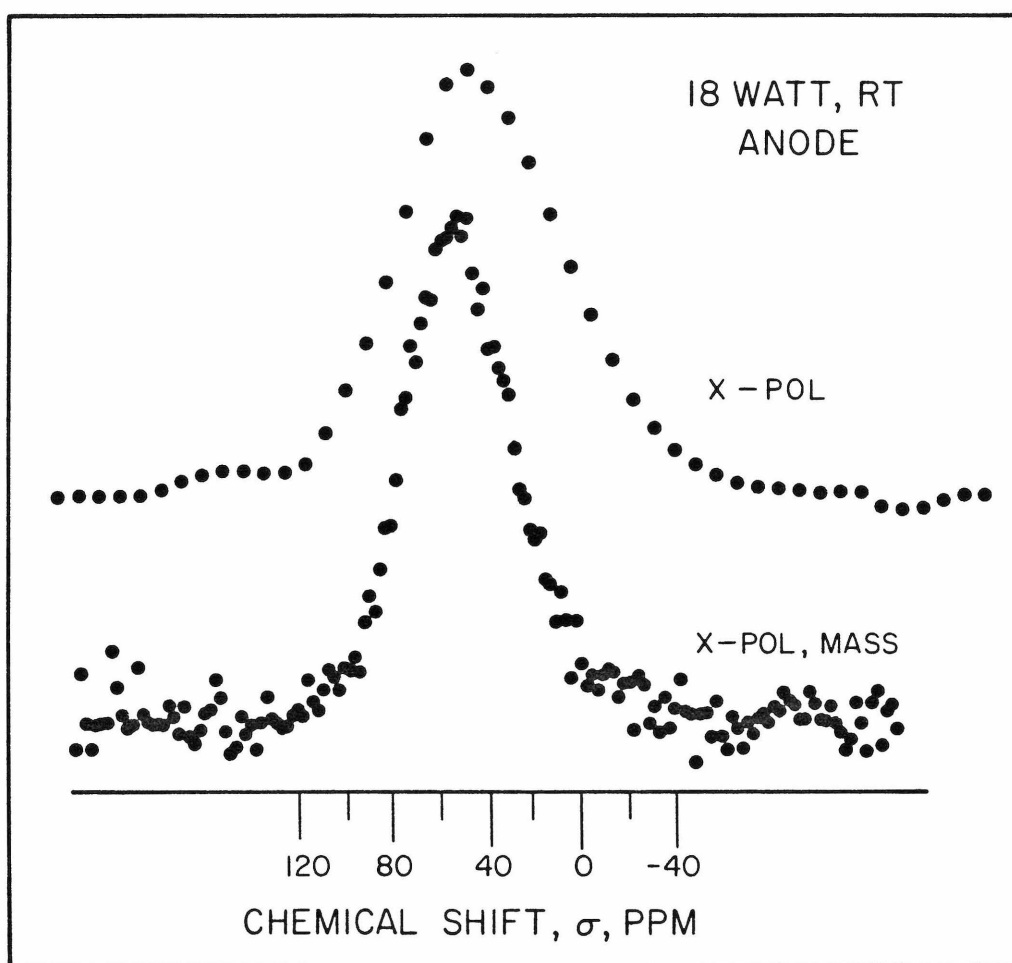
References

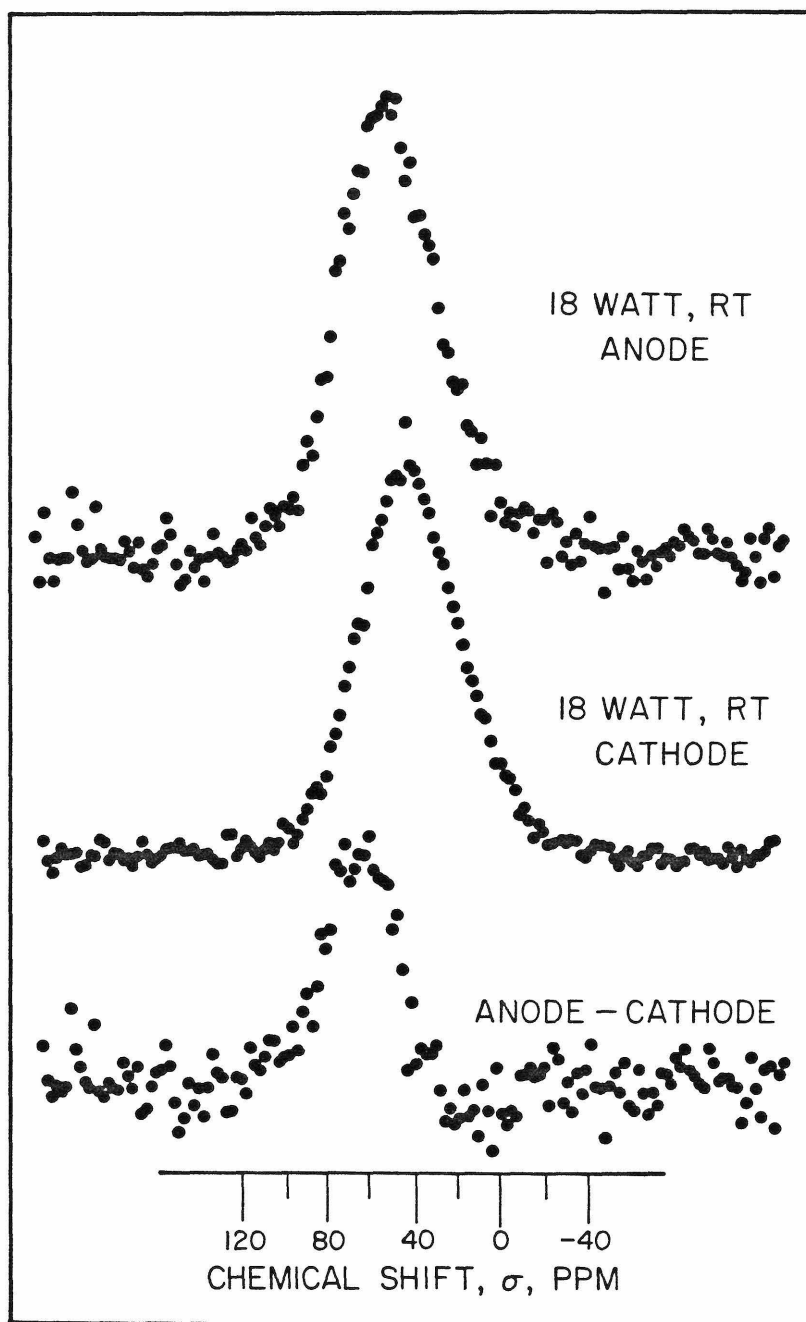
1. M. M. Brodsky, M. Cardona, J. J. Cuomo, Phys. Rev. B 16, 3556 (1977).
2. J. C. Knights, G. Lucovsky, R. J. Nemanich, Phil. Mag. B 37, 467 (1978).
3. G. Lucovsky, R. J. Nemanich, J. C. Knights, Phys. Rev. B 19, 2064 (1979).
4. J. C. Knights, G. Lucovsky, R. J. Nemanich, J. Non-Crys. Solids 32, 393 (1979).
5. E. R. Andrew, Prog. in NMR Spectroscopy 8, 1 (1971).
6. J. Schaefer, E. O. Stejskal, R. Buchdahl, Macromolecules 8, 291 (1975).
7. S. R. Hartmann, E. L. Hahn, Phys. Rev. 128, 2042 (1962).
8. A. Pines, M. G. Gibby, J. S. Waugh, J. Chem. Phys. 59, 569 (1973); J. Chem. Phys. 56, 1776 (1972).
9. F. Bloch, Phys. Rev. 111, 841 (1958).
10. L. R. Sarles, R. M. Cotts, Phys. Rev. 111, 853 (1958).
11. J. Schaefer, E. O. Stejskal, R. Buchdal, Macromolecules 10, 384 (1977).
12. A. N. Garroway, W. B. Moniz, H. A. Resing, ACS Symposia Series (1979).
13. A. N. Garroway, W. B. Moniz, H. A. Resing, Faraday Symposium 13 (1979).
14. M. Alla, E. Lippmaa, Chem. Phys. Lett. 15, 373 (1976).
15. D. L. VanderHart, A. N. Garroway, J. Chem. Phys. 71, 2773 (1979).
16. M. Mehring, High Resolution NMR Spectroscopy in Solids in NMR: Basic Principles and Progress 11 (Springer-Verlag, Berlin, 1976).

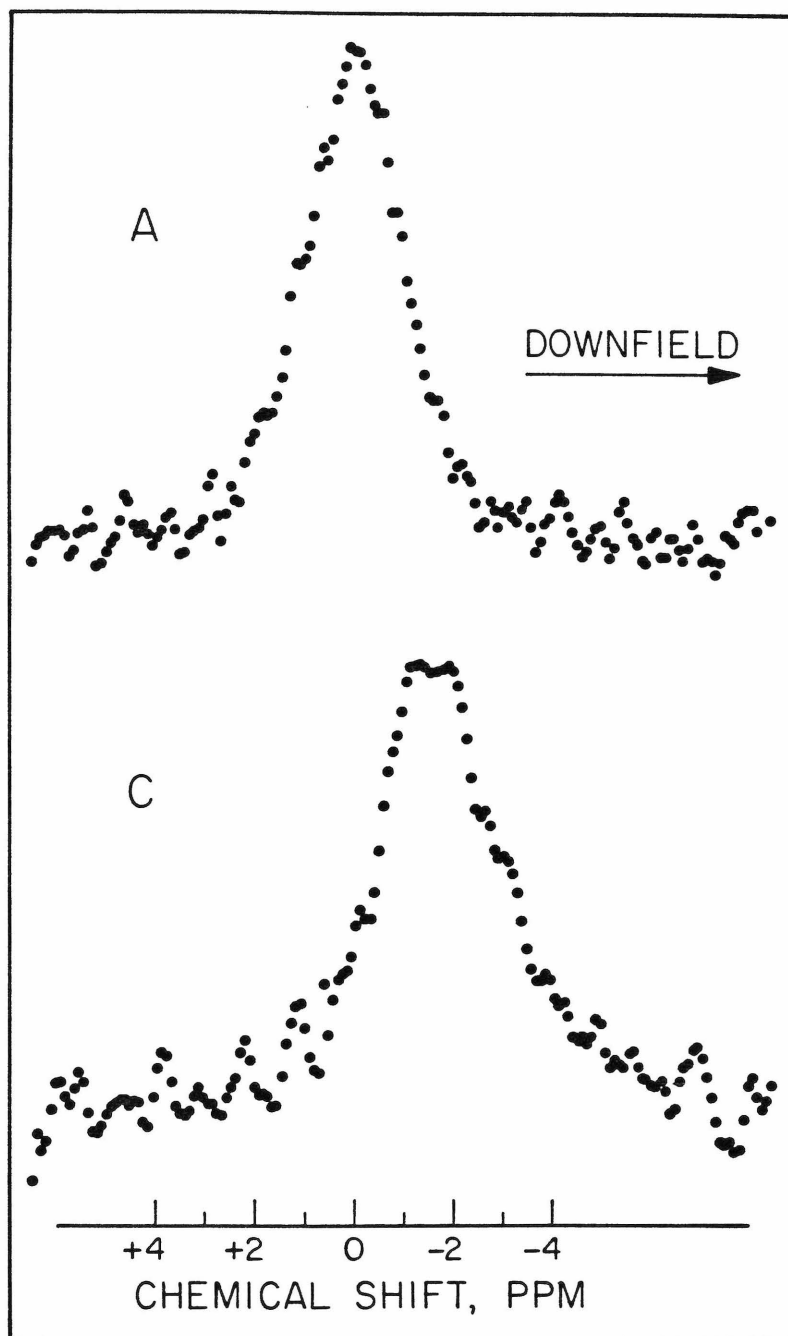
17. U. Haeberlen, High Resolution NMR in Solids in Adv. in Mag. Resonance Supp. 1 (1976).
18. D. P. Burum, W. K. Rhim, J. Chem. Phys. 71, 944 (1979).
19. L. M. Ryan, R. E. Taylor, A. J. Paff, B. C. Gerstein, J. Chem. Phys. 72, 508 (1980).
20. R. W. Vaughan, Ann. Rev. Phys. Chem. 29, 397 (1978).
21. G. R. Holzman, P. C. Lauterbur, J. H. Anderson, W. Koth, J. Chem. Phys. 25, 172 (1956).
22. G. C. Levy, J. D. Cargioli in Nuclear Magnetic Resonance Spectroscopy of Nuclei Other Than Protons, eds. T. Axenrod and G. A. Webb, Wiley and Sons, New York (1974).
23. B. C. Gerstein, C. Chow, R. G. Pembleton, R. C. Wilson, J. Phys. Chem. 81, 565 (1978), and references therein.
24. P. D. Murphy, PhD Thesis, Iowa State University, 1979.
25. P. D. Murphy, B. C. Gerstein, "The Design of a Single Coil Double Resonance NMR Probe for Combined Magic Angle Spinning Double Resonance Experiments", No. IS-4388, Ames Laboratory, DOE, Ames, Iowa 50011.
26. P. D. Murphy, B. C. Gerstein, "Analysis and Computerized Design of NMR Probe Circuits", No. IS-4436, Ames Laboratory, DOE, Ames, Iowa 50011.
27. R. A. Street, J. C. Knights, D. K. Biegelsen, Phys. Rev. B 18, 1880 (1978).
28. Varying the contact time allows for the determination of contributions to the ^{29}Si linewidth due to motion on the time scale of the cross-polarization time. For details see Reference 16.

Figure Captions

- Figure 1: Cross-polarization (top) and cross-polarization with magic-angle sample spinning (bottom) spectra for an 18 watt room-temperature anode amorphous silicon:hydrogen film. The full width at half maximum for the top spectrum is 81.5 ppm; 50.8 ppm for the lower spectrum. Increasing field is from right to left.
- Figure 2: Cross-polarization with magic-angle sampling spinning spectra of (top) the 18 watt room-temperature anode film and (middle) the 18 watt room-temperature cathode film. At the bottom is the difference (anode - cathode). Increasing field is from right to left.
- Figure 3: Combined proton multiple pulse magic angle sample spinning spectra for sample A (room-temperature anode) (top), and sample C (230^oC anode) (bottom). The chemical shift scale arbitrarily reference to the center-of-mass of sample A. Increasing field is from right to left.







Chapter 4

DISORDER MODES IN AMORPHOUS SILICON-HYDROGEN FILMS
AS DETERMINED BY PROTON SPIN-LATTICE RELAXATION

(Chapter 4 is essentially an article by J. A. Reimer, R. W. Vaughan and J. C. Knights entitled "Proton Spin-Lattice Relaxation in Plasma-Deposited Amorphous Silicon-Hydrogen Films". This paper has been submitted to the Physical Review B.)

ABSTRACT

Proton spin-lattice relaxation data are presented for several plasma-deposited amorphous silicon-hydrogen films when (i), homonuclear dipolar interactions are suppressed, (ii), deuterium is isotopically substituted for hydrogen, and (iii), films are annealed. These data are consistent with a model in which proton nuclei are relaxed by hydrogen-containing disorder modes. Analysis of these data shows that the density of disorder modes is ~30% higher in the low hydrogen density domain and that more than one hydrogen nucleus is associated with each disorder mode. The behavior of T_1 upon annealing indicates that a small fraction of unpaired spins or "dangling bonds" may be associated with the disorder modes. These results suggest that the role of hydrogen in amorphous silicon is more complex than passivation of "dangling bond" intrinsic defects.

1. INTRODUCTION

Hydrogenated amorphous silicon (a-Si:H) has attracted a great deal of attention recently because of its remarkable electronic properties vis-à-vis pure amorphous silicon. The hydrogenated material (1), prepared either by glow discharge of silane or reactive sputtering, has a large photoconductivity, efficient photoluminescence, and a very low concentration of unpaired electron spins associated with dangling bonds. Because the hydrogen apparently passivates (2) the large number of these unpaired spins found in pure amorphous silicon, controlled doping of hydrogenated films has led to the development of p,n and Schottky barrier junctions (3-5), as well as moderately efficient solar cells (6).

More recently, a variety of proton nuclear magnetic resonance (NMR) data have posed some new questions on the role of hydrogen in both electronic and structural properties of plasma-deposited inorganic films. Linewidth and lineshape results (7) have shown that plasma-deposited a-Si:H is characterized by two domains which differ in the local density of hydrogen. Furthermore, upon annealing (8) hydrogen in the less clustered domain diffuses internally concomitant with the reduction of paramagnetic center density (9). Proton spin-lattice relaxation measurements in a-Si:H have also been reported recently (10) and were explained by postulating the existence of hydrogen-containing disorder modes that may contribute to the electronic states within the band gap. In fact such disorder modes have been observed directly by us using proton NMR in amorphous boron, carbon, and silicon nitride (11).

The purpose of this work is to investigate the proton spin-lattice relaxation behavior in a-Si:H in detail in order to ascertain the validity of the disorder mode relaxation model and examine the structural details of both the disorder modes and their distribution in the film. An understanding of these details is expected to aid in discerning the relationship between film microstructure and defects which contribute to non-radiative recombination processes and limit luminescence efficiency. In this paper we present proton spin-lattice relaxation behavior when: (i), homonuclear dipolar interactions are suppressed; (ii), deuterium is isotopically substituted for hydrogen; and (iii), films are annealed under conditions which produce rapid changes in unpaired spin density and lumin-

escence efficiency. The data provide additional evidence for the relaxation model of Carlos and Taylor (10) and yield new information on the distribution of hydrogen-containing disorder modes within the film, the number of hydrogen nuclei within the disorder modes, and the association of "dangling bond" paramagnetic centers with the disorder modes.

2. EXPERIMENTAL

Magnetic resonance data were taken with an NMR spectrometer previously described (12) with an operating frequency of 56.4 Mhz (1.3Tesla). Proton spin-lattice relaxation times (T_1) were determined by the inversion recovery method (13). Proton spin-lattice relaxation times while homonuclear dipolar interactions were suppressed were determined by the T_{1y} method (14). We shall briefly review the T_{1y} technique since it is relatively new and only recently received attention in the literature (14,18,30).

In order to suppress homonuclear dipolar interactions an eight pulse cycle (15),

$$\tau^*-P_x-\tau-P_y-2\tau-P_y-\tau-P_x-2\tau-P_x-\tau-P_y-2\tau-P_y-\tau-P_x-\tau,$$

was applied to the spins. Here P_x , etc., denote 90° pulses in the directions x , etc., and τ and 2τ stand for the pulse separations. At the point τ^* in the cycle the magnetization is sampled and stored in a transient recorder. The cycle is repeated 1024 times, continuously, and the magnetization is thus "stroboscopically" observed. The effective rotating frame Hamiltonians for the spins under this pulse cycle have been calculated previously (15,19,20) via the Magnus expansion approach and yield the homonuclear dipolar interaction to be zero to second order. The chemical shift Hamiltonian becomes (15)

$$\overline{H}_{CS}^{(0)} = \sum_i \frac{\alpha(\Delta\omega + \omega_0\sigma_{ZZi})}{3} (I_{xi} + I_{zi})$$

where α is the chemical shift scaling factor, ω_0 the resonant frequency of the spins, $\Delta\omega$ the amount the applied rf differs from ω_0 , and σ_{ZZ} the chemical shift tensor component for the I spin. This Hamiltonian is thus in the (101) direction and, in geometric terms, the initial magnetization may be thought of as precessing about the (101) direction.

In the T_{1y} experiment a 90_x^0 or 90_{-x}^0 preparatory pulse is used to place the total thermally induced magnetization parallel to the y direction. While applying this eight pulse sequence on resonance a phase error of ~ 2 kHz in the x-pulses is introduced which gives rise to a y Hamiltonian,

$$\overline{H}_P(0) = \frac{2}{t_c} (-\phi_x + \phi_{-x}) I_y \quad ,$$

where t_c is the eight pulse cycle time and ϕ_x is the phase misadjustment of the x pulses. Under this Hamiltonian the magnetization is forced to precess about the y-axis (perpendicular to the 101 direction) and thus "second averages" (19,20) chemical shift and field inhomogeneities to zero. The small non-fluctuating phase error Hamiltonian does not affect relaxation times (14); hence, the observed decay is due only to spin-lattice relaxation. However, the effective frequency for relaxation is not the Larmor frequency as in conventional T_1 measurements, rather, it is given by the cycle time of the eight pulse sequence. This is analogous to $T_{1\rho}$ "spin-locking" measurements (31) where the effective field is defined by the magnitude of the locking field. For these data a 50 microsecond cycle time was used for the eight pulse sequence, and the 90^0 pulse widths were less than 2 microseconds. The 90_x^0 and 90_{-x}^0 preparatory pulses were alternately applied and the data were cosubtracted with 100-200 acquisitions accumulated to improve the signal-to-noise ratio and eliminate baseline artifacts.

The samples were prepared in an rf-diode deposition system, details of which have been published elsewhere (16). Five samples were prepared that represent a proton content of 31 to 7 atom % by varying the deposition parameters. The hydrogen content was determined by using the integrated proton spin density and the sample weight. The samples were deposited onto 2 inch diameter aluminum foil substrates in thicknesses of approximately 10 microns, resulting in sample masses of 50 milligrams after removal of the substrates with a dilute hydrochloric acid etch. The notation for the deposition conditions used in the text are as follows: (5% SiH_4/Ar , 18W, RT, C) refers to deposition from 5% silane diluted in argon, a rf power (net into matching network) of 18 watts, a substrate tempera-

ture of 25⁰C, and deposition onto the hot rf electrode (cathode), as opposed to the grounded electrode (anode). Some samples were then placed in a quartz NMR tube and isochronally annealed at various temperatures under flowing nitrogen for 20 minutes. The NMR data were taken after cooling the sample to room temperature subsequent to each increase of 50⁰C in the annealing temperature. The spectra of annealed samples were independent of temperature down to 80⁰K and field in the range 6.3 to 1.3 Tesla. All spin-lattice relaxation rates ($T_1^{-1} = R_1$) were also found to be field independent in the same range.

3. RESULTS

A. Proton Spin-Lattice Relaxation under Conditions of Suppressed Homonuclear Dipolar Interactions

Figure 1 shows the T_{1y} decay of the magnetization for a high (29 atom %) proton content sample (100% SiH₄, 2W, RT, A). The decay is clearly non-exponential. The curves are from models discussed later in the text.

Figure 2 shows the temperature dependence of the initial and final slopes of the T_{1y} decay on an Arrhenius plot. The activation energies from Figure 2 are 276 ± 30 calories·mole⁻¹ for the initial slope and 214 ± 50 calories·mole⁻¹ for the final slope.

Since the two-component dipolar-broadened spectra for these films are due to spatially isolated proton dipolar reservoirs (7), the non-exponentiality in Figure 1 may be due to the two proton environments having different relaxation times (T_{1y}). In order to test this hypothesis, the Fourier-transformed free induction decay spectrum of the sample shown in Figure 1 was compared to the spectrum after "spin-locking" the magnetization under T_{1y} conditions for a time equal to three times the initial T_{1y} of Figure 1. Figure 3 shows the "spin-locked" spectrum, (A), the normal spectrum, (B), and the difference. A fit of both spectra to the sum of a Gaussian (broad component) and a Lorentzian (narrow component) yields spectrum A to be 87.6% broad (12.4% narrow) and spectrum B to be 80.0% broad (20.0% narrow). Figure 3 thus shows the narrow component, on the average, has a shorter T_{1y} than the broad component.

B. The Effect of Deuteration on T_1 and T_{1y}

Table 1 shows the deposition conditions for four samples which may be considered in pairs. Each of the two pairs has deposition conditions that differ only by their dilutant gas. In one case, the gas is hydrogen and, in the other, deuterium. Neglecting isotopic effects in the plasma chemistry during film growth, Table 1 shows that between 20 and 40% of the hydrogen has been replaced by deuterium when films are deposited in deuterium. Included in Table 1 are the spin-lattice relaxation rates (T_1^{-1}) as well as the initial and final rates (T_{1y}^{-1}) when homonuclear dipole-dipole interactions are suppressed. Figures 4 and 5 show T_{1y} data for the four samples described in Table 1. These data clearly show T_{1y}^{-1} to be proportional to hydrogen content and T_1^{-1} almost insensitive to a factor of 3 change in hydrogen content.

C. The Effect of Annealing on T_1

Two samples, (5% SiH₄/Ar, 18W, RT, C) and (5% SiH₄/Ar, 18W, RT, A), were annealed and monitored for changes in hydrogen content and T_1 . Figure 6 shows the changes in hydrogen content for the two samples normalized to unity (as deposited, the samples have different hydrogen contents (7)). The apparent increase in the hydrogen content in the anode sample is not due to adsorption of atmospheric gases as the sample was kept under dry nitrogen. Also extended evacuation did not affect the NMR lineshape or hydrogen content. Figure 7 shows a comparison of the spin density determined by ESR (from Reference 9) and T_1 for the two annealed samples. Although the anode T_1 data follow the spin density, the sensitivity is quite low: a change of two orders of magnitude in spin density produces less than a factor of two change in T_1 . The cathode sample T_1 data have no straightforward relation to the spin density.

4. DISCUSSION

A. T_{1y} and Disorder Modes

A recent study (10) of NMR spin-lattice relaxation rates (T_1^{-1}) in a-Si:H films has shown that there is a maximum near 40 K and that the temperature and frequency dependence of T_1 are well described by a model which

assumes that a small fraction of the hydrogen atoms are coupled to disorder modes. One consequence of this model is that the observed relaxation rate is the result of two processes: (i) spin relaxation for nuclei at the disorder mode, and (ii) spin diffusion that occurs between neighboring spins. The model is analogous to relaxation in solids due to dilute paramagnetic centers (17) where spin diffusion carries to remote nuclear spins the information on the lattice temperature dispensed by electron spins. In these films, however, the role of the paramagnetic center is played by hydrogen nuclei experiencing rapidly fluctuating magnetic fields due to hopping over the potential barrier separating two equilibrium positions of a disorder mode.

Recent developments (14,18) in multiple pulse schemes for high-resolution NMR in solids (19,20) have furnished a means to measure proton spin-lattice relaxation times while suppressing homonuclear dipolar interactions with an eight-pulse cycle (15). This experiment allows for a determination of spin-lattice relaxation in a-Si:H in the absence of spin diffusion (21,22). According to the above model, such a measurement is expected to be analogous to spin-lattice relaxation of isotopically dilute spins, such as ^{13}C , by randomly distributed paramagnetic centers (23). Nuclei close to the disorder mode are expected to relax quickly, while nuclei far away should relax more slowly since (14), in the fast motion limit,

$$\frac{1}{T_{1y}} = \frac{2}{3} \Delta m_2 \tau \propto \frac{A}{r^6} \tau \quad (1)$$

where τ is the correlation time of the hydrogen nuclei in the disorder mode, Δm_2 the fluctuating field due to hydrogen in the mode, and r the distance between the disorder mode and the nucleus being relaxed. In a disordered material such as a-Si:H one might expect a random distribution of the disorder modes so that an expression $N(T_{1y})$ may be written based on Equation (1) which gives the number of nuclei at a given T_{1y} . The magnetization then behaves as (23)

$$m(t) = \int_0^{T_{1y}^{\text{MAX}}} N(T_{1y}) e^{-t/T_{1y}} dT_{1y} \quad (2)$$

One thus expects a non-exponential decay of the magnetization.

The data in Figure 1 show that the decay of the magnetization in the T_{1y} experiment is indeed non-exponential. This is consistent with the disorder mode model. Also, if we assume τ is due to a simple activated process,

$$\tau = \tau_0 e^{\Delta E/kT} \quad (3)$$

then a plot of $\ln(T_{1y})$ versus $\frac{1}{T}$ yields ΔE . Figure 2 shows the initial and final T_{1y} times to be consistent with Arrhenius behavior. The calculated ΔE of ~ 250 calories \cdot mole $^{-1}$ is slightly larger than that observed in the T_1 measurements (10), ~ 160 calories \cdot mole $^{-1}$. However, such differences are to be expected as sample preparation conditions differ between the two experiments.

Further insight on the distribution of disorder modes can be derived from these T_{1y} data according to explicit models for $N(T_{1y})$ given in Equation 2. Since the hydrogen atoms are in two spatially isolated regions of the film with differing spin densities (7), a particularly simple model may be the sum of two exponentials in which the weighting of the two terms is given by the proportion of hydrogen in the high and low density hydrogen domains and the time constants of the terms are given by the initial and final time constants in the T_{1y} decay shown in Figure 1 (32). This calculation yields the dotted line in Figure 1; clearly a poor match to the experimentally observed decay.

A second model for Equation 2 is one in which the disorder modes are distributed at random throughout the film. Using Equation (1) $N(T_{1y})$ may be calculated readily, and T_{1y}^{MAX} is determined by a fit to the data. The solid lines in Figure 1 show this calculation for two different values of T_{1y}^{MAX} , one to best fit the initial decay and the second to best fit the final decay. Neither is a good fit to the full range of experimental data. Clearly, these models for $N(T_{1y})$ in Equation (2) are insufficient to explain the data. The most appropriate model may be one which involves modifying Equation (2) to include two terms that differ only by $N(T_{1y})$. More precisely, two random distributions may be considered with the average density of disorder modes in each distribution differing. An interesting question would then be whether or not the two different domains of disorder mode density correspond

to the two different domains of hydrogen density. The results for an experiment designed to test this hypothesis are shown in Figure 3. By " T_{1y} spin-locking" the magnetization for a period of three times the initial time constant, we remove from the spectrum those components which decay quickly. If one domain of hydrogen has a higher density of disorder modes than the other, we would expect the lineshape due to that domain to be depleted relative to the other lineshape by spin-locking. Figure 3 shows that the spin-locked spectrum for the sample shown in Figure 1 is depleted in the narrow component relative to the normal spectrum. We conclude that the density of defect sites is higher in the less clustered hydrogen domain. The lineshape analyses show that the average density of hydrogen-containing disorder modes is a factor of 1.3 higher in the less clustered hydrogen domain.

B. Deuterium Dilution

At room temperature (far above the T_1 minimum) the spin-lattice rate $T_1^{-1}(R_1)$ is expected to be governed by spin diffusion (10,17). The spin-diffusion constant (24) is proportional to density of proton spins. Thus, deuterium dilution of the hydrogen in a-Si:H would proportionately affect T_1^{-1} . Assuming there are no isotopic effects during film growth, Table 1 shows hydrogen content and R_1 to be directly proportional upon dilution of hydrogen with deuterium. These data confirm the importance of spin diffusion on the observed R_1 data away from the T_1 minimum. The T_{1y} data, however, are very insensitive to deuterium dilution. Since the T_{1y} data are not affected by spin diffusion, any changes or lack of changes would be due to the distribution of hydrogen about the disorder modes (Equation 1 and $N(T_{1y})$ in Equation 2). If the disorder modes contained only one hydrogen nucleus, then the density of hydrogen-containing disorder modes (and T_{1y}) would be proportional to the hydrogen content. Inspection of Figures 4 and 5 as well as Table 1 shows that T_{1y} is not proportional to hydrogen content. We conclude that each disorder mode must contain more than one hydrogen atom. This rules out the possibility that the disorder mode corresponds to a single monohydride (SiH) species rapidly exchanging with an unpaired spin or "dangling bond" defect.

C. Annealing Behavior of T_1

The role the dangling bond defects play in spin-lattice relaxation is not straightforward. This is made clear by inspection of Figures 6 and 7 which show changes in hydrogen content and T_1 as the films are annealed. Previous studies (8,9,25) have shown changes in ESR spin densities, vibrational spectra, and proton NMR lineshapes upon annealing. The following is a summary of the data from this work:

- (i) despite the fact that the unpaired spin density is the same as deposited for the anode and cathode films, the T_1 's differ by a factor of ~ 4 .
- (ii) in the annealing range of 20-200^o C where unpaired spin densities rapidly decrease, the T_1 's for the anode sample increase whereas the cathode film T_1 's are roughly constant.
- (iii) in the range 200-400^o C where unpaired spin densities increase, both anode and cathode T_1 's decrease.
- (iv) the observed hydrogen content (as determined by NMR intensities) for the anode sample increases in the range 20-200. When allowed to self-anneal at room temperature for several months, the hydrogen content in this sample stabilizes at $\sim 32\%$ with slight changes in hydrogen clustering (28). The hydrogen content in the cathode sample changes in a straightforward fashion described previously (8).
- (v) a previous ESR study (29) has shown that electron spin lineshapes in anode samples motionally narrowed for $N_S > 10^{19} \text{ cm}^{-3}$. The electron spin T_1 's are, however, still too long (10,17) to explain these proton T_1 data. Thus, we may rule out effects on proton relaxation due to paramagnetic centers (17).
- (vi) anode films have shorter T_{1y} values than cathode films deposited under the same conditions, and the anode film T_{1y} values are less sensitive to deuteration than cathode film values.

In view of these observations, we propose that a fraction of the unpaired spins is associated with the disorder modes and, in anode films, hydrogen nuclei are clustered nearer to the disorder modes than in cathode films. This would explain points (i), (iv), and (vi). The close proximity of hydrogen nuclei to

the unpaired spins in the anode film would broaden those proton spectra to the point that they would appear to lack any contribution to the observed lineshape. Hence, an artificially low hydrogen content would be observed. The increased local density of disorder modes would yield shorter T_1 's, T_{1y} 's, and less sensitivity to deuterium dilution as observed in this study. Observation (ii) may be explained by noting that in the range 20-200 the total number of unpaired spins, hence, the number of disorder modes that contain some fraction of these spins, is rapidly decreasing. The anode film T_1 's, sensitive to the density of disorder modes, would then increase. The cathode film T_1 's are insensitive to the decrease in unpaired spins (hence, density of disorder modes) due to the proton clustering away from disorder mode sites (as deposited, longer T_1 's, T_{1y} 's, and more sensitive to deuteration). The interpretations for observation (iii) are unclear although we have shown previously (8) in cathode films at annealing temperatures $T_A > 200^\circ \text{C}$ hydrogen diffuses internally and thus allows hydrogen nuclei to diffuse closer, on the average, to disorder modes. We conclude that it is likely that the hydrogen-containing disorder modes responsible for proton spin-lattice relaxation may be associated with a small fraction of the unpaired electron spins. The relationship of the different microstructures seen in anode and cathode films vis-à-vis the distribution of hydrogen about the disorder modes should be considered.

5. CONCLUSIONS

By using deuterium dilution and spin-lattice relaxation times while suppressing homonuclear dipolar interactions, we have obtained evidence supporting a hydrogen-containing disorder mode model of proton spin-lattice relaxation in plasma-deposited amorphous silicon-hydrogen films. A small fraction of hydrogen nuclei at these disorder modes have very short relaxation times and act as "sinks" for proton spin-lattice relaxation. The temperature dependence of these data agree with the T_1 measurement of Carlos and Taylor. Deuterium dilution experiments have shown that: (i) spin diffusion between neighboring nuclei dominates T_1 relaxation at temperatures far above the T_1 minimum, and (ii) that each disorder mode contains more than one hydrogen atom. Effects on the proton lineshape due to spin-

locking while suppressing homonuclear dipolar interactions show that the density of disorder modes is ~30% higher in the less clustered hydrogen domain. Finally, we have argued from the T_1 behavior upon annealing that, in addition to hydrogen nuclei, the disorder modes may contain a small fraction of the unpaired spin(s). The relationship between film microstructure, the distribution of the disorder modes, and the optical properties of these films warrants further investigation.

6. ACKNOWLEDGMENTS

The authors wish to thank R. A. Lujan for his expert assistance with sample preparations. The authors are grateful to Drs. S. I. Chan and T. M. Duncan for their help in preparing this manuscript and Dr. A. J. Vega for helpful discussions. This work was supported by the National Science Foundation under grant # DMR-77-21394.

References

1. H. Fritzsche, C. C. Tsai, P. Persans, Solid State Tech., Jan. 1978 (p. 55).
2. M. H. Brodsky and D. Kaplan, J. Non-Cryst. Solids, 32, 431 (1979).
3. W. Paul, A. J. Lewis, G. A. N. Connell, T. D. Moustakas, Solid State Common. 20, 969 (1976); G. A. N. Connell and J. R. Pawlik, Phys. Rev. B13, 787 (1976).
4. W. F. Spear, P. G. Le Comber, S. Kinmond, M. H. Brodsky, Appl. Phys. Lett. 28, 105 (1976).
5. D. E. Carlson and C. R. Wronski, Appl. Phys. Lett. 28, 671 (1976).
6. D. E. Carlson, EIII Trans. on Electron Dev. ED-24, 449 (1977).
7. J. A. Reimer, R. W. Vaughan, J. C. Knights, Phys. Rev. Lett. 44, 193 (1980).
8. J. A. Reimer, R. W. Vaughan, J. C. Knights, Solid State Commun., submitted
9. D. K. Biegelsen, R. A. Street, C. C. Tsai, J. C. Knights, Phys. Rev. B20, 4839 (1979).
10. W. E. Carlos and P. C. Taylor, Phys. Rev. Lett. 45, 358 (1980).
11. J. A. Reimer, R. W. Vaughan, J. L. Knights, R. A. Lujan, Appl. Phys. Lett., submitted.
12. R. W. Vaughan, D. D. Elleman, L. M. Stacey, W.-K. Rhim, J. W. Lee, Rev. Sci. Inst. 43, 1356 (1972).
13. T. C. Farrar and E. D. Becker, Pulse and Fourier Transform NMR (Academic Press, New York, 1971).
14. A. J. Vega and R. W. Vaughan, J. Chem. Phys. 68, 1958 (1978).
15. W.-K. Rhim, D. D. Elleman, and R. W. Vaughan, J. Chem. Phys. 59, 3740 (1973).
16. R. A. Street, J. C. Knights, and D. K. Biegelsen, Phys. Rev. B18, 1880 (1978).
17. A. Abragam, The Principles of Nuclear Magnetism (Clarendon, Oxford, England, 1961).
18. A. J. Vega, A. D. English, and W. Mahler, Jour. Mag. Res. 37, 107 (1980).
19. U. Haeblerlen, Adv. Magn. Reson. Suppl. 1 (1976).
20. M. Mehring, NMR Basic Principles Prog. 11 (1976).
21. D. Tse and S. R. Hartmann, Phys. Rev. Lett. 21, 511 (1968).

22. J. I. Kaplan, Phys. Rev. B3, 604 (1971).
23. T. M. Duncan, J. T. Yates, Jr., and R. W. Vaughan, Jour. Chem. Phys., 73, 975 (1980).
24. Reference 17 shows $D \sim Wa^2$, where W is the probability of mutual spin flips between neighbors ($\sim \sqrt{M_2}/30$) separated by distance a . Light deuterium dilution is expected to change the second moment ($M_2 \propto \frac{1}{r^6}$), but the average value of "a" should remain roughly constant.
25. C. C. Tsai and H. Fritzsche, Solar Energy Mat. 1, 29 (1979).
26. J. C. Knights and R. A. Lujan, Appl. Phys. Lett. 35, 244 (1979).
27. A. J. Leadbetter, A. A. M. Rashid, R. M. Richardson, A. F. Wright and J. C. Knights, Solid State Comm. 33, 973 (1980).
28. J. A. Reimer, R. W. Vaughan, J. C. Knights, manuscript in preparation.
29. R. S. Title, M. H. Brodsky, and J. J. Cuomo, in Proceedings of the 7th International Conference on Amorphous and Liquid Semiconductors, edited by E. W. Spear (University of Edinburgh, Edinburgh, 1977), p. 424.
30. A. J. Vega and A. D. English, Macromolecules, scheduled for Nov. 1980.
31. M. Goldman, Spin Temperature and Nuclear Magnetic Resonance in Solids, (Oxford U. P. , London, 1970).
32. $T_{1y}^{\text{initial}} \sim T_{1y}^{\text{a}} \left[\frac{p_1 + p_b}{p_a} \right]$, where p_a and p_b are the populations of the narrow and broad components, respectively.

TABLE 1

(a) Sample	(b) Atom % H	(c) R_1 (seconds ⁻¹)	(c) $R_{1y}(\text{initial})$ (seconds ⁻¹)	(c) $R_{1y}(\text{final})$ (seconds ⁻¹)	$\frac{\text{atom\% H}_2}{\text{atom\% D}_2}$	$\frac{R_{1H_2}}{R_{1D_2}}$	$\frac{\text{initial } R_{1yH_2}}{\text{initial } R_{1yD_2}}$	$\frac{\text{final } R_{1yH_2}}{\text{final } R_{1yD_2}}$
5%SiH ₄ /H ₂ ,19W RT,A	25.7	0.63 ± .01	31.6 ± 0.1	10.6 ± 0.1				
					2.5	2.4	1.0	1.3
5%SiH ₄ /D ₂ ,18W RT,A	10.1	0.2 ± .01	32.5 ± 0.1	8.1 ± .01				
					4.4	4.0	1.2	2.2
5%SiH ₄ /H ₂ ,18W RT,C	31.1	0.67 ± 0.1	29.3 ± 0.1	6.1 ± 0.1				
					4.4	4.0	1.2	2.2
5%SiH ₄ /D ₂ ,18W RT,C	7.0	0.17 ± .01	23.5 ± 0.1	2.8 ± 0.1				

(a) Notation for sample preparation conditions is explained in the text.

(b) Determined from integrated proton spin density and sample weight.

(c) $R_1 = \frac{1}{T_1}$; $R_{1y} = \frac{1}{T_{1y}}$

FIGURE CAPTIONS

Figure 1: Decay of magnetization while suppressing homonuclear dipolar interactions (T_{1y}) for an a-Si:H sample prepared under the conditions shown. The dotted line is the sum of two exponentials weighted by the hydrogen content in the broad and narrow components of the Fourier transformed free induction decay. The two solid lines are calculations based on the random distribution of relaxation centers discussed in the text.

Figure 2: Initial and final slopes from T_{1y} data as a function of temperature. The activation energy from the initial decay (top) is 276 ± 30 calories/mole; the final decay (bottom) is 214 ± 50 calories/mole.

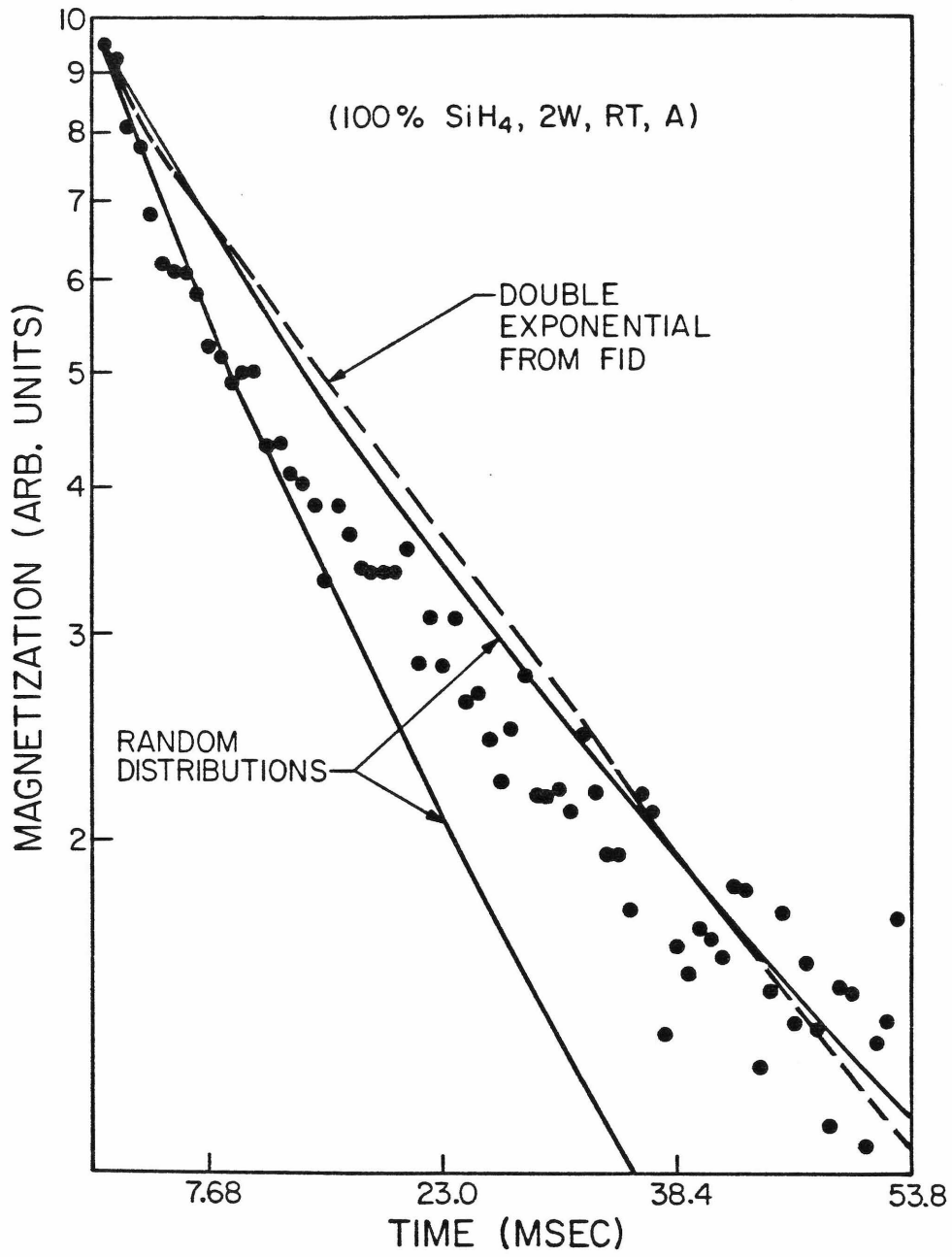
Figure 3: Fourier-transformed free induction decays for the (100% SiH₄, 2W, RT, A) sample. Spectrum A has been "spin-locked" under the conditions of the T_{1y} experiment (suppressed homonuclear spin diffusion) for a period of three times the initial decay time (Figure 1) and less than the final decay time. Spectrum B resulted from a single 90° pulse. At the bottom is the difference of A and B.

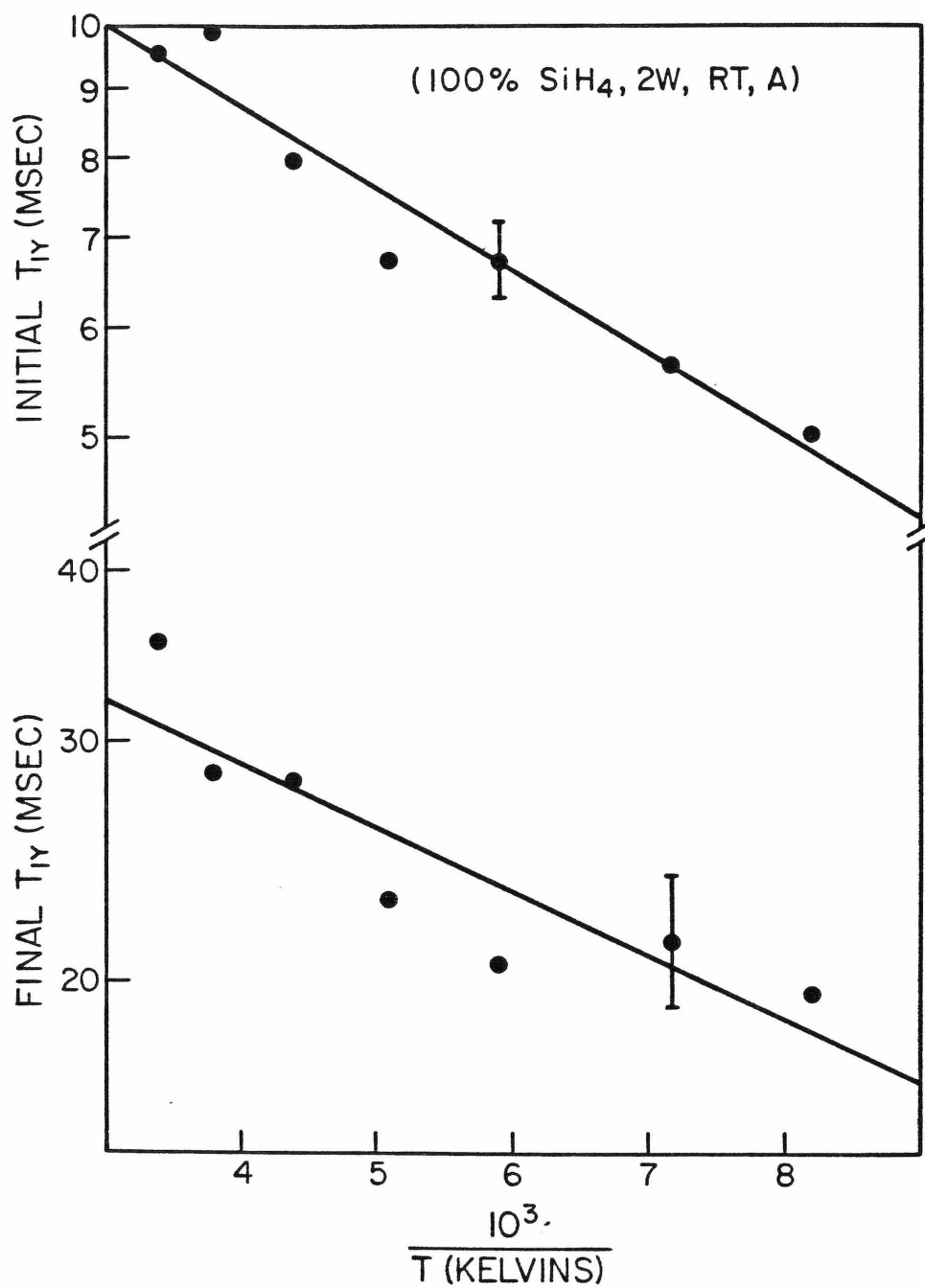
Figure 4: Comparison of T_{1y} decays for the samples deposited in deuterium and hydrogen on the hot rf electrode (cathode).

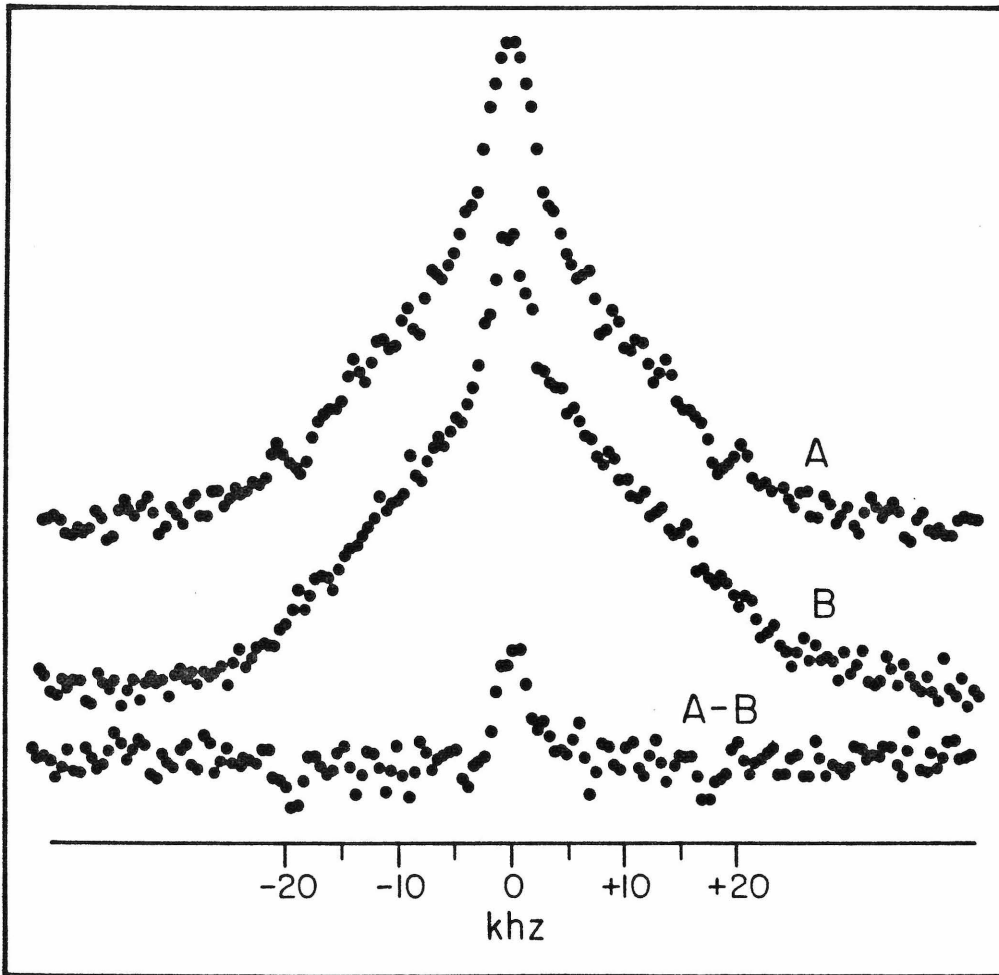
Figure 5: Comparison of T_{1y} decays for samples deposited in deuterium and hydrogen on the grounded electrode (anode).

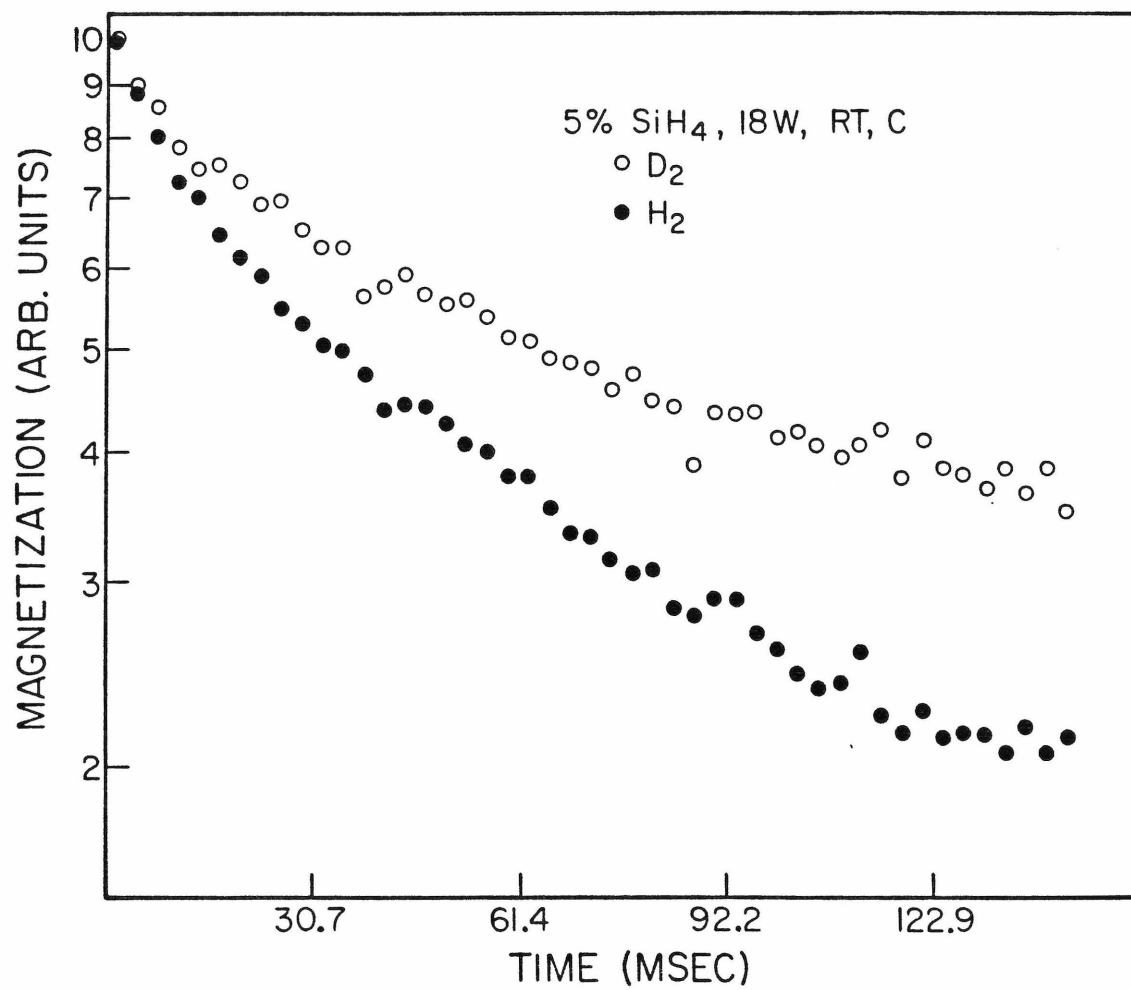
Figure 6: Hydrogen content as a function of annealing temperature for two films prepared from 5% SiH₄ in Argon.

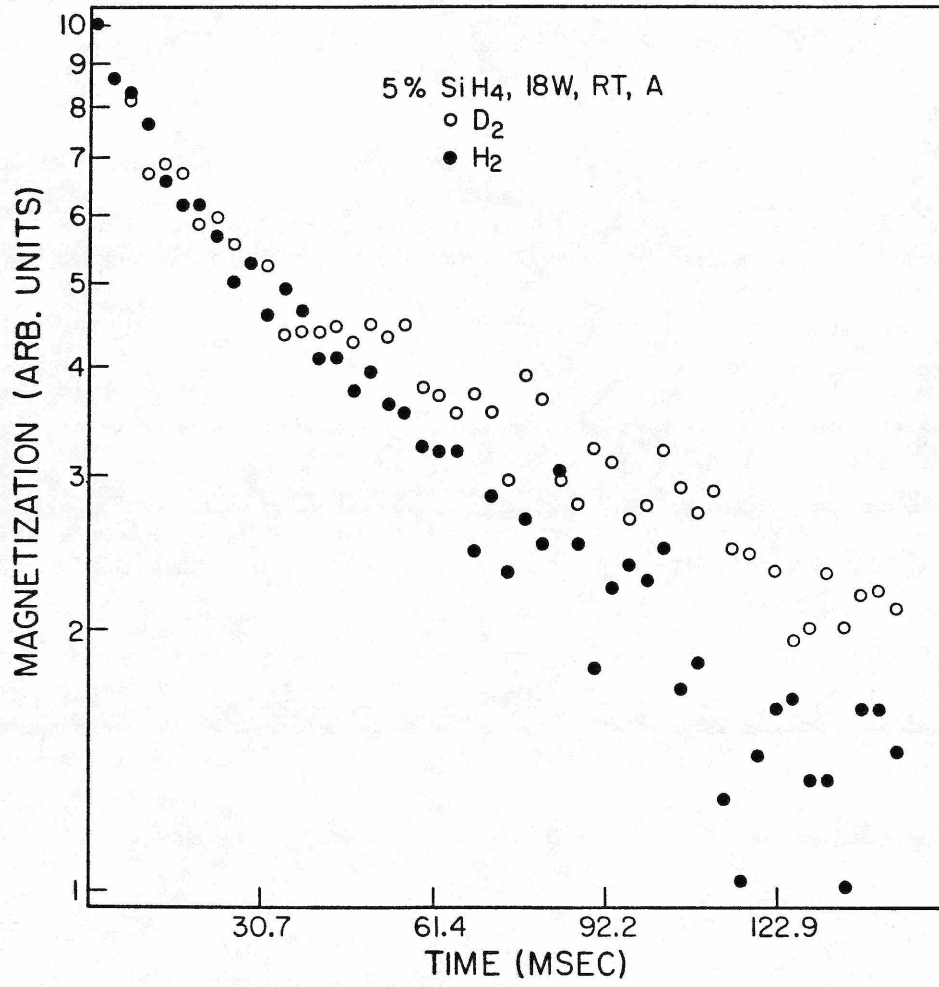
Figure 7: Proton spin-lattice relaxation times (T_1 , bottom) for the samples shown in Figure 6 as a function of annealing temperature. For comparison the ESR spin densities for similarly prepared samples (from reference 9) are shown at top.

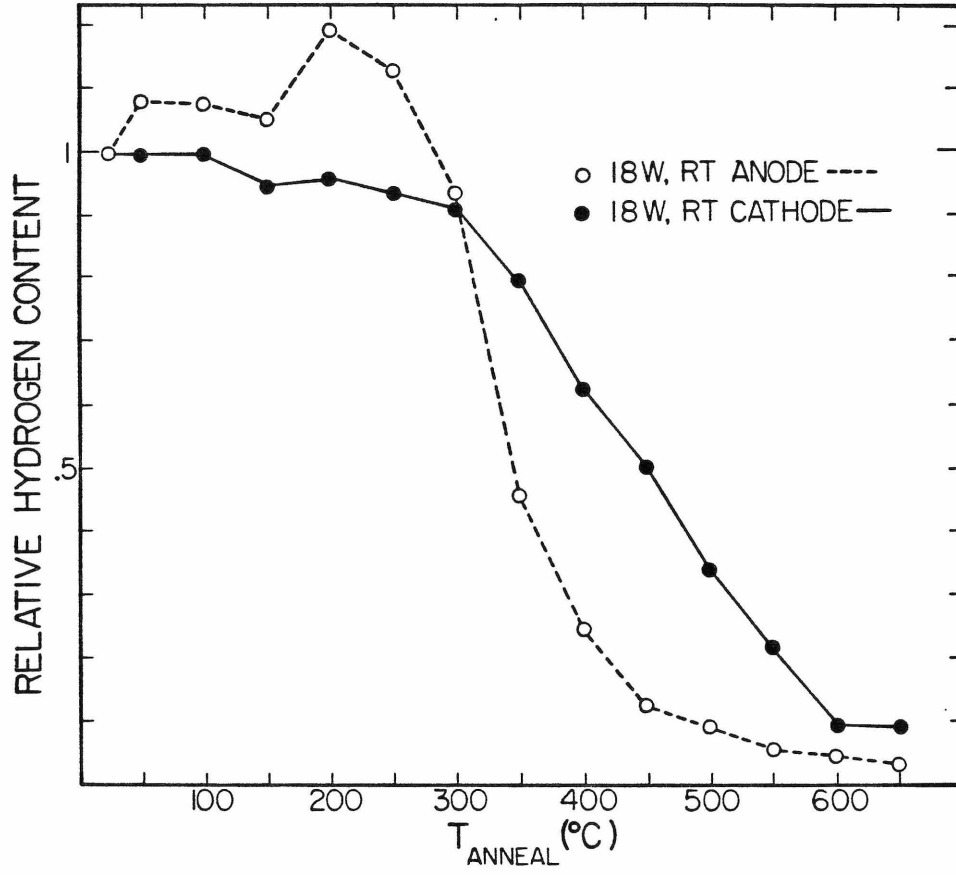


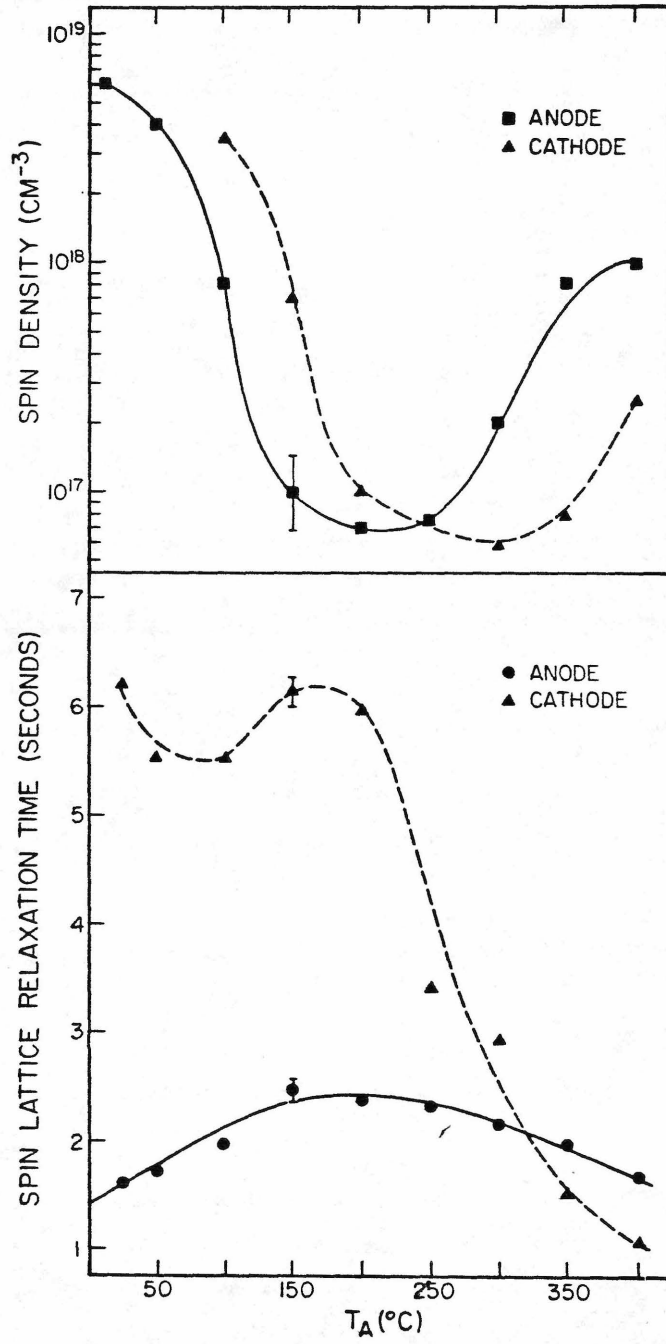












PART 2: SELECTIVE PROTON OBSERVED NMR IN SOLIDS

(Part 2 is essentially two articles by J. A. Reimer and R. W. Vaughan entitled "Selective High Resolution Proton NMR Spectra in Solids" and "Selective Proton Observed Heteronuclear Dipolar Modulated Chemical Shift Spectra in Solids". The former article appeared in Chemical Physics Letters 63, 163 (1979) and the latter is scheduled for the January 1981 issue of the Journal of Magnetic Resonance.)

Chapter 5

INTRODUCTION: SELECTIVE PROTON OBSERVED NMR

Recent years have seen the development of multiple pulse NMR techniques (1-3) allowing for the measurement of proton chemical shift spectra in solids. Application of these techniques has been limited largely to systems in which all the protons are crystallographically equivalent, since nonequivalent protons normally produce overlapping chemical shift powder spectra. For more complicated systems some investigators (3) have used single crystal rotation patterns to deconvolve overlapping chemical shifts, however, many chemically interesting systems such as biomacromolecules or surface adsorbed species are unavailable as single crystals. Another method for observing a selected chemical environment in a polycrystalline solid is to use other nuclei such as ^{13}C which have a dispersion of chemical shifts large enough to resolve different chemical environments. Double resonance techniques (1,2) have been developed to aid in the observation of such dilute spin nuclei. However, extensive signal averaging and/or high magnetic fields are still required to obtain spectra in even moderately complex systems. Thus, the motivation for this work was to develop a technique designed for observation of a selected chemical environment in complex polycrystalline solids while retaining the signal-to-noise advantage of observing protons.

A heuristic description of the technique we developed is shown in Figure 1. Consider a polycrystalline solid with several inequivalent protons where one type of proton is directly bonded to another spin- $\frac{1}{2}$ nucleus such as ^{13}C or ^{15}N . After suppressing the proton homonuclear dipolar interactions with a multiple pulse cycle, one obtains the spectrum diagrammed in Figure 1B. The protons bonded directly to the ^{13}C or ^{15}N nuclei are broadened by the heteronuclear dipolar interaction to the

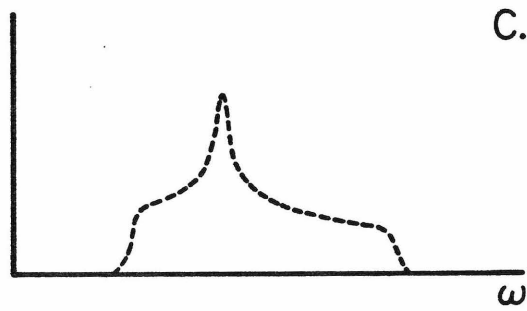
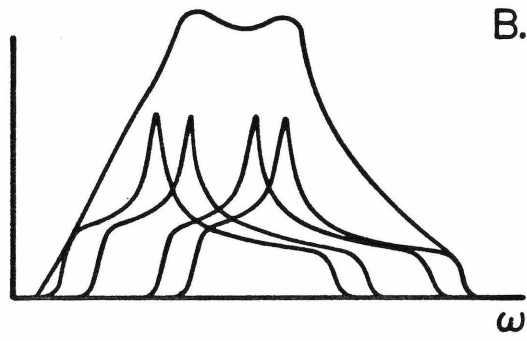
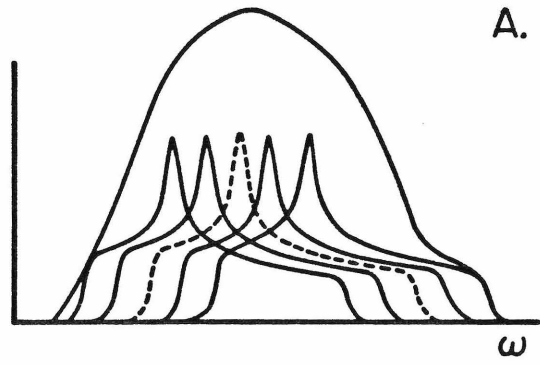
point that they appear to lack any contribution to the observed chemical shift spectrum. If one simultaneously decouples both the homonuclear and heteronuclear dipolar interactions, one obtains the spectrum shown in Figure 1A. In that case, all proton chemical shift spectra are observed. The difference of the two experiments, shown in Figure 1C, is the chemical shift powder spectra for only those protons bonded directly to the nucleus we chose to decouple (e.g. ^{13}C or ^{15}N). We thus achieve selective observation of a given chemical environment by a difference technique involving suppression of the homonuclear dipolar interaction while alternately suppressing the heteronuclear dipolar interaction. The next chapter describes this technique in detail as well as showing how the technique may be modified to obtain geometrical (bond distances and angles) information. Finally, Chapter 7 describes the application of these techniques to two chemical problems.

References

1. R. W. Vaughan, *Ann. Rev. Phys. Chem.* 29, 397 (1978).
2. M. Mehring in: MMR-Basic Principles and Progress, Vol. II, Eds. P. Kiehl, E. Fluck and R. Kosfield (Springer, Berlin, 1976).
3. U. Haeberlin in: Advances in Magnetic Resonance, Supplement 1, Ed. J. S. Waugh (Academic Press, New York, 1976).

Figure Caption

Heuristic description of the difference technique discussed in the text. Top: Overlapping chemical shift spectra with both homonuclear and heteronuclear dipolar interactions suppressed. The dotted spectrum corresponds to those protons bonded directly to another spin- $\frac{1}{2}$ nucleus. Middle: Overlapping chemical shift spectra with homonuclear dipolar interactions suppressed. Bottom: Difference spectrum (top - middle).



Chapter 6

SELECTIVE PROTON OBSERVED HETERONUCLEAR DIPOLAR
MODULATED CHEMICAL SHIFT SPECTRA IN SOLIDS

Abstract

The production of heteronuclear dipolar modulated chemical shift spectra of specific protons within polycrystalline solids is described by consideration of explicit double resonance pulse schemes which remove both heteronuclear and homonuclear dipolar interactions. These spectra furnish an accurate method of determining bond distances in local environments of complicated chemical systems. When used in conjunction with selectively observed chemical shift spectra, these schemes present a means for characterization of both geometrical and electronic properties in the solid state.

Introduction

The use of the heteronuclear dipolar interaction between two spin- $\frac{1}{2}$ nuclei together with the chemical shift interaction to furnish geometrical information has been widely discussed in the recent literature (2-8). The creation of dipolar-modulated chemical shift powder patterns has been described for observation of dilute spins, ^{13}C (3-7), and abundant spins, ^1H , when all the abundant spins occupy equivalent sites (8). In a recent communication (1), we reported an experimental scheme to isolate the chemical shift spectrum of chemically distinct protons in complex polycrystalline solids where the protons of interest are coupled by the heteronuclear dipolar interaction to another spin- $\frac{1}{2}$ nucleus. Such a technique allows for the observation of a selected proton environment at the exclusion of all others. We concluded that it may be possible to create selective proton observed dipolar modulated powder patterns and use such spectra to determine molecular frame geometry (bond distances and bond angles) and orient the chemical shift principal axes in the molecular frame.

The purpose of this chapter is to consider the proton selective technique in detail. In addition to selective chemical shift spectra, we show how to produce selective proton observed heteronuclear dipolar modulated chemical shift spectra and thus demonstrate the ability to characterize geometrical properties of local hydrogen environments in polycrystalline or amorphous solids.

The Proton Selective Multiple Pulse Technique

When using a multiple pulse technique (9,10) to suppress homonuclear dipolar interactions in a typical polycrystalline solid, one usually obtains for the abundant I spins an inhomogeneously broadened spectrum because of the overlapping chemical shift spectra. In the case where some of the I spins are dipole-dipole coupled to S spins, the multiple pulse spectrum of those protons will have an additional broadening due to the heteronuclear dipolar (I-S) interaction. In typical rigid solids, or at least where motional averaging is not complete, the heteronuclear dipolar interaction is much greater than the chemical shift interaction for $I = {}^1\text{H}$. The proton selective technique relies on this fact because under multiple pulse those protons bonded directly to an S spin will be broadened to the point where they appear to yield no contribution to the overlapping chemical shift powder patterns of the other protons. Thus, by suppressing the heteronuclear dipolar broadening of those I spins coupled to the S spins concurrently with a multiple pulse cycle and subtracting the resultant spectrum from a multiple pulse spectrum in which the I-S dipolar interaction is not suppressed, one obtains only the multiple pulse spectrum of the I spins bonded directly to the S spins.

While there are a variety of ways in which one may remove the heteronuclear dipolar interaction (9), the pulse decoupling scheme (12) in the present experiment must necessarily take into consideration the multiple pulse sequence used to suppress the I-I homonuclear dipolar interaction. For the data shown here, the MREV-8 cycle (11) was used to remove the homonuclear dipolar interaction, although other pulse cycles such as the

BR-24 cycle (13,14) could be used as well. Figure 1 shows the timing of the I and S spin pulse sequences including the effects of finite pulse widths. The S spin π -pulses are adjusted to fit within the "windows" of the I spin eight pulse sequence and alternate in sign with each eight pulse cycle to eliminate the accumulation of pulse errors. In the event that there is insufficient rf power to produce such short pulses, one may overlap the S spin π -pulses with the I spin $(\pi/2)_Y$ and $(\pi/2)_{-Y}$ pulses as described previously (1). The effect of these finite pulse widths on the heteronuclear dipolar Hamiltonian, calculated via the Magnus expansion approach (11), may be shown to vanish from symmetry arguments. In these experiments, if one suppresses the heteronuclear I-S interaction with the four pulse scheme every other acquisition while suppressing the homonuclear dipolar interaction, one obtains the chemical shift spectrum of that I spin coupled to the S spin by alternately adding and subtracting acquisitions.

The above scheme is particularly well suited for studying molecules that have only one inequivalent S spin, such as can be realized for a small molecule adsorbed to a surface. To obtain selectivity in larger molecules, one must in general isotopically enrich the S spin bonded directly to the proton of interest. Such enrichment is common practice in the case of observing isotopically dilute spins such as ^{13}C or ^{15}N .

Selective Proton I-S Dipolar Oscillations

The extension of the above technique to obtain selective proton observed dipolar modulated chemical shift spectra is straightforward, as shown in Figure 1B. For every other acquisition, one simply delays the

start of the four pulse heteronuclear decoupling sequence by an integral number of the proton eight pulse cycle times. During the delay time the heteronuclear dipolar interaction evolves and modulates the chemical shift powder pattern of the proton bonded directly to the S spin. By alternately adding and subtracting the acquisitions with and without the delay (Figures 1A and 1B), one then obtains the difference between the normal chemical shift spectrum of the proton and the chemical shift spectrum that has been modulated by the I-S interaction. The present experiment differs from the dilute spin observed (3-6) experiments where one obtains the dipolar modulated spectra directly. In addition, one has the advantage of much greater signal-to-noise due to the larger gyromagnetic ratio of protons. Here the selectivity occurs because those protons not bonded directly to an S spin will have their spectra unaffected by the delay, hence are cancelled out by the co-subtraction of acquisitions with and without the delay.

To consider the production of selective I spin heteronuclear dipolar modulated spectra, we extend on the formalism used to describe dipolar modulation of dilute spins in polycrystalline solids (3-6). The effective zeroth-order Hamiltonians associated with a polycrystalline solid consisting of inequivalent spin- $\frac{1}{2}$ I spins with dilute spin- $\frac{1}{2}$ S spins under an eight pulse sequence are:

$$H_{CS}^I = \sum_i \frac{\alpha(\Delta\omega + \omega_0 \sigma_{zzj})}{3} (I_{xi} + I_{zi}) \quad (1)$$

$$H_{CS}^S = \sum_j (\Delta\omega + \omega_0 \sigma_{zzj}) S_{zj} \quad (2)$$

$$H_{IS} = \frac{\alpha B_{ij}}{3} (I_{xi} + I_{zi}) S_{zj} \quad (3)$$

where

$$B_{ij} = \left(\frac{\gamma_i \gamma_j h}{r_{ij}} \right) (1 - 3 \cos^2 \theta_{ij})$$

are r is the internuclear distance, θ the angle between r and the applied field, ω_0 the resonant frequency of the I or S spins and $\Delta\omega$ the amount the applied rf differs from ω_0 , and σ_{zz} the chemical shift tensor component for either the I or S spin. Equations (1) and (2) are the effective chemical shift Hamiltonians and Equation (3) the heteronuclear dipole-dipole Hamiltonian. Since the effective Hamiltonians commute, one may calculate easily the time evolution of the density matrix and hence predict the observed chemical shift spectrum. For example, when H_{IS} is allowed to evolve for a time τ , the effective zeroth-order density matrix for the coupled I spin evolves as

$$\rho^I(t) = \exp \{-i[H_{IS}\tau + H_{CS}^I t]\} \rho(0) \exp \{i[H_{IS}\tau + H_{CS}^I t]\}. \quad (4)$$

We have used this approach to calculate the time dependence of the density matrix for the more complicated case of the difference scheme shown in Figures 1A and 1B. The effective zeroth-order density matrix for the difference scheme is then used to calculate the time dependence of the magnetization which, upon Fourier transformation, yields the dipolar modulated spectrum

$$F(\omega, \tau) =$$

$$\int_0^{2\pi} \int_0^{\pi} \left[1 - \cos \left\{ \frac{\alpha \gamma_I \gamma_S \hbar \tau}{3\sqrt{2} r^3} \left(1 - 3[\sin\chi \cos(\phi - \psi) \cos\chi \cos\theta]^2 \right) \right\} \right] \sin\theta d\theta d\phi \left\{ \frac{\frac{\alpha}{3\sqrt{2}} (\Delta\omega + \omega_0 (\sigma_x \sin^2\theta \cos^2\phi + \sigma_y \sin^2\theta \sin^2\phi + \sigma_z \cos^2\theta) - \omega)^2}{\omega^2 + 1} \right\}$$

(5)

In this expression, $(\sigma_x, \sigma_y, \sigma_z)$ are principal components of the I spin tensor (note the multiple pulse scaling factor $\alpha/3\sqrt{2}$), (χ, ψ) are the polar angles of the I-S vector with respect to the principal axes of the chemical shift tensor, and ω is the half-width of a Lorentzian broadening function assumed for the chemical shift powder pattern. The experimental spectra, obtained as a function of τ , may be fitted to Equation (5) in order to obtain the orientation of the I-S vector in the chemical shift principal axis system as well as determine the I-S bond distance.

In the event that there is insufficient resolution of the proton chemical shift tensor to use Equation (5), the areas of the dipolar modulated spectra are sufficient to determine the I-S internuclear distance. If $A(\tau)$ is the area of the proton spectrum after dipolar evolution for a time τ , then the observed areas for the selective scheme shown in Figures 1A and 1B are given by

$$\frac{A(0) - A(\tau)}{A(0)} = 1 - \frac{1}{4\pi} \int \cos \left\{ \left[\frac{\alpha \tau \gamma_I \gamma_S \hbar}{3\sqrt{2} r_{IS}} \right] [1 - 3\cos^2\theta_{IS}] \right\} d\Omega \quad (6)$$

Figure 3A gives the result for three I-S distances where $I = {}^1\text{H}$ and $S = {}^{15}\text{N}$. Note that I-S internuclear distances differing by only 0.1 angstroms may be discriminated readily so that fairly accurate bond lengths may be obtained by this approach.

A more recent 24-pulse scheme (13,14) which removes the homonuclear dipolar interaction to fourth order may also be used in conjunction with a heteronuclear decoupling pulse scheme to obtain selective dipolar oscillations. As with the eight pulse sequence, care must be taken to insure no pulse errors accumulate due to finite overlap of the I and S spin pulses. The 24-pulse cycle is particularly useful in furnishing increased resolution for protons with small chemical shift anisotropies as well as for tightly coupled protons such as AX_2 systems. Under this 24-pulse cycle, the relevant zeroth-order Hamiltonians still commute and are given by

$$H_{\text{CS}}^{\text{I}} = \sum_i \frac{\alpha(\Delta\omega + \omega_0 \sigma_{\text{ZZ}i})}{3} (I_{\text{x}i} - I_{\text{y}i} + I_{\text{z}i})$$

$$H_{\text{IS}} = \sum_i \frac{\alpha\beta_{ij}}{3} (I_{\text{x}i} - I_{\text{y}i} + I_{\text{z}i}) \quad (7)$$

Thus, Equations (5) and (6) still describe the production of dipolar modulated chemical shift spectra provided the appropriate chemical shift scaling factor is used. It is important to note that this scheme provides a more direct method for determining I-S internuclear distances in AX_n systems than dilute spin observation experiments where sum and difference frequencies (3-6) are required to interpret bond distances from spectral areas. Hence, structural information in more complicated systems may be

readily obtained.

Experimental

While π -pulses for $S = {}^{13}\text{C}$ could be set by direct observation of the ${}^{13}\text{C}$ spins, in the case of $S = {}^{15}\text{N}$ such tuning could be tedious due to the low signal-to-noise for ${}^{15}\text{N}$. Here, one can take advantage of an I spin resonance offset due to the presence of the S spin irradiation to tune the S spin pulse amplitudes. Since the S spin pulse is given by

$$\theta = \gamma H_1 t_p = \omega_1 t_p ,$$

for ${}^{15}\text{N}$ when $\theta = \pi$ and $t_p = 11$ microseconds, H_1 must be 105.3 Gauss. Given the duty cycle for the S spin pulse scheme shown in Figure 1, the average rf field strength, $\overline{\omega_1}$, must be 197,000 hertz. The effect of this irradiation of frequency ω_S and effective amplitude $\overline{\omega_1}$ on the proton resonance may be calculated by going to the proton rotating frame and ignoring Bloch-Siegert terms (9). For $H_1 = 105.3$ Gauss, we find that a liquid sample of protons on resonance is shifted by 384 hertz when the S spin pulse decoupling field is present. Hence, given the S spin and the time required for the pulse and the duty cycle, H_1 may be set by its effect on the I spin resonant frequency.

This offset poses a minor irritation on the actual difference experiments once the S spin pulses are tuned. Two methods of avoiding this offset are: (i) using a programmable synthesizer for the I spins that offsets the shift produced by the S spin irradiation, and (ii) accumulating the desired spectra with the I spin synthesizer set to take into account the S spin irradiation and then subtracting the same number of

acquisitions from the original spectrum with the S spin irradiation off and the I spin synthesizer returned to its original value. Both methods were used to obtain the results shown in Chapter 8. For dipolar modulated chemical shift spectra, the delay time is never long enough to remove this offset, hence, no programmable synthesizer is required to furnish these spectra.

Conclusions

In conclusion, we have reviewed an experimental method for obtaining selective proton observed chemical shift and heteronuclear dipolar modulated chemical shift spectra in polycrystalline solids as well as presenting an average Hamiltonian formalism for the selective dipolar oscillations. In the next chapter we shall see how these techniques may be applied to the study of surface adsorbed species as well as hydrogen bonds in solids. As we shall see, in both cases information could be derived from the spectra which elucidate local bonding environments. We conclude that selective observation of proton NMR parameters may be useful in studying local geometrical and electronic properties in complicated polycrystalline of amorphous solids.

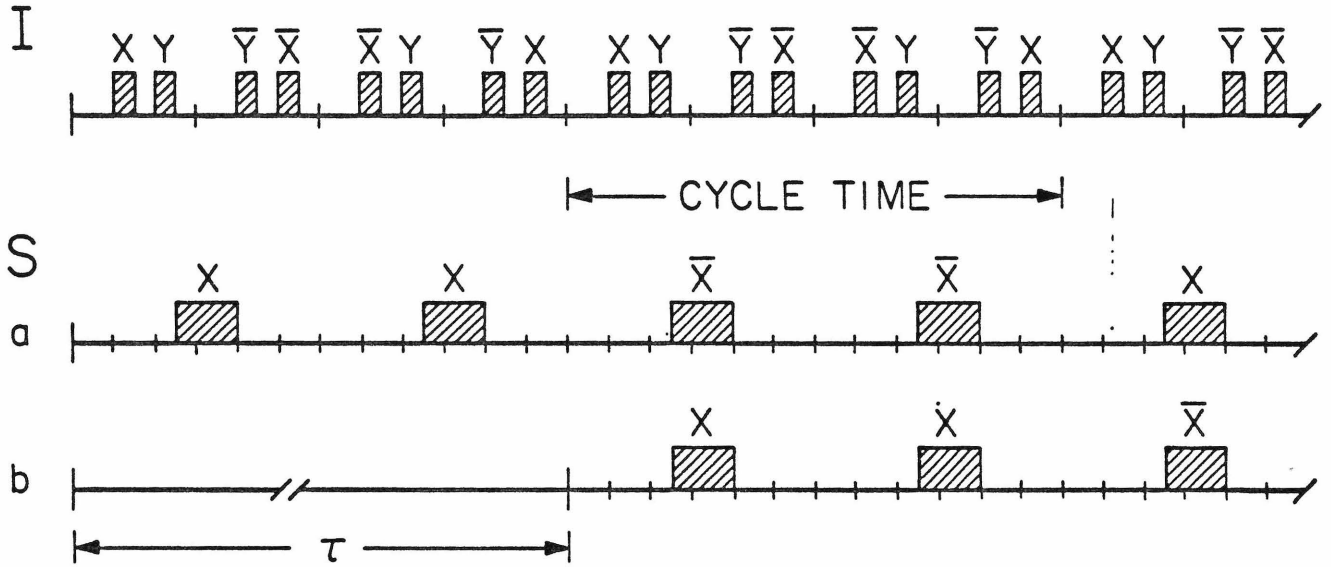
References

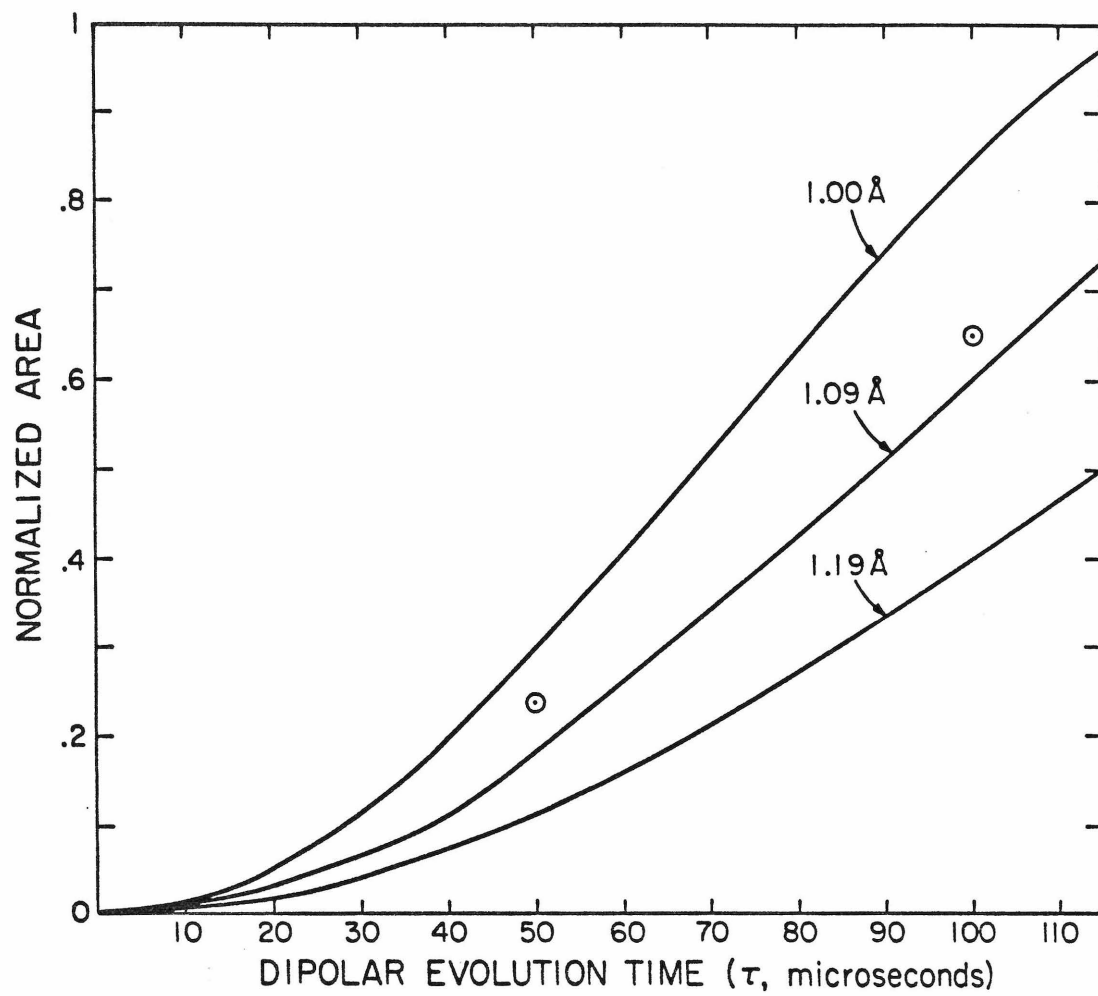
1. J. A. Reimer and R. W. Vaughan, Chem. Phys. Lett. 63, 163 (1979).
2. R. W. Vaughan, Ann. Rev. Phys. Chem. 29, 397 (1978).
3. M. E. Stoll, A. J. Vega, R. W. Vaughan, J. Chem. Phys. 65, 4093 (1976).
4. M. E. Stoll, A. J. Vega, R. W. Vaughan, XIX Congress Ampere, Heidelberg, 1976.
5. J. S. Waugh, Proc. Natl. Acad. Sci. 73, 1394 (1976).
6. R. K. Hester, J. L. Akerman, B. L. Neff, J. S. Waugh, Phys. Rev. Lett. 36, 1081 (1976).
7. E. F. Rybaczewski, B. L. Neff, J. S. Waugh, J. S. Sherfinski, J. Chem. Phys. 67, 1231 (1977).
8. M. E. Stoll, A. J. Vega, R. W. Vaughan, J. Chem. Phys. 69, 5458 (1978).
9. M. Mehring in: NMR-Basic Principles and Progress, Vol. 11, Eds. P. Kieh1, E. Fluck and R. Kosfield (Springer, Berlin, 1976).
10. U. Haeberlen in: Advances in Magnetic Resonance, Supplement 1, ed. J. S. Waugh (Academic Press, New York, 1976).
11. W.-K. Rhim, D. D. Elleman, L. B. Schreiber, R. W. Vaughan, J. Chem. Phys. 11, 4595 (1974).
12. M. Mehring, A. Pines, W.-K. Rhim, J. S. Waugh, J. Chem. Phys. 54, 3239 (1971).
13. D. P. Burum, W.-K. Rhim, J. Chem. Phys. 71, 944 (1979).
14. D. P. Burum, PhD Thesis, California Institute of Technology, 1979.

Figure Captions

Figure 1: Schematic diagram showing S spin π -pulses properly timed to eliminate accumulation of pulse errors. X and \bar{X} refer to the relative phase of the rf pulse with \bar{X} being 180° out of phase to X . The eight pulse cycle applied to the I spins consists entirely of $\pi/2$ pulses with relative phases as shown. A delay of the start of the S spin π -pulse decoupling scheme is shown in (b) and produces heteronuclear dipolar-oscillated chemical shift spectra.

Figure 2: Equation (6) from the text for $I = {}^1\text{H}$ and $S = {}^{15}\text{N}$, showing the relative area of the difference spectrum as a function of dipolar evolution time τ . The curves show three different values of N-H bond lengths. The two open circles show the data points for the N-H...O hydrogen bond in acetanilide and yield an N-H distance of $1.05 \pm 0.01 \text{ \AA}$.





Chapter 7

THE APPLICATION OF SELECTIVE PROTON NMR TO THE STUDY OF
SURFACE ADSORBED FORMIC ACID AND POLYCRYSTALLINE ACETANILIDE

Abstract

Selective proton-observed NMR results are presented for the carbonyl proton of adsorbed formic acid on ammonium-Y zeolite and the hydrogen bonded proton in polycrystalline acetanilide. Chemical shift information for the adsorbed formic acid shows a chemisorbed species consistent with formate ions. The data for the amide bond in polycrystalline acetanilide show a hydrogen bond with a chemical shift anisotropy of 17.7 ppm and a N-H distance of $1.05 \pm .01 \text{ \AA}$.

Introduction

Two frontiers addressed frequently in the literature are the chemistry of surface-adsorbed molecules and the nature of hydrogen bonding in both liquids and solids. The former research area has implications for catalysis and the latter for biomacromolecules and cooperative phenomena in solids. In both problems, a wide variety of spectroscopic and experimental techniques are employed in an attempt to elucidate local geometrical and electronic environments. There have been few attempts, however, to utilize modern high resolution NMR techniques to study these phenomena because of their chemical complexity. As discussed in Chapter 6, selective proton observed NMR allows for the selective observation of a local hydrogen environment at the exclusion of all others, and hence, is a technique well suited for both surface and hydrogen bond studies.

In this chapter, I will present selective proton NMR data for formic acid adsorbed to ammonium- γ zeolites and the amide bond in polycrystalline acetanilide. In the formic acid study, I will show the selectively observed chemical shift spectrum of the carbonyl proton on the admolecules. The proton chemical shift indicates that the admolecule is a formate ion. In polycrystalline acetanilide, in addition to the selective chemical shift spectrum, I show heteronuclear dipolar oscillation results for the amide bond and thus demonstrate the ability to characterize geometrical parameters in polycrystalline or amorphous materials.

Experimental

Materials

Acetanilide 95% ^{15}N -enriched was obtained from Prochem (Lot #12x9) and was used without further purification, spin-lattice relaxation times were approximately 90 seconds and approximately 1000 averages were accumulated for a typical spectrum. A 20% deuterium-exchanged sample was prepared by recrystallization of the ^{15}N -enriched acetanilide from a 20% $\text{D}_2\text{O}/\text{H}_2\text{O}$ solution and the difference spectrum signal was found to decrease by 20%.

A sample of 90% ^{13}C formic acid (H^{13}COOH , Prochem) adsorbed on ammonium-Y zeolite was prepared by T. M. Duncan. Formic acid was introduced (3) into the dry zeolite to a concentration of 25 formic acid molecules per unit cell. The unit cell has the molecular formula $\text{Na}_2(\text{NH}_4)_{48}(\text{AlO}_2)_{50}(\text{SiO}_2)_{142} \cdot 267\text{H}_2\text{O}$, hence the formate proton contributes only 3% to the total protons present in the sample. Proton spin-lattice relaxation times were less than one second so that a difference spectrum could be obtained in an hour.

Method

Magnetic resonance spectra were taken with an NMR spectrometer described previously (1) at a proton resonance frequency of 56.4 Mhz ($^{13}\text{C} = 14.2$ Mhz, $^{15}\text{N} = 5.7$ Mhz). Proton τ values were 4.17 microseconds and the proton $\pi/2$ pulse widths were typically 2 microseconds. S spin pulses were set at approximately 11 microseconds. The S spin field strengths were 42.5 Gauss for $S = ^{13}\text{C}$ and 105.3 Gauss for $S = ^{15}\text{N}$.

Both the ^{15}N -H and ^{13}C -H double resonance probes were of the single coil doubly tuned type (2). Nominal values for ^{13}C -H and ^{15}N -H, respectively, were $C_1 = 590$ pf, 1270 pf; $C_2 = 1760$ pf, 6600 pf; $C_3 = 30$ pf, 30 pf; $C_4 = 108$ pf, 120 pf. The ^{15}N -H probe Q's were 25 and 90, respectively, and those of the ^{13}C -H probe were 70 and 100.

Discussion of Results

Figure 1 shows the selective observation of the chemical shift spectrum of the carbonyl proton of H^{13}COOH adsorbed to ammonium-Y zeolite. Zeolites (or molecular sieves) are composed of SiO_4 and AlO_4 tetrahedra arranged in various geometrical patterns. The key structural feature of the sieves is the narrow uniform channel system that becomes available after the zeolitic water has been driven off by heating and evacuation (4a). Ammonium-Y zeolite specifically catalyzes the decomposition of formic acid to CO and H_2O (46). Duncan and Vaughn (3) were able to use the spectrum shown in Figure 3 in conjunction with ^{13}C NMR and infrared data to elucidate binding site geometry and distributions for the adsorbed formic acid. The reader is referred to their work for a complete description of the formic acid zeolite adsorption. We point out here three conclusions that are a direct result of the spectrum shown in Figure 1. The first conclusion is that at least some of the adsorbed formic acid has an intact C-H bond that is rigid enough to allow the heteronuclear interaction to be sufficiently large to yield a difference spectrum. This leads to the conclusion that the molecule is chemisorbed and not physisorbed to the surface as has been suggested previously (5).

Second, the average chemical shift $\bar{\sigma}$ of the carbonyl proton (-12.3 ppm) is consistent with formate ion structures and not the acid itself (6), implying that the adsorbed species are formate ions. Third and finally, the linewidth of the carbonyl proton is relatively narrow (6 ppm) giving an upper bound on the inhomogeneous broadening (e.g. ^{27}Al heteronuclear dipolar) observed in ^{13}C NMR chemical shift spectra (3). This latter result confirmed the interpretation of the broadening in ^{13}C chemical shift spectra as being due to site distributions and local motions. Selective dipolar oscillations were not performed on this sample since previously attempted dilute spin observation experiments showed no geometrical information due to motional effects (3). Finally, we note that this particular difference spectrum was accumulated in approximately one hour compared with eight hours for the equivalent signal-to-noise in a ^{13}C observed cross-polarization spectrum. Hence, the selective proton observation experiment should prove useful in the study of low surface area or low coverage adsorption experiments.

Figure 1 also shows the selective observation of the chemical shift spectrum of the intermolecular hydrogen bonded proton in polycrystalline acetanilide. The crystal structure of acetanilide (7) shows molecules of acetanilide are linked together in chains by N-H...O hydrogen bonds characterized by an N-H...O length of 2.969 Å. The presence of these N-H...O hydrogen bonds has been confirmed by infrared studies (8) and is currently under investigation in a search for cooperative phenomena in solids (9). The spectrum in Figure 1 shows a near axially symmetric tensor with an anisotropy $\Delta\sigma$ of 17.7 ppm. A least-squares fit of this spectrum yields $\sigma_1 = 4.6$ ppm, $\sigma_2 = -13.0$ ppm, and $\sigma_3 = -13.1$ ppm with a

Lorentzian broadening of 16 ppm and center mass $\bar{\sigma} = -7.2$ ppm. The open circles in Figure 2 of Chapter 6 show the relative areas for selective observation of dipolar oscillation spectra with τ values of 50 and 100 microseconds. These areas yield a N-H bond length of $1.05 \pm .01$ Å. Because of the residual broadening of the observed tensor, an exact determination of the orientation of the principle axis of the chemical shift tensor in the N-H molecular frame was not possible. However, the observed data are qualitatively consistent with O-H...O NMR studies (10) which show the most shielded component of the chemical shift tensor to be parallel to the hydrogen bond.

To this author's knowledge, the amide proton tensor is the first observation of the NMR of protons in an N-H...O hydrogen bond in the solid state. It is useful to compare these data with those found in the numerous studies of O-H...O systems (10,11). Berglund and Vaughan (11) found an excellent correlation between the isotropic chemical shift $\bar{\sigma}_{\text{abs}}$ [referenced to the bare proton on an absolute scale where $\bar{\sigma}_{\text{TMS}} = 30.4$ ppm (12)] and the O...O distance in O-H...O hydrogen-bonded systems. Figure 2 is taken from reference (11) and shows this correlation with the addition of the data from this N-H...O study and the known N...O distance from X-ray studies (7). We find excellent agreement with the trend for O-H...O systems that $\bar{\sigma}_{\text{abs}}$ increases with increasing O...O distances. This trend is also in agreement with *ab initio* studies (13) of H₂O and H₂O...H₂O dimers. The data in Figure 3, also from reference (11), show the correlation between anisotropy of the proton chemical shift $\Delta\sigma$ and the O...O distance. These N-H...O data of Figure 3 are also in agreement with O-H...O trends of decreasing $\Delta\sigma$ with increasing X...O distances.

Deviations from this correlation for these N-H...O data may be related to the difference between oxygen and nitrogen donor atoms. These correlations show the need for further theoretical studies of hydrogen bonds.

The observed N-H bond length of $1.05 \pm .01 \text{ \AA}$ is in good agreement with ^{14}N NMR single crystal studies in N-acetyl valine (14) and consistent force field (CFF) calculations (15) for hydrogen bonds between carbonyl groups and amino groups in various amide crystals. This observed bond length is also in good agreement with correlations between N...O and N-H distances as determined by neutron diffraction studies (16,17). Thus, the proton selective dipolar oscillation methods seem practical for structural determinations in complex polycrystalline systems.

In summary, we have presented the selective observation of protons on a surface admolecule, formic acid on ammonium-Y zeolite, and in an N-H...O hydrogen bond, polycrystalline acetanilide. In both cases, information could be derived from the spectra which elucidate local bonding environments. We conclude that selective observation of proton NMR parameters may be useful in studying local geometrical and electronic properties in complicated polycrystalline or amorphous solids.

References

1. R. W. Vaughan, D. D. Elleman, L. M. Stacey, W.-K. Rhim, J. W. Lee, *Rev. Sci. Instrum.* 43, 1356 (1972).
2. M. E. Stoll, A. J. Vega, R. W. Vaughan, *Rev. Sci. Instrum.* 48, 800 (1977).
3. T. M. Duncan and R. W. Vaughan, submitted *J. Catalysis*.
4. (a) P. B. Venuto and P. S. Landis, *Adv. in Catalysis*, Vol. 18, 259 - 371 (1968).
(b) P. Mars, J. J. F. Scholten, P. Zweitering, *ibid.* 14, 35 (1963).
5. K. Hirota, K. Fueki, K. Shinko, Y. Nakai, *Bull. Chem. Soc. Japan* 32,
6. J. A. Reimer and R. W. Vaughan, *Chem. Phys. Lett.* 63, 163 (1979).
7. C. J. Brown and D. E. C. Corbridge, *Acta Cryst.* 7, 711 (1954).
8. (a) N. B. Abbott and A. Elliott, *Proc. Roy. Soc. (London)*, Series A, A234, 247 (1955).
(b) C. Sandorfy in: Hydrogen Bond II, Eds. P. Schuster, G. Zundel, C. Sandorfy, 612 (North-Holland, Amsterdam, 1976).
9. G. Careri in: Cooperative Phenomenon, Eds. H. Haken and M. Wagner, 391 (Springer-Verlag, Berlin, 1973).
10. U. Haeberlen in: Advances in Magnetic Resonance, Supplement 1, ed. J. S. Waugh (Academic Press, New York, 1970).
11. B. Berglund and R. W. Vaughan, *J. Chem. Phys.* 73, 2037 (1980).
12. W. D. Phillips, W. E. Cokke, D. Kleppner, *Phys. Rev. Lett.* 35, 1619 (1975).
13. R. Ditchfield, *J. Chem. Phys.* 65, 3121 (1976).

14. R. E. Stark, R. A. Haberkorn, R. G. Griffin, J. Chem. Phys. 68 (4), 1996 (1978).
15. A. T. Hagler and S. Lifson, J.A.C.S. 96, 5327 (1974); A. T. Hagler, E. Huler, S. Lifson, J.A.C.S. 96, 5319 (1974).
16. I. Olovsson and P.-G. Jönsson in: Hydrogen Bonding II, Eds. P. Schuster, G. Zundel, C. Sandorfy, 393 (North-Holland, Amsterdam, 1976).
17. T. F. Koetzle and M. S. Lehmann, *ibid.*, 457.

Figure Captions

Figure 1: Selective proton observed chemical shift spectra for H^{13}COOH adsorbed to ammonium-Y zeolite and the amide proton $(\text{C}_6\text{H}_5)\text{CO}^{15}\text{NHCH}_3$ in acetanilide. The carbonyl proton represents only 3% of the total number of protons present in the sample. Note the chemical shift scale is in σ not δ units.

Figure 2: Absolute chemical shift (see text) versus O...O distances from O-H...O hydrogen bonding studies (taken from Reference 23). Included is the absolute shift for the N-H proton in acetanilide and this shows the excellent correlation between hydrogen bond strength and absolute shift.

Figure 3: Proton chemical shift anisotropy ($\Delta\sigma$) versus X...O distances in X-H...O hydrogen bonded systems. Filled circles are for O-H...O hydrogen bonds [from Reference (23)] and the open circle is from acetanilide. These data show good correlation between chemical shift anisotropy and hydrogen bond strength over a large range of anisotropies.

